

# Facilities for production of bulk amorphous metals, and evaluation thereof using alloy $Zr_{55}Cu_{30}Al_{10}Ni_5$

---

**Erno Soinila**





Facilities for production of bulk  
amorphous metals, and evaluation  
thereof using alloy Zr55Cu30Al10Ni5

**Erno Soinila**

Doctoral dissertation for the degree of Doctor of Science in  
Technology to be presented with due permission of the School of  
Engineering for public examination and debate in Auditorium K216  
at the Aalto University School of Engineering (Espoo, Finland) on the  
13th of July 2012 at noon (at 12 o'clock).

**Aalto University  
School of Engineering  
Department of Engineering Design and Production  
Engineering Materials**

**Supervisor**

Hannu Hänninen

**Instructor**

Sven Bossuyt

**Preliminary examiners**

Dr. Nele Van Steenberge, ArcelorMittal Global R&D Gent OCAS NV, Belgium

Prof. Vincent Keryvin, Université de Bretagne Sud, France

**Opponents**

Dr. Nele Van Steenberge, ArcelorMittal Global R&D Gent OCAS NV, Belgium

Prof. Juha-Pekka Hirvonen / DG JRC JRC, Institute for Energy and Transport, Petten, Netherlands

Aalto University publication series

**DOCTORAL DISSERTATIONS 88/2012**

© Erno Soinila

ISBN 978-952-60-4691-4 (pdf)

ISSN-L 1799-4934

ISSN 1799-4934 (printed)

ISSN 1799-4942 (pdf)

Unigrafia Oy

Helsinki 2012

Finland

The dissertation can be read at <http://lib.tkk.fi/Diss/>

**Author**

Erno Soinila

**Name of the doctoral dissertation**

Facilities for production of bulk amorphous metals, and evaluation thereof using alloy Zr55Cu30Al10Ni5

**Publisher** School of Engineering

Unit Department of Engineering Design and Production

Series Aalto University publication series DOCTORAL DISSERTATIONS 88/2012

Field of research Material science, engineering design

Manuscript submitted 9 March 2012

Manuscript revised 23 May 2012

Date of the defence 13 July 2012

Language English

 Monograph Article dissertation (summary + original articles)**Abstract**

Bulk metallic glasses (BMG) are alloys that can be solidified into a diameter larger than 1 mm without detectable crystallization. The resulting amorphous solid state satisfies the thermodynamic definition of a glass: upon heating above a glass transition temperature, they reach a metastable super-cooled liquid region before crystallizing. There are many known methods for producing amorphous metals. The material properties and the ease of manufacturing amorphous metal specimens depend on the manufacturing methods and facilities used. Studying and developing such facilities contributes both to practical applications of these materials and to advances in basic science of liquid and amorphous states of matter. In this thesis, the merits of different facilities for producing bulk metallic glass are evaluated anecdotally using literature and interviews, and then in practice by designing, building and finally using different facilities to make various metallic glass specimens with composition Zr55Cu30Al10Ni5 (at.%).

The results demonstrate that the process and equipment for producing metallic glass can be significantly simplified by constructing a combined arc melter and tilt casting furnace. A novel design for such a furnace, using ultra-high vacuum fittings making it possible to tilt the entire chamber, eliminates the need to use separate furnaces for alloying and for casting, and enables a practical manner to produce metallic glass specimens of the highest purity and highest mechanical quality.

Further shaping of bulk metallic glass preforms into large aspect ratio metallic glass parts was shown to be feasible, without elaborate process control, in a tensile viscous flow configuration. Induction heating specially designed preforms results in a self-stabilizing thermoplastic forming process for metallic glass wires.

Magnetron sputtering was used to produce amorphous coatings of the same nominal composition as the BMG specimens, directly attached to heat sensitive polymeric materials. Adhesion was found to be controllable via sputtering process parameters.

**Keywords** amorphous metal, bulk metallic glass, arc melting, physical vapor deposition, induction heating

**ISBN (printed)****ISBN (pdf)** 978-952-60-4691-4**ISSN-L** 1799-4934**ISSN (printed)** 1799-4934**ISSN (pdf)** 1799-4942**Location of publisher** Espoo**Location of printing** Helsinki**Year** 2012**Pages** 148**The dissertation can be read at** <http://lib.tkk.fi/Diss/>



**Tekijä**

Erno Soinila

**Väitöskirjan nimi**

Amorfisten metallien valmistuslaitteistot ja niiden arvionti seoksen Zr55Cu30Al10Ni5 avulla

**Julkaisija** Insinööritytieteiden korkeakoulu

Yksikkö Koneenrakennustekniikan laitos

Sarja Aalto University publication series DOCTORAL DISSERTATIONS 88/2012

Tutkimusala materiaaliteknikka, koneenrakennus

**Käsikirjoituksen pvm** 09.03.2012**Korjatun käsikirjoituksen pvm** 23.05.2012**Väitospäivä** 13.07.2012**Kieli** Englanti **Monografia** **Yhdistelmäväitöskirja (yhteenveto-osa + erilisartikkelit)****Tiivistelmä**

Makroskooppisiksi metallisiksi laseiksi (bulk metallic glass, BMG) kutsutaan metalliseoksia, jotka on pystytty jäähyttämään yli millimetrin paksuisina koko alijäähyneen alueen läpi lasiisirymälämpötilaan asti ilman, että on päässyt tapahtumaan havaittavaa kiteytymistä. Jäähytyksessä syntynyt amorfinen metalli täyttää lasin termodynamiisen määritelmän: kuumennettaessa yli lasiisirymälämpötilan metastabiili alijäähyneen sulan alue esiintyy ennen kiteytymistä. Amorfisten metalliseosten tuottamiseen tunnetaan monia menetelmiä. Tuotettujen amorfisten metallikappaleiden materiaalimaisuudet ja valmistettavuus riippuvat käytetyistä valmistusmenetelmiä ja laitteistoista. Näiden valmistuslaitteistojen tutkiminen ja kehittäminen edistää sekä amorfisten metallien käytännön sovelluksia että edistää sulien ja amorfisten materiaalien perustieteitä. Tässä väitöstyössä tutkitaan eri valmistuslaitteistojen kykyjä ensin kirjallisuutta ja haastatteluja käyttäen, seuraavaksi käytännössä laitesuunnittelun ja laiterakennuksen keinoin ja lopuksi koostumuksen Zr55Cu30Al10Ni5 (at.%) amorfisia koekappaleita valmistaen eri valmistuslaitteistoja käyttäen.

Tutkimustyön tulokset osoittavat, että metallisten lasien valmistusprosesseja ja valmistuslaitteistoja voidaan merkittävästi yksinkertaistaa rakentamalla yhdistetty valokaarisulatus- ja kallistusvalulaitteisto. Uudenlainen valmistuslaitteisto, jossa käytetään erittäin korkean tyhjötiiveyden edellyttämää irto-osia mahdollistaa koko tyhjökammion kallistamisen, poistaen tarpeen käyttää kahta erillistä laitetta, yhtä seossumutukseen ja toista valamiseen. Tämä mahdollistaa korkeimman puhtauden ja parhaan mekaanisen laadun metallisten lasikappaleiden valmistuksen. Metallisesta lasista valmistettujen aihioiden jatkomuovaus suuren sivusuhteen metallisiksi lasiosiksi näytettiin toteuttamiskelpoiseksi, ilman erittäin tarkkaa prosessinhallintaa käyttäen viskoosia virtausta vетojännyksen alaisena. Erityisen muotoisten metallisten lasi-aihioiden induktiokuumennus vетojännyksen alaisena synnyttää itsevakauttavan läpömuovausprosessin metalliselle lasilangalle.

Magnetronisputterointia käytettiin samaa nimellistä BMG koostumusta olevien amorfisten pinnoitteiden kiinnittämiseen lämpöherkille polymeerisubstraateille. Amorfinen pinnoite saatiin kiinnitetyä polymeerisubstraatille sopivia sputterointiparametrejä käyttäen.

**Avainsanat** amorfinen metalli, metallinen lasi, valokaarisulatus, induktiokuumennus, magnetronisputterointi**ISBN (painettu)****ISBN (pdf)** 978-952-60-4691-4**ISSN-L** 1799-4934**ISSN (painettu)** 1799-4934**ISSN (pdf)** 1799-4942**Julkaisupaikka** Espoo**Painopaikka** Helsinki**Vuosi** 2012**Sivumäärä** 148**Luettavissa verkossa osoitteessa** <http://lib.tkk.fi/Diss/>



# Preface

The work for this thesis was started as a part of Tekes (Finnish Funding Agency for Technology and Innovation) funded project AMORFISET which studied bulk metallic glasses. The work was continued with the funding from the IA-GGraduate School and the Graduate School Concurrent Mechanical Engineering (GSCME). Also the funding from TULLI-project for the patenting of the next version of the custom-built arc melter is much appreciated. The participating companies in the TEKES project were Nokia, Savcor and Luvata. I gratefully acknowledge the project for funding and the opportunity to study for a year in the Inoue group at Tohoku University's the Institute for Materials Research in Sendai, Japan. Also the possibility to see the metallic glass production facilities used at Professor Johnson's laboratory in CalTech and at Arcelor Mittal's research center in Ghent are much appreciated. I express my gratitude to Professor Hannu Hänninen for his advice and guidance. In addition I wish to thank the entire staff of the Laboratory of Engineering Materials, the entire staff of Institute for Materials Research at Tohoku University and the staff of Savcor Coatings for their help in magnetron coating experiments. In particular I wish to thank Professor Akihisa Inoue, assistant professor Yoshiko Yokoyama, assistant professor Parmanand Sharma, Dr. Markku Heino, PhD. Matti Ryynänen, M.Sc. Paula Kainu and Dr. Sven Bossuyt for sharing their knowledge. Also, and especially Tuomas Pihlajamäki, Jarmo Raiskio, Samuli Laine, Heikki Vestman and Jari Hellgren were instrumental for the equipment building.

Espoo, June 13, 2012,

Erno Soinila



# Contents

<b>Preface</b>	<b>7</b>
<b>Contents</b>	<b>9</b>
<b>Research hypothesis and original features</b>	<b>11</b>
<b>List of Publications</b>	<b>15</b>
<b>Author's Contribution</b>	<b>17</b>
<b>List of abbreviations and symbols</b>	<b>19</b>
<b>1 Introduction</b>	<b>21</b>
1.1 Bulk amorphous metals . . . . .	21
1.2 Bulk amorphous metal applications . . . . .	27
1.2.1 Mechanical applications for bulk amorphous metals .	28
1.2.2 Coating applications for bulk amorphous metals . .	31
1.2.3 3D MEMS/NEMS applications for bulk amorphous metals . . . . .	34
1.2.4 Challenges and recent advances . . . . .	38
<b>2 Methods frequently used to study the properties of bulk amorphous metals</b>	<b>43</b>
2.1 X-ray diffraction of amorphous metals . . . . .	43
2.2 Calorimetry of amorphous metals . . . . .	44
2.3 Mechanical testing . . . . .	46
2.3.1 Compression test . . . . .	47
2.3.2 Instrumented indentation . . . . .	50
<b>3 Production facilities for alloying a glass-forming alloy and casting it without crystallization</b>	<b>53</b>

3.1	High-purity induction melting and casting . . . . .	54
3.2	High-purity induction levitation melting and casting . . . . .	57
3.3	High-purity arc melting and low pressure induction die casting . . . . .	58
3.3.1	High pressure die casting . . . . .	64
3.4	High-purity arc melting and tilt casting with suction . . . . .	65
3.4.1	An example of BMG ingot melting with tilt and suction casting . . . . .	67
3.4.2	Tilt casting more complex annular shapes . . . . .	76
3.4.3	Tilt casting with cap casting . . . . .	77
<b>4</b>	<b>Production facilities for thermoplastic forming of bulk amorphous metal</b>	<b>79</b>
4.1	Effect of friction between metallic glass and mold in thermoplastic forming of metallic glass . . . . .	80
4.2	Effect of reheating rate on thermoplastic forming of metallic glass . . . . .	83
4.3	An example of thermoplastic flow facility construction and its use for tensile viscous flow forming . . . . .	85
4.3.1	Finite element modeling of induction heating . . . . .	86
<b>5</b>	<b>Production facilities for bulk amorphous coating with physical vapor deposition</b>	<b>91</b>
5.1	Magnetron sputtering target manufacturing . . . . .	91
5.2	Bulk amorphous metal coating of polymers with magnetron sputtering . . . . .	93
5.2.1	Methods to improve the metal-polymer adhesion . . . . .	98
<b>6</b>	<b>Discussion</b>	<b>101</b>
<b>7</b>	<b>Conclusions</b>	<b>105</b>
<b>Bibliography</b>		<b>109</b>
<b>Publications</b>		<b>115</b>

# **Research hypothesis and original features**

For this thesis, the merits of different facilities for producing bulk metallic glass were evaluated first anecdotally using literature and interviews, and then in practice by designing, building and finally using different facilities to make various metallic glass specimens with composition  $Zr_{55}Cu_{30}Al_{10}Ni_5$  (at.%). The research hypothesis of this thesis is that there remain significant opportunities for improvement of processing facilities used in bulk metallic glass research. Bulk metallic glasses are relatively new materials. A variety of processing routes have shown that many of the properties of these materials are indeed remarkable, and could be practically useful. However, there has not been a pressing need to optimize the processing routes. In a research laboratory context, it is more interesting to use existing facilities to study something new than to make marginal improvements to those facilities. So when the need to build new facilities for bulk metallic glass processing in our lab was identified, this presented a rare opportunity to re-imagine those facilities.

This thesis, then, presents an original overview of some of the issues in producing metallic glass specimens, and features several original designs for metallic glass processing facilities. These facilities now exist and were tested, which is a tangible result of unique circumstances. The visit to Prof. Inoue's lab at Tohoku University, and the discussions there with Prof. Yokoyama about their production facilities, informed the re-imagination exercise. The machine shop and knowledge base available in-house at the Department of Engineering Design and Production allowed to reduce it to practice. The initial results obtained with  $Zr_{55}Cu_{30}Al_{10}Ni_5$  specimens to test it, confirmed that it was worthwhile. Three categories of metallic glass processing facilities are considered in this thesis: alloying and casting facilities, thermoplastic forming facilities and physical vapor deposition facilities.

An outstanding original feature of the alloying and casting facility developed in this thesis is that high-purity arc melting and tilt casting can be done in a single furnace, without compromising on process purity of the arc melting or on the capabilities of the tilt casting. Provisions were also made for including cap casting into the construction. That innovation is the subject of a patent application [1], which was approved during the preparation of this thesis. It is not presented in this thesis. The combined tilt-casting arc-melting facility allows the entire process from starting materials to the cast specimen to proceed without exposing the sample to atmosphere. Furthermore, it uses single arc melting power source instead of three, a single high vacuum pumping and measuring system instead of two and occupies a single machine space instead of two. Some mechanical engineering was required to tilt the entire vacuum chamber, but the result is a uniquely compact and quite practical facility for making the highest quality bulk metallic glass specimens.

The original feature of the thermoplastic forming facility is the way induction heating is used to locally soften that part of the material that is to be deformed. Superplastic forming of bulk metallic glass had been reported previously, but the method was impractical due to the need to machine a specimen where the part of the material that is to be deformed already has a smaller cross section than the part that is gripped to apply the tensile load. In contrast, the thermoplastic forming facility developed in this thesis is designed to use specimens that are easy to make. Crucially, non-uniform heating of the specimen is exploited to keep the ends that are gripped relatively cool, so that the material's flow stress is higher at the grips. Thus, the flow stress is not exceeded where the applied stress is highest, but rather where the material is most softened. Furthermore, this facility was upgraded to create an asymmetric induction heating field in which an asymmetric specimen can be deformed in a steady state. No machining at all is required for those specimens, as the wires through which force is applied to the specimen are integrated in the specimen already during the casting process. In principle, as long as the preform does not run out and does not crystallize, the steady state deformation process can produce wires of arbitrary length.

The original feature of the physical vapor deposition study of  $Zr_{55}Cu_{30}Al_{10-Ni_5}$  on heat sensitive technologically interesting polymer substrates is that some of the methods tried are already used in mass production with other alloys. Being able to achieve good adhesion to these polymers allows

for a fast transition to mass production, when a suitable application need for amorphous metal coatings on polymer substrates emerges.



# List of Publications

This thesis consists of an overview and of the following publications which are referred to in the text by their Roman numerals.

- I** Erno Soinila, Parmanand Sharma, Markku Heino, Kaj Pischedow, Akihisu Inoue, Hannu Hänninen. Bulk metallic glass coating of polymer substrates. *Journal of Physics: Conference Series*, 144, 012051, 1–4, doi:10.1088/1742-6596/144/1/012051, 2009.
- II** E. Soinila, K. Antin, S. Bossuyt, H. Hänninen. Bulk metallic glass tube casting. *Journal of Alloys and Compounds*, 509S, 210–213, doi:10.1016/j.jallcom.2010.12.145, 2010.
- III** Sven Bossuyt, Erno Soinila, Henri Penttinen, Ville Pulkki, Hannu Hänninen. Thermoplastic wire drawing from bulk metallic glass. *2010 MRS Fall Meeting*, 1–6, MRSF10-1300-U08-04.R1, 2010.
- IV** E. Soinila, T. Pihlajamäki, S. Bossuyt, H. Hänninen. A combined arc-melting and tilt-casting furnace for the manufacture of high-purity bulk metallic glass materials. *Review of Scientific Instruments*, 82, 1–4, doi:10.1063/1.3606444, 2011.
- V** E. Soinila, S. Bossuyt, H. Hänninen. Steady-state tensile viscous flow forming of bulk metallic glass. *Journal of Alloys and Compounds*, Available online (doi:10.1016/j.jallcom.2012.01.153) from 7th of February 2012.



# Author's Contribution

## **Publication I: “Bulk metallic glass coating of polymer substrates”**

The author did the industrial purity magnetron sputtering experiments, castings and compression tests. Parmanand Sharma did the Tohoku experiments with the help of the author. The author did the energy dispersive X-ray spectroscopy (SEM-EDS) measurements, X-ray diffraction (XRD), differential scanning calorimetry (DSC) and compression strength tests. The author did the transmission electron microscopy (TEM) imaging and selected area diffraction (TEM-SAD) tests with the instruction of Janne Ruokolainen. The final text was written as a collaborative effort with co-authors.

## **Publication II: “Bulk metallic glass tube casting”**

The author found the idea for doing metallic glass tube casting when discussing with Kim Antin. The author did the X-ray diffraction, the differential scanning calorimetry and the instrumented indentation tests. The custom mold was designed with Kim Antin. Author did most of the casting experiments with the help of Kim Antin and Sven Bossuyt. The final text was written as a collaborative effort with co-authors.

## **Publication III: “Thermoplastic wire drawing from bulk metallic glass”**

The author found the idea for doing metallic glass musical string when discussing with Ville Pulkki and Henri Penttinen. The author did the finite element simulations with the instruction of Sven Bossuyt. The au-

author did the castings, X-ray diffraction, differential scanning calorimetry and instrumented indentation tests. The author and Sven Bossuyt did the wire drawing tests. The final text was written as a collaborative effort with co-authors.

**Publication IV: “A combined arc-melting and tilt-casting furnace for the manufacture of high-purity bulk metallic glass materials”**

The author had the central idea for the device, i.e., the use of tilting of the chamber after detailed discussions with Yoshiko Yokoyama about the merits of various previously tested custom-built casting facilities. The author designed the detailed construction together with Tuomas Pihlajamäki. The impact tests were done with Sven Bossuyt. The author did the X-ray diffraction, the differential scanning calorimetry and most of the casting tests. The final text was written as a collaborative effort with co-authors.

**Publication V: “Steady-state tensile viscous flow forming of bulk metallic glass”**

The author did the finite element simulations with the instructions of Sven Bossuyt. The author did the castings, X-ray diffraction, differential scanning calorimetry and instrumented indentation tests. The author and Sven Bossuyt did the wire drawing tests. The author did the castings, with the help of Sven Bossuyt. Author and Sven Bossuyt performed the wire drawing experiments. The author did the X-ray diffraction and differential scanning calorimetry tests. The final text was written as a collaborative effort with co-authors.

# List of abbreviations and symbols

Abbreviation or symbol	Description
BMG	Bulk metallic glass
XRD	X-ray diffraction
DSC	Differential scanning calorimetry
SEM	Scanning electron microscopy
EDS	Energy dispersive X-ray spectroscopy
TEM	Transmission electron microscopy
SAD	Selected area diffraction
BCE	Before common era
DLC	Diamond-like carbon
MEMS	Micro electro mechanical systems
NEMS	Nano electro mechanical systems
$d$	Fracture process zone size
$T$	Temperature
$\tau$	Shear stress
$\dot{\gamma}$	Shear strain rate
$\mu$	Shear modulus
$T_\ell$	Liquidus temperature
$T_G$	Glass transition temperature
$\sigma_{yield}$	Stress
$K_C$	Fracture toughness
FIB	Focused ion beam
PVD	Physical vapor deposition
AFM	Atomic force microscopy
$G_{1C}$	Fracture toughness
$n$	Order of diffraction

<b>Abbreviation or symbol</b>	<b>Description</b>
$d'$	Lattice constant
$\lambda$	Wave length
$\theta$	Angle of the incoming beam
$H_c$	Crystallization heat of the composite
$H_a$	Crystallization heat of the fully amorphous material
$\sigma_y$	Elastic limit
$\epsilon$	Strain
$I$	Indentation modulus
$\nu$	Poisson ratio
$E$	Young's modulus
$P_{\max}$	Peak indentation load
$A$	Projected indenter contact area
$H$	Hardness
TIG	Tungsten inert gas
$F$	Figure of merit
$\eta$	Viscosity
$T_X$	Crystallization temperature
FEM	Finite element modelling
PC	Polycarbonate
PMMA	Polymethyl methacrylate
PA	Polyamide
PAA	Polyarylamide
GF	Glass fiber
PPS	Polyphenylene sulfide
UHV	Ultra high vacuum
PBT	Polybutylene terephthalate

# 1. Introduction

## 1.1 Bulk amorphous metals

Man-made glass objects date back to 2000 BCE or even to 3500 BCE, depending on the source [2, 3], for recovered and dated archeological findings of oxide glass objects. When compared to the long history of oxide glasses and even the more recent technologically important amorphous semiconductors and organic polymers, metallic glasses are a relatively new discovery, yet to enter the wider public awareness. Unlike in the often transparent electrically insulating polymer and oxide glasses, the interatomic bonding in metallic glasses is of the metallic type. There may be some directionality of the interatomic potentials, reminiscent of covalent bonding, and significant short-range order in the nearest neighbor shells, but there is no long-range orientational order in the atomic structure. The density of free electrons is typical of that of crystalline metals, with scattering lengths on the order of the interatomic distance, resulting in metallic luster and electrical conductivity comparable to stainless steel. Also, unlike oxide glasses, metallic glasses can show plastic deformation in compression. In polymers, the use of glassy polymers is often restricted by their low modulus compared to crystallized polymers, as a result, glassy polymers are often thought less strong than crystalline ones. On the contrary in metals, glassy metals are found to be of higher strength than crystalline ones because they possess much higher yield strain and not much lower stiffness than crystalline metals. All these glasses, however, solidify into precise shapes undisturbed by uneven crystalline growth shrinkage, and can be used in net-shape manufacturing directly from the molten state. Since metallic glasses are much stronger than polymer glasses and can be made much less brittle than silicate glasses, they provide new possibilities in engineering and stir up sci-

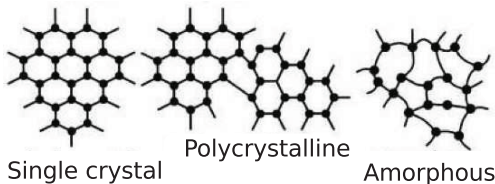


**Figure 1.1.** The difference between monocrystalline, polycrystalline, and amorphous structure [7].

tific curiosity.

The distinctive feature of amorphous metals is the lack of long-range order in the microstructure. This means that the positions of the neighboring atoms can not be predicted in the way that is possible within a crystalline structure, as schematically illustrated in figure 1.1. Figure 1.4 illustrates the necessary cooling rates for glass formation in pure metals, marginal glass forming metal alloys and in bulk metallic glasses. Bulk metallic glasses are a new class of metal alloys that can be cast with amorphous microstructure to a copper mold with diameters larger than 1 mm, often exceeding several centimeters as shown in figure 1.3. This stability is achieved with suitable alloying (Inoue empirical alloying rules) that produces short-range order without crystallinity as schematically illustrated in figure 1.2. BMG alloys (Bulk Metallic Glass, where the glass refers to exceptionally high thermal stability when compared to traditional amorphous metallic alloys) offer many advantageous properties directly from the mold without thermomechanical treatment when compared with crystallized metals. These properties include: high strength, as shown in figure 1.5, good wear resistance, good resistance against corrosion and staining due to the lack of grain boundaries, accurate surface finish with wanted surface roughness, isotropic properties that can be scaled to nanometer range without grain size related problems, exceptionally high elastic deformation, possibility to have plastic deformation before failure, superplastic deformation when heated above glass transition temperature, and high tailorability of alloy properties for specific applications and functional properties such as soft and hard magnetic properties. [4–6]

The difficulty in producing large glassy metal products has traditionally been the need to achieve a very high quenching rate. This is no longer the case. Several alloy groups have sufficient stability (meta-stability) to enable casting diameters of more than 10 mm thick in copper-mold

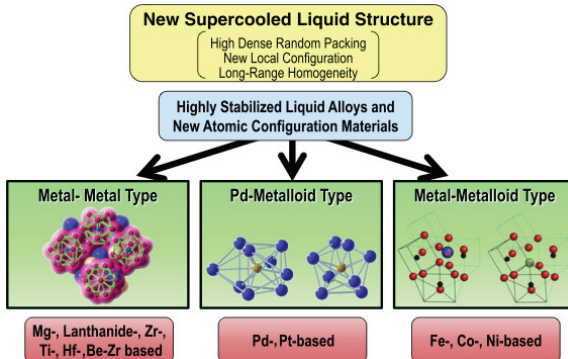


**Figure 1.2.** Amorphous state stabilizing short-range structures detected in BMG alloys [8].

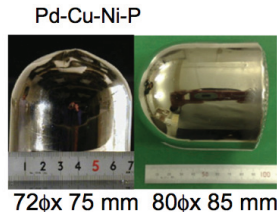


**Figure 1.3.** Fully amorphous Pd-Cu-Ni-P BMG alloy [8].

casting, as shown in figure 1.3. The best alloys can be quench cast in thickness of about 100 mm [9]. The current problem obstructing large scale BMG applications is the necessity of using high-purity materials and high-purity manufacturing processes, which can make the end product more expensive. Nevertheless, there are some promising exceptions to this rule for some specific alloys. Also, and perhaps even more importantly, compared to smaller parts, larger sized objects exhibit more quasi-brittle behavior. When the smallest part dimension is smaller relative to the fracture process zone size,  $d$ , more ductile material behavior is expected. In effect, when the smallest part dimension size is kept below the fracture process zone size ( $d < 1 \text{ mm}$ ), the detrimental effect of shear banding on the macroscopical ductility is avoided [10]. Thus, to accommodate the size limitations due to mechanical property and cost considerations, the most promising application areas for metallic glasses are those which require complex shapes, little material, and exceptional mechanical integrity. Some examples of such applications are: small high-strength parts for the electronics industry, coatings to create hybrid materials (such as a BMG coating on polymer substrate for visual and wear-resistance applications) and use of very high surface quality from casting for functional and visual applications. To evaluate the added value of

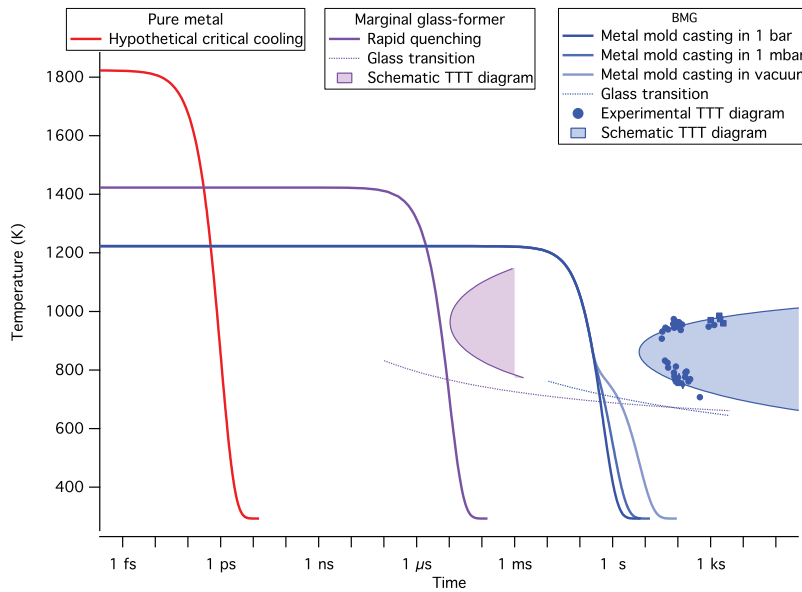


**Figure 1.4.** A schematic TTT diagram for illustrating the differences between: a pure metal, a marginal glass former, and a bulk metallic glass. The crystalline phases, that need to be avoided for glass formation, and curves for  $T_G$  have been illustrated for the marginal glass-former and the bulk metallic glass. Since pure metals crystallize on experimental liquid cooling rates, no crystallization phase or  $T_G$  is shown. For bulk metallic glasses, the influence of casting atmosphere for low pressure metal mold die casting cooling rates is also illustrated.

amorphous metals in these solutions, the material properties obtained in research studies need to be evaluated and compared with alternative technologies. This information is then used to refine the plans for application-oriented BMG research, focusing on issues that are important for the use cases that are most likely to become viable practical applications.

Depending on the temperature, stress and strain-rate, different deformation behavior is expected for metallic glasses [2, 6]. The strength values presented in figure 1.5 were obtained at room temperature. When the test temperature is raised, or very slow deformation speeds are used, the deformation becomes viscoplastic rather than elastoplastic. The deformation behavior of metallic glasses can be schematically illustrated over a range of temperatures ( $T$ ) and shear stresses ( $\tau$ ) with a deformation map, such as the one shown in figure 1.6 [11]. The schematically illustrated lines represent temperature dependence at constant shear strain rate ( $\dot{\gamma}$ ). The shear stresses ( $\tau$ ) have been divided by shear modulus ( $\mu$ ) and plotted logarithmically, whereas the temperatures ( $T$ ) have been scaled to the liquidus temperature ( $T_\ell$ ) resulting in a universal normalized deformation

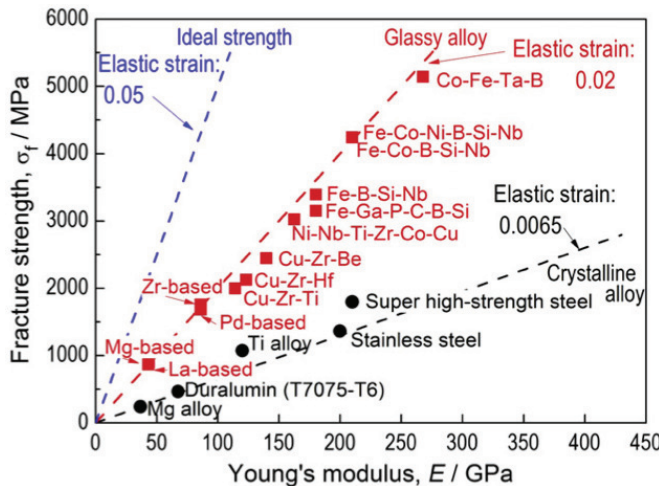


**Figure 1.5.** Strength to Young's modulus comparison for a selection of BMG alloys, also illustrated for comparison are ideal strength and crystalline alloy values [8].

map. At temperatures below ( $T_G$ ) metallic glass behaves like a solid, that will experience homogeneous flow (creep) with low stresses and will undergo inhomogeneous flow with high stresses. In the vicinity of  $T_G$  the deformation behavior exhibits relaxation phenomena and above  $T_G$  the metallic glass becomes purely viscous, and undergoes large deformations with little applied force. Recently there has been some debate as to the conditions under which metallic glasses exhibit inhomogeneous flow, because some indentation experiments showed the disappearance of flow serrations both at high and at low strain rates [2, 12]. Further research with non-indentation methods has started to elucidate the thermodynamics of serrated flow [13], even if the precise relationship with shear band initiation, propagation and arrest is not yet clear.

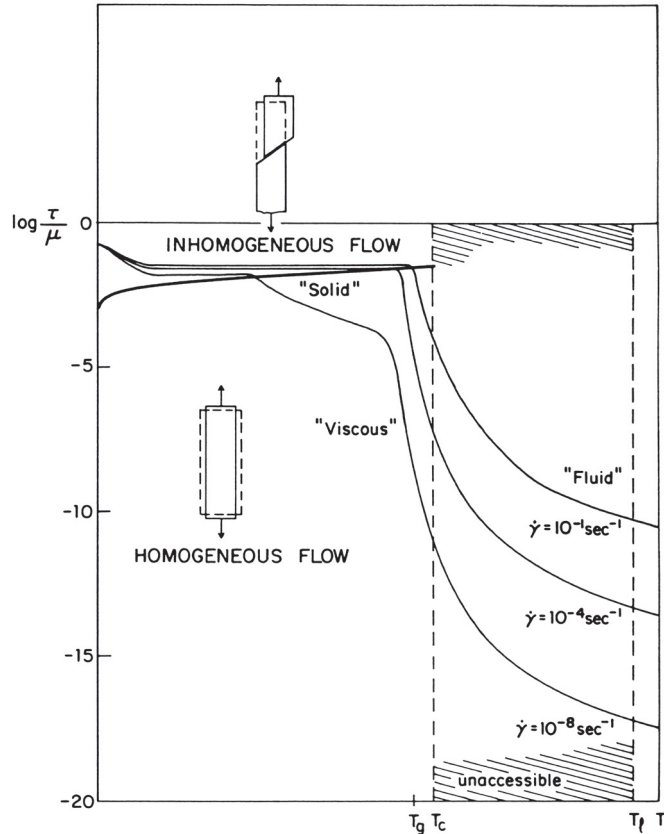


**Figure 1.6.** Metallic glass deformation map, with the constant shear strain rates ( $\dot{\gamma}$ ) drawn in as lines. Depending on the horizontal axis temperature ( $T$ ) on the constant shear strain rates ( $\dot{\gamma}$ ), different vertical axis shear stresses ( $\tau$ ) are needed to maintain a steady state shear strain rate ( $\dot{\gamma}$ ) deformation. The shear stresses ( $\tau$ ) have been divided by shear modulus ( $\mu$ ), and the temperatures ( $T$ ) have been divided by the liquidus temperature ( $T_l$ ) to normalize the values. The crystallization temperature ( $T_c$ ) and the glass transformation temperature ( $T_g$ ) are marked on the temperature scale [11].

## 1.2 Bulk amorphous metal applications

One of the most promising advantages of BMGs for practical applications is that they can be conveniently formed into complex shapes, with excellent surface finish and precise tolerances. Without cold working or heat treatment, the very impressive mechanical properties shown in figure 1.5 are achieved: purely elastic deformation up to a yield strain of typically 2%, resulting in tensile strength from 1500 MPa to 5500 MPa, with Young's modulus from 70 GPa to 275 GPa, depending on alloy composition. As discussed in section 1.1, at temperatures below  $T_G$ , metallic glass behaves like a solid that will experience inhomogeneous flow with high stress. In the inhomogeneous flow region, a monolithic metallic glass specimen typically deforms by shearing on a one major shear band, that extends across the width of the specimen, as is schematically illustrated on the top of figure 1.6 for tensile stress. This shear banding problem limits the macroscopic ductility of most of the known monolithic metallic glass compositions. In the more constrained modes of loading, like bending or compression, the amount of forming shear bands increases as the characteristic metallic glass specimen dimension decreases [14]. This leads to macroscopically more plastic behavior in smaller specimens, such as the bent beam in figure 1.7, than is seen in their larger counterparts. The relationship between shear band density and characteristic metallic glass specimen dimension is illustrated in figure 1.8.

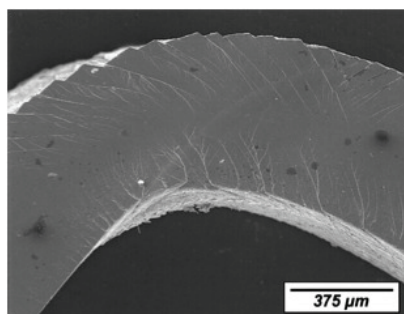


**Figure 1.7.** Electron micrograph of bent metallic glass beam, showing multiple shear bands. An example of increased macroscopic ductility from decreased characteristic dimension, i.e. thickness of the bent ribbon [14].

For a more precise rule on when macroscopically quasi-brittle behavior is unlikely, the concept of fracture process zone size  $d$  discussed in chapter 1.1 is revisited in more detail.

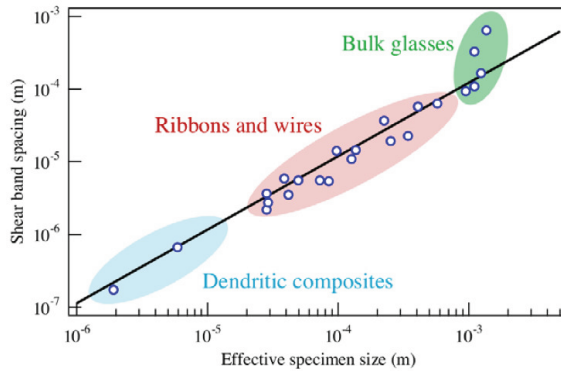


**Figure 1.8.** Average shear band spacing as a function of characteristic specimen dimensions for a variety of metallic glasses (and some derivate composites) deformed in constrained modes of loading [6].

$$d = \frac{K_C^2}{\pi \sigma_{yield}^2}, \quad (1.1)$$

where  $K_C$  is the fracture toughness,  $\sigma_{yield}$  stress. When the  $K_C$  is known for a metallic glass alloy, then the process zone size can be known and used as an application design guideline. Besides the mechanical properties, also the economical considerations need to be taken into account for evaluating potential bulk metallic glass applications. The potential applications for BMG alloys can be estimated by comparing the specific price 33\$/kg [15] with material costs in figure 1.9, which confirms the commonly held view that currently the most potential BMG applications can be found from small niche parts, where the required material amounts are small and some of the BMG special properties are needed. In the following subchapters of this Introduction, several application examples are presented. Most of these application examples presented in chapters 1.2.1, 1.2.2, 1.2.3 and 1.2.4 keep the smallest part dimension below the fracture process zone size ( $d < 1$  mm) and also use small amounts of BMG material.

### 1.2.1 Mechanical applications for bulk amorphous metals

Because all the shrinkage from the molten state of a BMG alloy to the room temperature is due to thermal expansion and not to crystallization, the shrinkage is very evenly distributed. Also, if a pressure is applied on the cooling glass before  $T_G$  is reached, additional net-shape-forming precision can be achieved from the viscous flow forming of the cooling specimen against the mold surface. Examples of BMG net forming precision

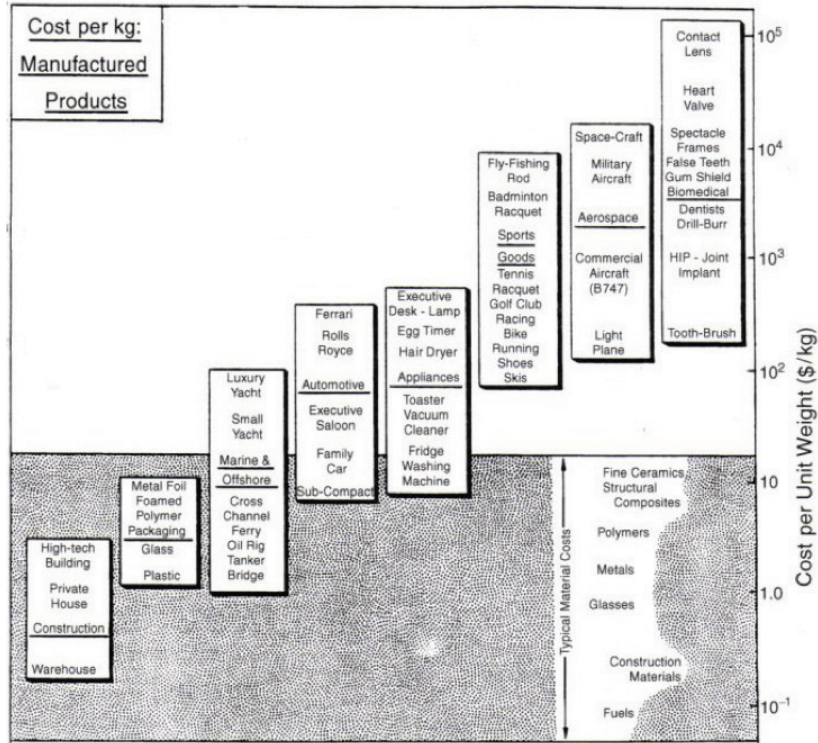


**Figure 1.9.** Potential BMG applications, based on 33 USD/kg materials cost [16]. The 33 USD/kg materials cost is illustrated as a drawn horizontal line.

are shown in figures 1.10 and 1.11. The motor in figure 1.10 is an example of the BMG alloys' potential for miniaturization that is not feasible with polycrystalline metals, where the uneven properties in near grain size components drastically limit the achievable mechanical properties. The high performance but still difficult to manufacture motor is planned for medical instruments, such as endoscopes, where small size components with high performance make large difference in performance. The competing crystalline gear size is limited to diameter 2.4 mm [4, 8].

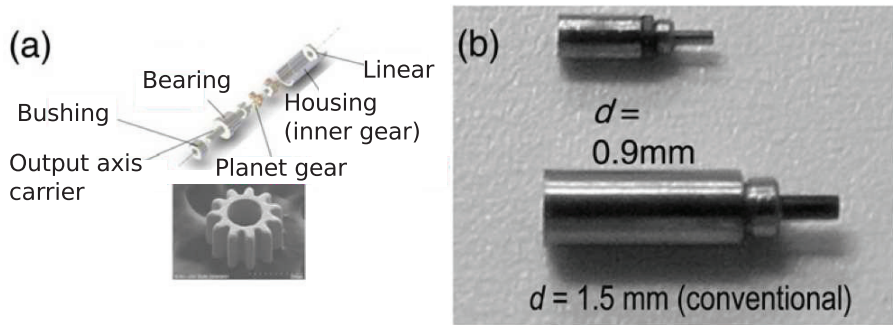


**Figure 1.10.** The world's smallest planetary gear is made of BMG alloy: a) schematically illustrated planetary gear structure, b) constructed 0.9 mm motor–planetary gear combination shown here together with the previous record holder 1.5 mm BMG geared motor [8].

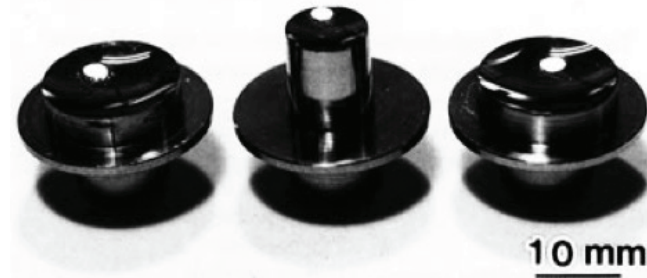


**Figure 1.11.** High-accuracy Zr-Al-Ni-Cu BMG-mirrors produced by superplastic forming between glass transition temperature ( $T_G$ ) and crystallization temperature ( $T_X$ ) [17].

### 1.2.2 Coating applications for bulk amorphous metals

The general topic of coating of crystalline substrates with amorphous, or partially amorphous coating with various means for improving wear resistance has a very large range of different techniques well outside the scope of this work. Amorphous coatings, and metallic glasses have been sought for wear resistance because of their large hardness, but the differences of plastic flow between crystalline materials and amorphous materials significantly complicate the efforts to extract any simple answers. Hardness can predict wear resistance within a given class of amorphous alloy. However, the relative wear resistances of different alloy classes can be affected not only by hardness but also by oxidative processes and changes of wear regime. Studies done indicate that amorphous alloys can have very good resistance to sliding and abrasive wear [18].

Although, the primary motivation for the coating use of BMG alloys is usually to improve corrosion resistance and the wear properties of the substrate [18, 19], recent results have shown that it is also possible to improve fatigue endurance and improve surface quality by BMG coating of crystalline metals as shown in figure 1.12 [20]. The results in figures 1.12 and 1.13 show how a very thin magnetron sputtered BMG coating can be used to improve fatigue endurance of crystalline metals. Part of the improvement is thought to come from the reduction of surface roughness, as shown in figure 1.13. The large elastic deformation capability of the BMG coating is thought to resist the fatigue-crack formation as shown in figure 1.14. The coating elongates elastically nearly to 2%, while at the same time showing good adhesion to the substrate and reducing the surface roughness as shown in figures 1.13 and 1.14.

Magnetron sputtering is a low temperature, low yield coating method, which enables the use of low process temperatures and very high surface quality finishes [21]. Compared to other coating methods, magnetron sputtering can be performed at room temperature when sufficient adhesion can be ensured. In amorphous microstructure there are practically no natural limits to achievable surface quality such as grains and grain boundaries. In practice the best achieved machining accuracy with current equipment is about 11 nm with Focused Ion Beam (FIB) as shown in figure 1.15 [22]. These properties can be used to produce very accurate surface patterns with optical or hydrophobic properties. One example that is considered is the production of the micro-lens arrays [23] used

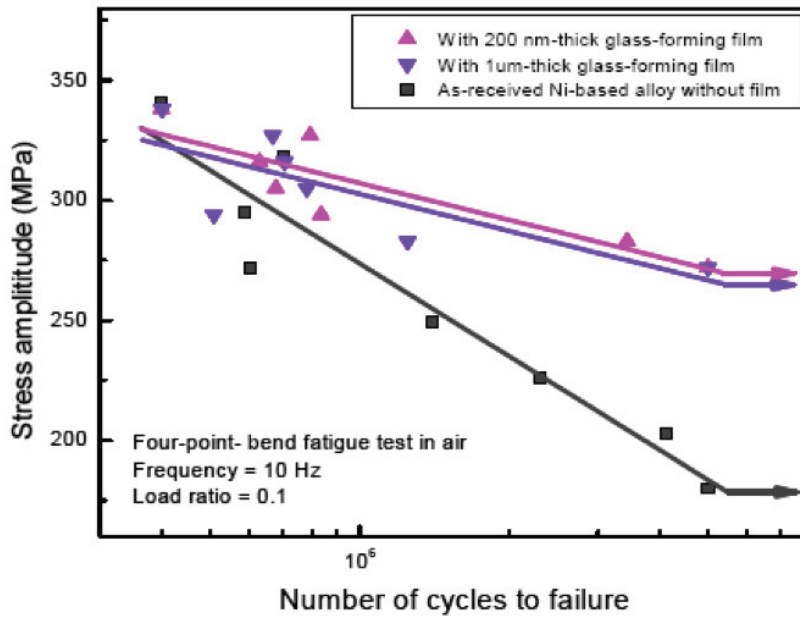


**Figure 1.12.** Increasing the fatigue endurance of Ni-based crystalline alloy with 200 nm thick magnetron sputtered BMG coating [20].

in 3D image recording digital cameras [24]. These can be produced by hot embossing them accurately with a BMG mold on a PMMA polymer substrate, which is later coated to be reflective by magnetron sputtering [23]. It is known that BMG alloys can be used to produce very accurate optical components, like the high-accuracy mirror in figure 1.11 [17].

Little has been published about the visual properties such as colors that can be produced with BMG alloys. Polymers can also be coated with BMG alloys when sufficient adhesion is achieved (thesis Paper I). Furthermore, BMG alloys can be coated with diamond-like carbon (DLC) with enough adhesion to withstand wear tests [19]. Thus, it is possible to manufacture with very high resolution surface patterns into BMG alloy for optical applications and optionally protect these from wear with a DLC coating. In addition to enhancing the surface of polymer parts, it is also possible to stiffen small polymer parts with BMG coating enabling the use of thinner parts. This also requires sufficient adhesion between the substrate and the coating, which can be best achieved with ion-bombardment during the deposition. The practical thicknesses possible with physical vapor deposition (PVD) methods such as magnetron sputtering are limited by the heating of the substrate and the amount of time that the deposition takes. In practice this means the method is practical only for (MEMS/NEMS) parts or requires good substrate cooling.

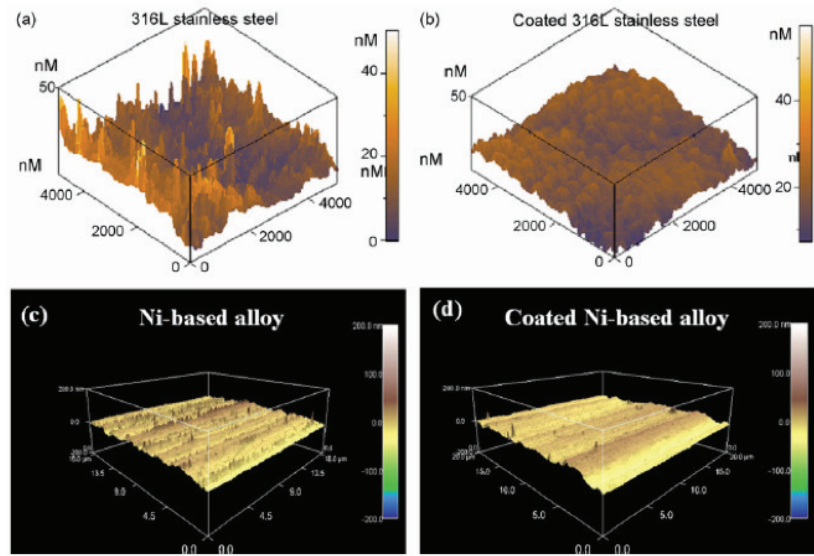


**Figure 1.13.** Reducing the surface roughness with a BMG alloy coating. a) Stainless steel surface quality before coating. b) Stainless steel surface quality after BMG coating. c) Ni-based crystalline alloy surface quality before coating. d) Ni-based crystalline alloy surface quality after BMG coating [21].

Shear bands and microstructures are of critical importance to understand the fatigue-crack initiation

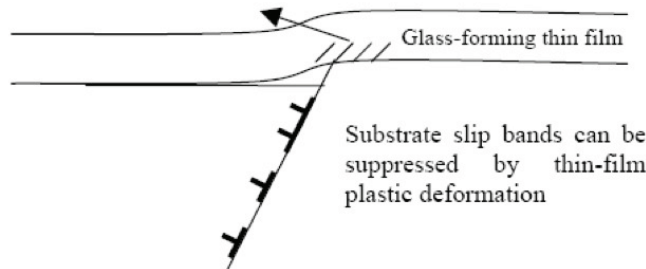


**Figure 1.14.** The hypothetical mechanism of crystalline metal fatigue endurance improvement, proposed by Liu et al., showing fatigue-crack initiation (typically due to dislocation pileups and surface offsets) suppressed by the unique elastic deformation of glass-forming films [20].

### 1.2.3 3D MEMS/NEMS applications for bulk amorphous metals

There is a lot of research aimed at nanotechnology research, i.e. the production of controlled structures under the 100 nm size limit. The properties of crystalline materials are severely affected when the feature size approaches the crystal size. The mechanisms that provide ductility (and uniformity of properties more generally) in polycrystalline materials stop working, and grain boundaries become a weak link in the structure, severely limiting the reliability of the part. Also the part performance varies too much from one produced part to the next depending on the crystal orientation and location of grain boundaries in crystalline metals. As was discussed in chapter 1.1, the distinctive feature of amorphous metals is the lack of long-range order in the microstructure, i.e. the isotropic properties can be scaled to nanometer range without the problems associated with miniaturizing polycrystalline materials. Since BMG-materials simply lack this problem they can be miniaturized from their maximum critical casting diameter all the way to tens of nanometers. As was discussed in chapter 1.2, the smaller size improves the ductility of BMG materials, because stress localization becomes less severe due to decreasing shear band spacing, as shown in figure 1.8 [14]. This makes BMG-materials attractive for joinable, high-strength, elastic, superplastically deformable and thermally stable complex shaped structures in the under 100 nm region as shown in figure 1.15. The alloy used in figure 1.15 has a 30 mm critical casting radius, which means that the same alloy can be used for components at least in the range from 17 nm to 30 mm [25].

In figures 1.16, 1.17 and 1.18 there is an example of the use of BMG alloy in a magnetron sputtered thin film for 3D-MEMS device manufacture. In the example the 3D shape can be achieved in two alternate methods:

1. By heating the spring first to between the glass transition temperature ( $T_G$ ) and crystallization temperature ( $T_X$ ) and then viscous flow deforming it by drawing it to the desired zero force length. In other words, the length of the spring when no force is acting on it is changed by deforming it in the supercooled liquid region.
2. By elastically deforming the spring to the desired zero force length and then heating it between  $T_G$ - and  $T_X$ -temperatures to relax elastic stresses leaving the spring in the elongated form after external stresses are removed.

The relatively large size of the actuator is thought to be a result of the

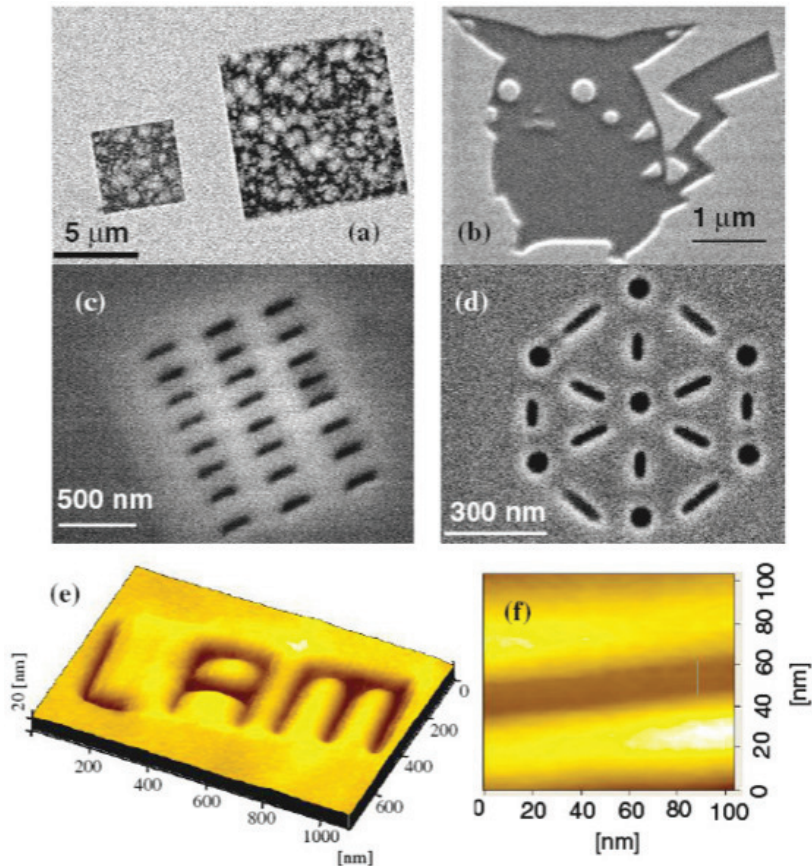
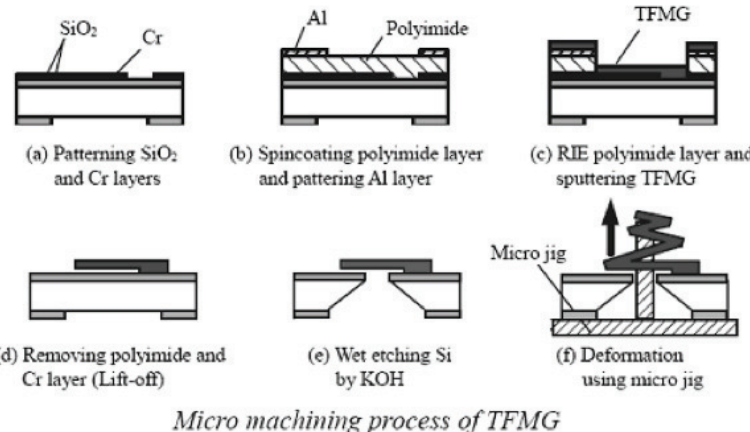


**Figure 1.15.** The benefit of stable amorphous structure in thin film focused ion beam (FIB) machining. a) Low microstructural stability, i.e., crystallization of the deposited platinum limits the achievable FIB machining accuracy in crystalline metals. The effect of crystallization in limiting the FIB machining accuracy of deposited platinum. b) BMG stability against crystallization allows very accurate FIB machining of the deposited metal ('Pikachoo') (SEM). c) FIB patterning test on BMG. d) Tohoku Institute for Materials Research (IMR) logo FIB machined on deposited BMG. e) FIB machined IMR subunit Laboratory of Advanced Materials (LAM) logo on BMG as seen with atomic force microscopy (AFM). f) Magnification of the LAM logo showing 17 nm line width [22].



*Micro machining process of TFMG*

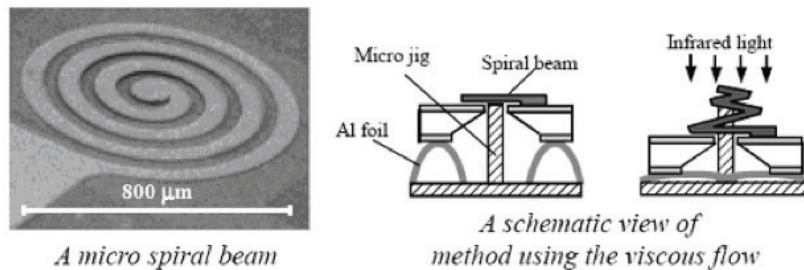


**Figure 1.16.** Manufacturing of a 3D-actuator by using the viscous flow formability of a BMG alloy. The finished actuator uses the high elastic limit of the BMG alloy to ensure durability in use [26].

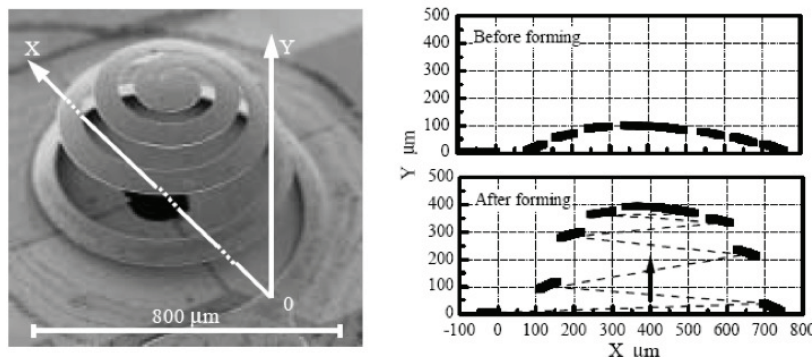


**Figure 1.17.** The elastic deformation and subsequent heat treatment plastically viscous flow deforms the spring from a plane to the 3D elongated form [26].

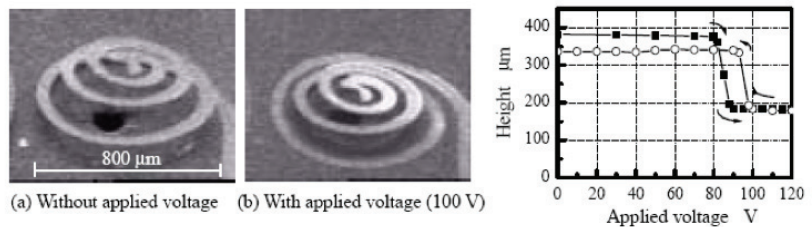


**Figure 1.18.** The results of an actuator test run [26].

available equipment and the amount of resources. There is a lot of resources directed at the study of the macroscopic properties of BMG alloys. The presented actuator case is a well suited method for directly integrating BMGs to the microchip. For stand-alone MEMS part production, the hot-scraping technique, schematically illustrated in figure 1.19 is seen as particularly efficient method [27].

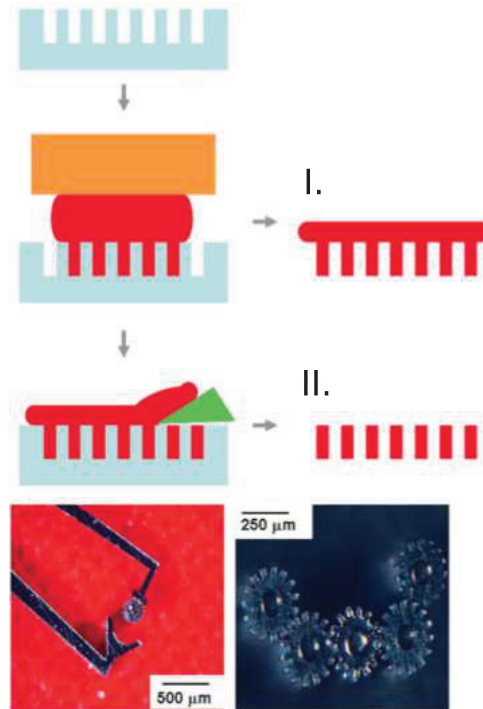


**Figure 1.19.** A schematic illustration of the hot-scraping method for producing stand-alone MEMS structures, and example hot-scraped metallic glass gears [27].

### 1.2.4 Challenges and recent advances

The work for developing bulk metallic glasses into a more commonly economically competitive material can, and needs to happen on multiple fronts. The ongoing work is presented below as an itemized list of challenges faced by the bulk metallic glass use, and the *state-of-the-art* response at the time of writing this thesis.

- Problem: The lack of ductility due to high strain localization into dominant shear bands in most BMG alloys.
  - At least three monolithic BMG compositions have been found where multiple shear bands lead to significant ductility and excellent toughness: Pd<sub>79</sub>Ag<sub>3.5</sub>P<sub>6</sub>Si<sub>9.5</sub>Ge<sub>2</sub> [28], Pt<sub>57.5</sub>Cu<sub>14.7</sub>Ni<sub>5.3</sub>P<sub>22.5</sub> [29], and Pd<sub>81</sub>Si<sub>19</sub> [30]. Some monolithic metallic glasses also show tensile ductility at room temperature [28, 31, 32].
  - Promising mechanical properties can be achieved with phase separated glass-glass composites [33].
  - Extrinsic toughening mechanisms in glass-crystal composites, formed *in situ* by partial crystallisation of bulk metallic glasses [34–36], can give rise to ductility and apparent strain hardening [37, 38]. Ultra-high fracture toughness can be achieved with BMG composite alloys ( $G_{1C} \sim 1000 \text{ kJ m}^{-2}$ ) [39].
  - Using one small dimension to counter the small fracture process zone size ( $d$ ) in BMG alloys. Thin BMG specimens can be bent repeatedly 180° without fracture [14]. The same principle is used in BMG foams [40].

- Problem: Manufacturing defects decrease fatigue strength.
  - Tilt casting has been shown to produce exceptionally good fatigue strengths at least for Zr-based alloys. Also the use of water-cooled metal crucibles in tilt casting avoids melt contamination [41, 42].
  - Clamp casting has shown some promising mechanical properties [43].
  - Casting with water quenching has shown good fatigue strength potential, because the molten alloy has a lot of time to properly fill the mold, thus avoiding casting defects.
  
  
  
  
  
  
- Problem: The dependence of the mechanical properties on the degree of relaxation of the amorphous structure.
  - The amount of structural relaxation varies in amorphous alloys, depending on their thermal history and composition. However, the relaxation behavior can be controlled to some degree with suitable alloying. For example, in Zr-based alloys the detrimental relaxation can be reduced with Pd-alloying, which increases the fatigue strength of the produced specimens [42].
  
  
  
  
  
  
- Problem: The required high quenching rates, and often high-purity requirement in most amorphous alloys severely limit manufacturing sizes or the number of possible alloys and increase the costs of manufacturing.
  - One of the smallest known critical cooling rates in amorphous alloys is  $0.01 \text{ K s}^{-1}$  in Pd-Ni-Cu-P alloys [4]. A 100 mm critical casting diameter has been achieved in nominal composition  $\text{Pd}_{40}\text{Cu}_{30}\text{Ni}_{10}\text{P}_{20}$  alloy [9].
  - In addition to the Pd-based alloys, Zr-based alloys also have critical casting diameters that exceed 30 mm. For example, the nominal composition alloy  $\text{Zr}_{55}\text{Cu}_{30}\text{Al}_{10}\text{Ni}_5$  has a critical casting diameter of 30 mm [25].

- The BMG alloys with critical casting diameter of more than 10 mm have been known the longest in the La-, Mg-, Zr- and Pd-alloy groups [44]. Recently (2004–2006) this limit has been exceeded also in Fe-, Co-, Ni- and Cu-alloy groups [45].
- Spark plasma sintering from atomized BMG alloy powder can be used to produce larger than critical casting diameter BMG specimens. The size is limited by the size of the sintering machine [46].
- Some BMG alloys can be cast in air atmosphere: select steel [47], Misch metal alloys [48] and noble metal alloys.
- Some Pt-based BMG alloys can be superplastically compressed into seamless specimens from amorphous precursor granules by applying pressure between  $T_G$  and  $T_X$  [49] temperatures ('thixoforming / thixo-casting')
- Many BMG alloys can be superplastically formed in air atmosphere [50].
- The low  $T_G$  alloys enable viscous flow forming at exceptionally low temperature of 90 °C. The forming has been demonstrated in hot water [51].
- Spark plasma sintering from atomized BMG alloy powder to produce BMG specimens with complex shapes, and with larger sizes than critical casting diameter would allow in casting, however this compromises on the achievable net-forming precision available in BMG casting [46].
- Magnetron sputtering with BMG alloy has been shown to work with at least three BMG alloys on silicon, crystalline metals and polymer substrates [22, 26, 52].
- The new inexpensive Fe- and Cu-based BMG alloys.
- Some Ni-, Fe-, and Pd-based BMG alloys can be de-oxidized with  $B_2O_3$ -fluxing and cast with water quenching [53] in temporary molds (quartz).

- Recycling the raw material, and reducing impurities, like oxygen with salt bath electrolysis can significantly lower the costs of BMG part production, even in Zr- and Ti- containing alloys. Also the starting materials used may be less expensive due to the lower purity requirements required with salt bath electrolysis [54].



## 2. Methods frequently used to study the properties of bulk amorphous metals

Presenting all the methods used to study bulk amorphous metals is outside the scope of this thesis. However, certain methods that are used in the thesis papers I–V, are routinely used in metallic glass research literature. It is the purpose of this chapter to provide a short primer to these use of the methods in metallic glass research.

### 2.1 X-ray diffraction of amorphous metals

The X-ray diffraction measurement is an often used method for studying sample microstructure. Bragg's law describes the connection between microstructure and the produced diffraction pattern. Bragg's law states that  $n\lambda = 2d' \sin(\theta)$ , where the positive integer  $n$  is the order of diffraction,  $d'$  is the lattice constant,  $\lambda$  is the wave length and the  $\theta$  is the angle of the incoming beam. These variables and the diffraction of a crystalline material are schematically illustrated in figure 2.1.

The long range periodic spacing of atoms in crystalline materials produces a set of X-ray diffraction peaks, which are usually easy to distinguish from the background noise. An example of X-ray diffraction peaks from silicon powder can be seen in figure 2.2. The lack of long-range order in amorphous materials produces no high intensity peaks in X-ray diffraction, only broad maxima can be seen in the diffraction pattern. The displayed maximum or two represent common atomic spacing in the amorphous material. An example of common oxide glass  $\text{SiO}_2$  X-ray diffraction pattern is shown in figure 2.3. Examples of nominal composition  $\text{Zr}_{55}\text{Cu}_{30}\text{Al}_{10}\text{Ni}_5$  (at.%) X-ray diffraction patterns from amorphous coating made with physical vapor deposition, copper mold cast metallic glass bar and a partially crystallized arc-melting ingot are shown in figure 2.4.

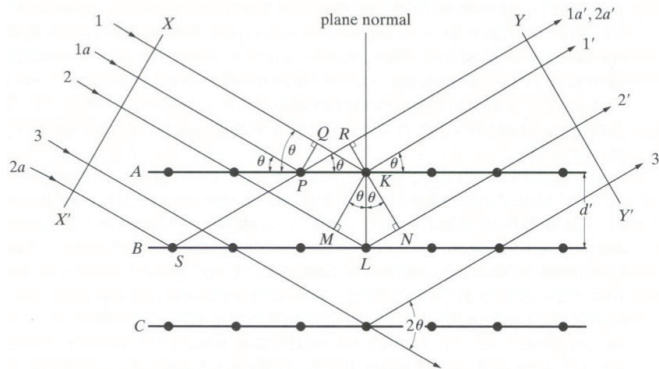


**Figure 2.1.** The variables for Bragg's law and a schematic illustration of the X-ray diffraction process [55].

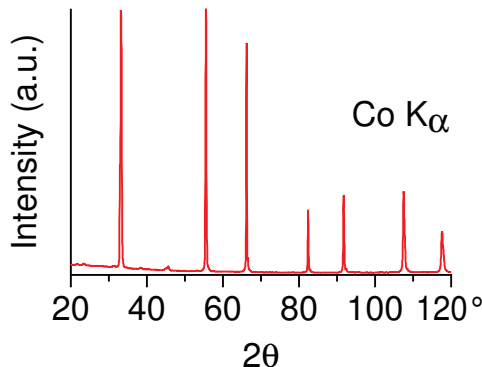


**Figure 2.2.** A typical crystalline X-ray diffraction pattern from silicon powder showing well-defined intensity peaks.

## 2.2 Calorimetry of amorphous metals

Calorimetric measurements provide information about the transition processes occurring in the microstructure of the material. In first order transitions, like melting and crystallization, the transition is marked by a usually easily observed heat of transformation. In second order transitions, such as the glass transition, the heat capacity of the alloy changes, without heat of transformation, although there may be a purely kinetic heat of relaxation effect which complicates the precise calorimetric determination of the transition temperature.

The glass transition is of particular interest in the study of bulk metallic glasses. During the undercooling of a glass-forming alloy melt, the viscosity of the melt increases rapidly. If the viscosity of the undercooled melt reaches a value of  $\sim 1 \times 10^{12}$  Pa s, giving a typical shear modulus of  $\sim 10 \times 10^9$  Pa, the timescale for mechanical relaxation of deviations

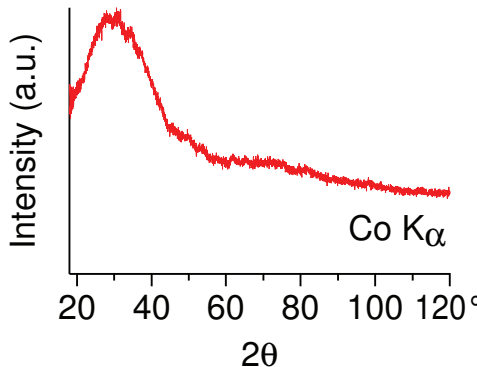


**Figure 2.3.** An example of amorphous X-ray diffraction pattern from silicate glass shows only low a broad intensity maxima with no crystalline peaks.

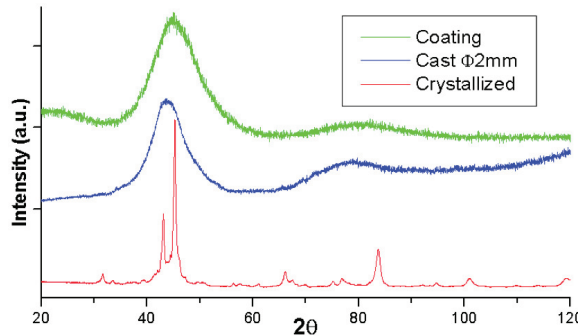


**Figure 2.4.** X-ray diffraction (Co K $\alpha$ ) patterns of deposited coating (top), cast bulk sample (middle) and arc-melted ingot (bottom) (thesis Paper I).

from the (metastable) thermodynamic equilibrium liquid configuration becomes comparable to the laboratory timescale, and the liquid freezes to a glass [56]. Thus, the glassy state is a non-ergodic state, with a liquid-like configuration that is not able, within the experimentally available time, to reach the equilibrated configuration at that temperature. The reason for the higher heat capacity of the liquid compared to the glass can be rationalized to result from the additional degrees of freedom associated with configurational changes that do happen above  $T_G$ , but not below it. The energy partitioned into these additional degrees of freedom, compounded with the rate at which these degrees of freedom become accessible with increasing temperature, manifests itself as an excess heat capacity over the isoconfigurational heat capacity measured below  $T_G$ .

The calorimetry of amorphous metals is used to determine the glass transition  $T_G$  and crystallization  $T_X$  temperatures of a glass-forming amorphous alloy. If the alloy was cooled fast enough, the  $T_G$  can be measured. The presence of  $T_G$  is a sign of the existence of an amorphous phase in

the sample. When a relatively stable composite structure of crystalline inclusions in an amorphous matrix is tested with differential scanning calorimetry (DSC) [57], the amount of crystallinity can be measured as the  $(H_c/H_a) * 100\%$ , where  $H_c$  and  $H_a$  are the crystallization heats of the composite and fully amorphous phases, respectively.

The  $T_G$ - and  $T_X$ -temperatures provide information about the microstructure and the thermal stability of an amorphous alloy. If crystallization happens at a higher temperature than glass transition, the alloy may be processed with thermoplastic forming between the two temperatures. The DSC measurement shown in figure 2.5 shows a temperature region suitable for thermoplastic forming (thesis Paper V).

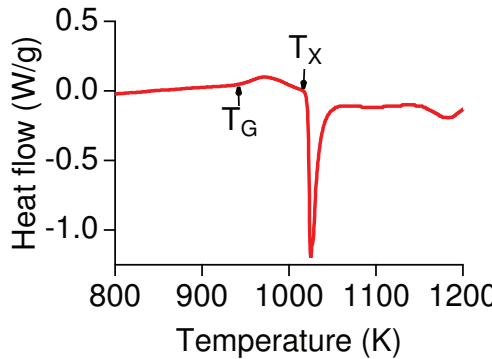


**Figure 2.5.** An example of glassy metal glass transition and crystallization in heating. Differential scanning calorimeter (DSC) measurement of the drawn wire with glass transition  $T_G$  and crystallization temperatures  $T_X$ , 668.6 K and 748.6 K, respectively (thesis Paper V).

## 2.3 Mechanical testing

As was discussed in chapters 1.1, 1.2.3 and 1.2.4, the macroscopic mechanical response of metallic glass depends on the applied strain rate, temperature, the size of the specimen and the mode of loading. Although some metallic glasses show tensile ductility at room temperature [28, 31, 32], more usually the localization of strain into narrow shear bands severely limits macroscopic tensile ductility in monolithic metallic glass specimens. However, in more constrained modes of loading, such as compression, bending and indentation, some plasticity can often be observed. Therefore, as often done in the metallic glass literature, thesis papers I–V use some of these more constrained loading mode methods to measure the mechanical response of  $Zr_{55}Cu_{30}Al_{10}Ni_5$  specimens prepared by different

methods.

### 2.3.1 Compression test

The compression tests of metallic glasses, reported in (thesis Paper I), were carried out with the setup shown in figure 2.6. The tungsten carbide blocks serve to protect the compression testing fixture, since the metallic glass specimens have high enough yield strength to damage the hardened steel compression test grips. The strain-gage is used to measure the deformation in the elastic region and sometimes also successfully in the plastic deformation region. Often the strain-gage loses adhesion to the sample, when the specimen starts to deform along a dominant shear-band, especially when large localized plastic deformation is observed. In these cases the strain measurement in the plastic deformation part of the stress-strain curve falls back on cross-head displacement data. The curve shown in figure 2.7 shows typical stress-strain test behavior for a  $Zr_{55}Cu_{30}Al_{10}Ni_5$  metallic glass sample. The loading curve exhibits essentially a linear increase until the elastic limit  $\sigma_y$  is reached. After the elastic limit is reached, the primary shear band forms and the sample begins to deform in an almost perfectly plastic manner, involving a very small volume of material in the shear band. Even though the strain in the shear band is very large, the amount of macroscopic plasticity remains very low because only a small volume of the material deforms plastically. Depending on the load frame compliance of the compression testing rig, a number of flow serrations may be observed in the stress-strain curve of the deforming metallic glass [13, 58, 59]. In figure 2.7, at least three such serrations can be observed. Eventually the shear band propagates catastrophically and the specimen fractures. An example of a fractured nominal composition  $Zr_{55}Cu_{30}Al_{10}Ni_5$  specimen with one dominant shear band is shown in figure 2.8.

In compression testing, any spurious misalignment in the compression fixture or between the sample top and bottom planes can cause deviations from the uniaxial stress-strain curve, which could be misinterpreted as increased ductility. To get reliable results, extra attention is paid to grinding the specimen ends parallel to each other and perpendicular to the specimen axis, using a dedicated grinding fixture shown in figure 2.9. Also a dry  $Al_2O_3$  spray is used to lubricate the contact surfaces between the specimen and the tungsten carbide blocks. These measures still leave

at least one major source of variability in the results, namely the amount of structural relaxation the specimen has experienced during its thermal history. For example specimens from the bottom of a low-pressure die casting bar mold are often cooled faster than the specimens nearer the top of the mold. To remove those effects, a suitable heat treatment was carried out in glass vials under high vacuum pumped high-purity Ar atmosphere, shown in figure 2.10. Detailed investigation of the effects of different heat treatments on the deformation behavior are beyond the scope of this work.

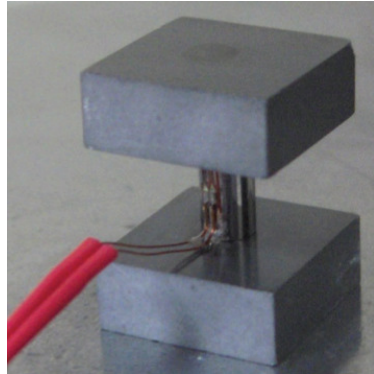


**Figure 2.6.** The set-up used for uniaxial compression testing. The compression fixture in a universal testing machine is protected from wear by using tungsten carbide blocks on the ends of the cylindrical test specimen. The deformation is measured with a strain gauge glued onto the specimen (thesis Paper I).

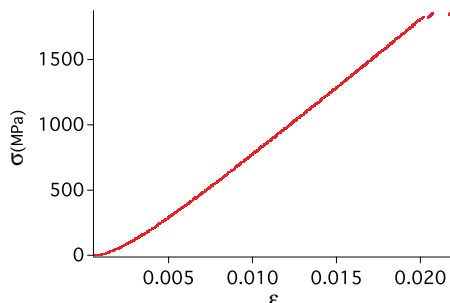


**Figure 2.7.** An example of a typical stress-strain compression curve for nominal composition  $Zr_{55}Cu_{30}Al_{10}Ni_5$  specimen. The behavior is linear elastic initially, until the yield limit where the specimen starts to deform locally in a perfectly plastic fashion, deformation being concentrated to one dominant shear band.



**Figure 2.8.** An example of a typical fractured nominal composition  $Zr_{55}Cu_{30}Al_{10}Ni_5$  test specimen. Two shear bands can be seen, but often only one dominant shear band forms.



**Figure 2.9.** The fixture for ensuring parallel ends for a compression sample. The sample is positioned in the white holder on the left of the figure, which is fastened in the cylinder opening at the end of the arm which moves on a linear bearing for grinding.

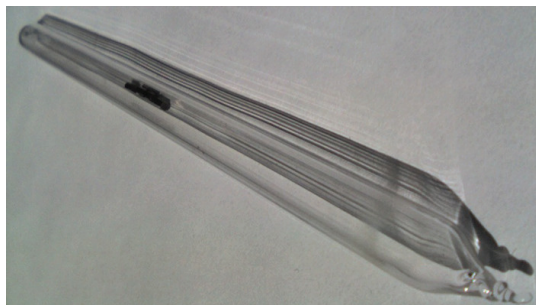


**Figure 2.10.** A sample after heat-treatment to achieve a reproducible relaxation state. An acetylene torch was used to seal the sample in a fused quartz vial under inert atmosphere (thesis Paper I).

### 2.3.2 Instrumented indentation

Depth-sensing indentation, also known as instrumented indentation or as NanoIndentation [60], differs from traditional hardness measurements by recording the load-displacement behavior during the test instead of examining the size of the indentation after the test has been completed. Once the indenter tip is characterized by measuring the indentation of a reference material (a fused quartz plate), studying the size and shape of the indentation made is not necessary for each specimen to get results in this method, and the load-displacement curve yields additional information.

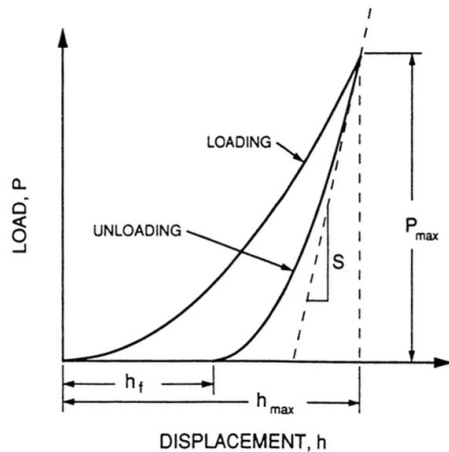


**Figure 2.11.** A schematic illustration of load versus indenter displacement in indentation experiment. The peak indentation load is  $P_{\max}$ , the indenter displacement at peak load  $h_{\max}$ , the final depth of the contact impression after unloading  $h_f$  and initial stiffness  $S$  [60].

The indentation modulus ( $I$ ) is measured directly from the tangent at initial unloading, illustrated in figure 2.11. If a value for the material's Poisson ratio ( $\nu$ ) is known or assumed, Young's modulus can be calculated from the measured indentation modulus as

$$E = I(1 - \nu^2). \quad (2.1)$$

The peak indentation load ( $P_{\max}$ ) and the projected indenter contact area ( $A$ ) are used to calculate the hardness [60]

$$H = \frac{P_{\max}}{A}. \quad (2.2)$$

Instrumented indentation provides more information than just hardness. The thermal history, i.e. the state of structural relaxation of an amorphous metal can be qualitatively estimated with instrumented indentation Young's modulus measurements. Also, since it is not necessary

to see the indentation marks with microscopy, smaller indentations can be used, which in turn enables measurement from smaller samples, such as thin films. The rule of thumb here is that the indentation thickness should be less than 1/10 of the layer thickness.

The amount of research effort needed to determine Young's modulus from compression tests is much larger than with the relatively fast instrumented indentation measurements. Also, in instrumented indentation, the main test preparation needed is a smooth enough surface on the test specimen and some knowledge of the thickness of the measured material layer. Instrumented indentation is frequently used in the study of amorphous metals. Examples of use in this thesis include the measurement of mechanical properties from a deposited coatings (thesis Paper I), the measurement of hardness profiles (thesis Paper II) and the measurement of mechanical properties from a cross-section of thermoplastically drawn amorphous wire, shown in figure 2.12 (thesis Paper III).

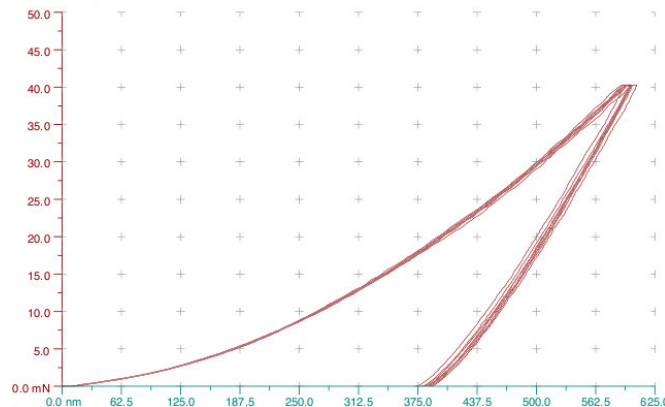


**Figure 2.12.** An example of the use of instrumented indentation to measure mechanical properties from a nominal composition  $Zr_{55}Cu_{30}Al_{10}Ni_5$  viscous flow-formed metallic glass wire cross-section. The sample wires were first embedded in an epoxy button. The button was subsequently polished to  $1\text{ }\mu\text{m}$  diamond paste finish to minimize any surface roughness effects on the results. The actual indentation measurements took less than an hour to accomplish (thesis Paper III).



### **3. Production facilities for alloying a glass-forming alloy and casting it without crystallization**

Bulk metallic glasses (BMG) are alloys that can be solidified with copper mold casting into a diameter larger than 1 mm without detectable crystallization. Amorphous metals can be manufactured with an extremely wide range of techniques [18, 61, 62]. Metallic glasses are also amorphous metals, usually with very similar properties as found in similar composition non-glassy amorphous metals. However, strictly speaking metallic glasses only result from a sufficiently fast cooling of a glass-forming alloy melt through its glass transition temperature without crystallization. For example, to make a magnetron-sputtered amorphous BMG alloy coating into metallic glass, it needs to be reheated above its glass transition temperature and re-cooled fast enough through its glass transition temperature without crystallization. Similarly, mechanical alloying can be used to produce metallic glasses from elemental particles, and once compacted above  $T_G$ , a metallic glass can result [61]. However, because the properties of the same composition amorphous metals and metallic glasses are very similar, the terms are often interchanged in literature.

A general trend in all amorphous metal manufacture is, as coined by Turnbull, the need to first 'energize' the material away from crystalline equilibrium conditions and then 'quench' it fast enough to retain the non-equilibrium structure [62]. Amorphous metal layers can be produced for example by ion deposition stainless steel with  $B^+$ , where at the layer end composition approaches the marginal glass forming composition  $Fe_{81}B_{19}$  [18]. Thin amorphous coatings can also be made with other physical vapor deposition methods, which are discussed in greater detail in chapter 5. Sometimes the glass forming composition is even achieved from diffusion at the interphase of two different materials [61]. A very limited set of amorphous alloys can be deposited electrochemically. However, ever since the advent of bulk glass forming alloys, the 'energized' state has

been metastable enough for bulk glass formation with the cooling rates found in metal mold casting. Often, depending on the actual alloy, the most straightforward method for producing large quantities of amorphous metal with wide range of compositions is to physically melt the elements with induction heating or by arc-melting. This melt can then be vitrified, i.e. made glassy by casting it into a metal mold. The casting must fulfill two distinct conflicting requirements, firstly to provide the wanted shape and vitrify the melt by cooling it fast enough. Another useful way of shaping metallic glass specimens, is to shape them in their viscous flow region, i.e. between  $T_G$  and  $T_X$  temperatures. These methods will be covered in more detail in chapter 4.

Because both the ease of manufacturing and the mechanical properties of the produced amorphous metal specimens are dependent on the manufacturing methods and facilities used, the study and development of these facilities is an important part of advancing metallic glass and amorphous metal usability in applications. In this chapter, the different facilities for the bulk metallic glass manufacturing are studied based on literature, interviews, facility design, facility construction and finally facility evaluation using the atomic percentage nominal composition alloy  $Zr_{55}Cu_{30}Al_{10}Ni_5$ .

### 3.1 High-purity induction melting and casting

The first tested BMG manufacturing method was the combination of induction melting alloying on a water-cooled copper crucible and induction melting casting in a quartz crucible. With induction, the melting can be done in vacuum or with inert gas environment. This experimental research work was published as a Master's thesis study of copper-based BMG alloys in Outokumpu PoriCopper in 2004–2005 [63]. The study included the trial of alloy preparation with existing equipment and the construction of capable equipment and testing of this equipment, as shown in figures 3.1, 3.3, and 3.4. The melting apparatus in figure 3.1 for glass-forming alloy alloying can be seen as a research scale version of a larger scale skull casting furnace illustrated in figure 3.2. Instead of having multiple water-cooled copper segments, as are needed for larger ingots in the 5 kg to 50 kg range, only one "copper claw" is used.

The construction of a high vacuum water-cooled copper crucible induc-

tion melter and a high vacuum quartz crucible induction casting furnace provided the possibility to study the high process purity manufacturing and high-purity raw material requirements of the current BMG alloy majority.

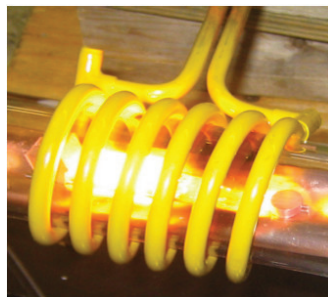


**Figure 3.1.** Induction melting on a water-cooled copper crucible in a high vacuum [63].

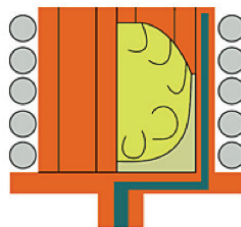


**Figure 3.2.** Cold copper crucible (skull-casting). Individual water-cooled copper crucible elements permit induction currents to melt the alloying elements inside the crucible. Process usually takes place inside a high vacuum chamber [64].

The equipment built was found to be labor intensive to use, because of the need to repeatedly break the vacuum during the alloying. This was necessary because there was no outside manipulator in the furnace and during the first melting all the ingredients did not always form a single ingot without manipulation as can be seen from figure 3.1. Also the breaking of the vacuum was necessary to flip the ingot to ensure homogeneous mixing of the alloying ingredients. Also the expensive quartz crucibles could only be used once. Often the quartz crucible softens and the required gas pressure is lost resulting in partial fill of the mold as shown in figure 3.4. The built equipment was found to be able to produce BMG castings, but it was found to be impractical for BMG part manufacturing. More specifically, the opening and closing of the alloying induction melter required a lot of care not to drop any of the alloying elements of the through, when the chamber was closed by rotating an end cap against the quartz tube. The melting of metal in a vacuum atmosphere risked coating the inside of the quartz crucible with evaporated metal, however

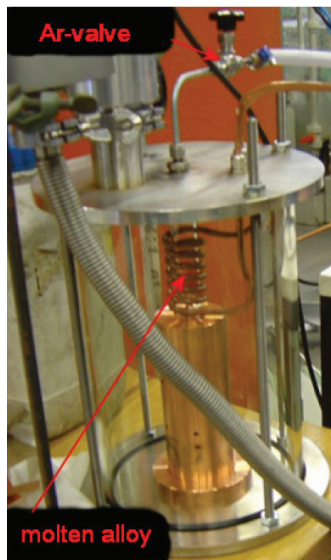


**Figure 3.3.** Induction melting of a BMG alloy in a quartz crucible in a high vacuum [63].



**Figure 3.4.** Cast BMG alloy with the used partially broken quartz crucible and the used copper mold [63].

since there was no shut off valve in the pumping system, regular disassembly of the system was required to re-use transparent portions of the quartz chamber. Despite its shortcomings, the alloying melting furnace was in much better working condition after repeated use than the casting furnace. The biggest shortcoming of the casting furnace was its *ad-hoc* epoxy sealing of the induction coil high-vacuum feedthrough, which required constant maintenance.

### 3.2 High-purity induction levitation melting and casting

A variation of cold copper crucible induction melting is to use the produced Lorenz force for melt levitation [65–68]. The process parameters and coil shape need to be carefully selected to avoid the melt leaking from the center axis of the coil. This method has the advantage when compared to cold copper crucible induction melting, that no crucible contact takes place. Usually the levitated melts are below 100 g [65–68], but much larger melts can be processed with partial levitation, i.e. using magnetic levitation only to keep the sides of the melt away from the container walls and allowing the coldest spot of the melt take support from a water-cooled copper crucible. In the partial levitation cases the melting takes place in a similar cold copper crucible as that shown in figure 3.2.

For alloying metallic glass alloys the added benefits of partial levitation as compared to skull casting are unclear, but as with skull casting, relatively large batches of about 5 kg to 50 kg glass forming alloy can be produced. Usually there is no attempt to cast this alloy directly fast enough for glass formation, instead a separate casting furnace is used.

For metallic glass induction levitation casting a mold can be placed below the coil, and the casting can be performed by cutting the power to the induction coil, after the desired casting temperature is reached. This mold geometry can also include suction casting, if the process is done in an inert atmosphere instead of vacuum.

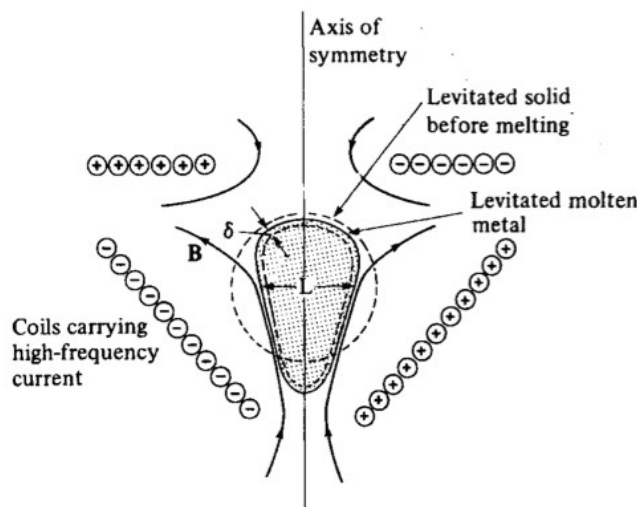


**Figure 3.5.** A typical axisymmetric levitation device [65].

### 3.3 High-purity arc melting and low pressure induction die casting

The second studied BMG manufacturing method was the combination of high vacuum purity arc melting and high vacuum induction casting. The possibility to study the method came with a one year visit to Tohoku University in Professor Inoue's group. The alloying is done by arc melting with the furnace shown in figure 3.8. The principle and the construction of the furnace are similar to those shown in figure 3.6 and more clearly, with less detail in figure 3.7.

On top of the furnace is a handle that is used to move the tungsten electrode inside the vacuum chamber above the water-cooled copper crucible shown in figure 3.9. The possibility to move the electrode makes it possible to direct the heating in X, Y and Z axes very accurately, making it possible to melt several ingots without breaking the vacuum. For example, in the furnace shown in figures 3.8 and 3.9 five ingots can be prepared with one pumping. The center trough is reserved for the titanium getter, which is always melted first to remove any leaked oxygen from the reduced pressure high-purity argon atmosphere. The arc is lit first on the titanium and then after sufficient gettering moved to melt the ingots. After melting, the ingots are flipped to ensure that the undersides of the ingots are also sufficiently melted.

Flipping, i.e., turning the ingot upside down between melting runs is done to ensure even composition. Usually the ingots need to be melted five times and flipped four times before even composition is achieved. The ingot can be flipped with the electrode tip or more comfortably with both the electrode tip and a separate high vacuum manipulator without breaking the vacuum. The high vacuum manipulator has been removed from the furnace shown in figure 3.8 to improve the vacuum.

After arc melting an ingot such as the one shown in figure 3.10 is produced. This ingot is broken into several pieces for one or more casts. The quartz crucible used was a cylindrical 10 mm diameter tube with a V-shaped tip [43]. The bottom orifice size was prepared by grinding the initially closed crucible tip until orifice of desired size was reached. The orifice size was selected based on the mold used.

After the crucible was ready, pieces of the prepared ingot were placed inside it and the crucible was carefully positioned inside the furnace shown in figure 3.11 to correctly align it with the mold orifice when the piston on top of the furnace was down, i.e., in casting position. The motion of

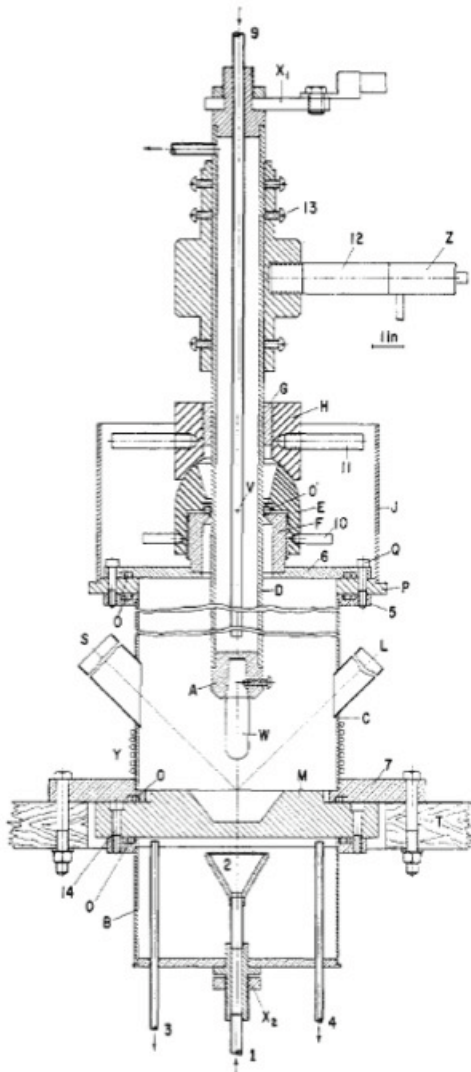


**Figure 3.6.** Laboratory arc melter. The arc melting works by making sure that the amount of heat brought in by the arc plasma is sufficient to melt the ingot metal (placed on M, not shown) on top of the hearth but at the same time insufficient to raise the temperature of the hearth itself too much. The hearth is kept cool with the high thermal conductivity of its material, usually copper and by water-cooling. Also, it is good practice to minimize the thermal conductivity between the molten metal and the hearth by using high surface tension melt-hearth material combinations. As a result, the melting point of the hearth material can be exceeded in the ingot material melt with only the ingot materials melting and not sticking to the *cold copper crucible*. The technical difficulties lay in the detail that this process is done inside a high vacuum chamber. O' marks the rubber O-ring, which allows vertical motion and rotation about the point V of the tungsten-tipped electrode W inside the chamber above the water-cooled copper crucible M [69].

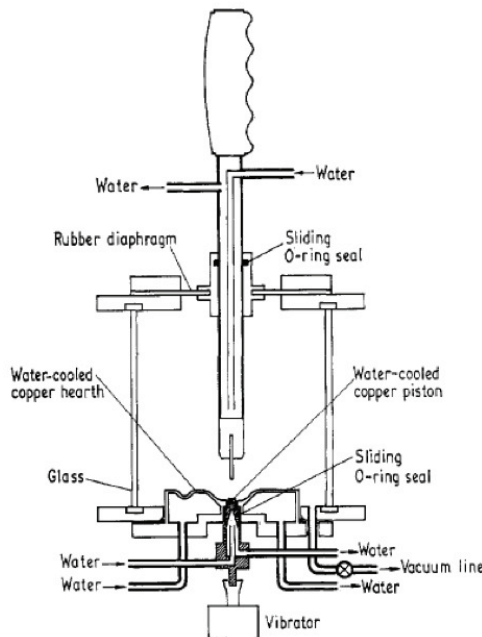


**Figure 3.7.** A laboratory arc melter with a vibrating crucible. The basic principle is same as in figure 21, but the rotation of the electrode is done by the deformation of a rubber diaphragm and only the linear motion requires the use of a sliding O-ring seal [70].



**Figure 3.8.** Water-cooled copper crucible arc melter used for alloying.

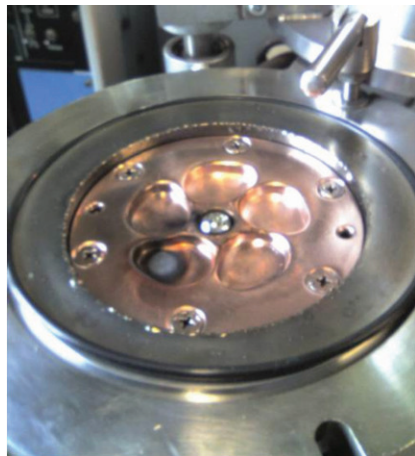


**Figure 3.9.** Water-cooled copper crucible with titanium in the center and five melting troughs for melting five ingots with one vacuum pumping. The titanium is melted first to purify the vacuum chamber from any remaining oxygen impurities.

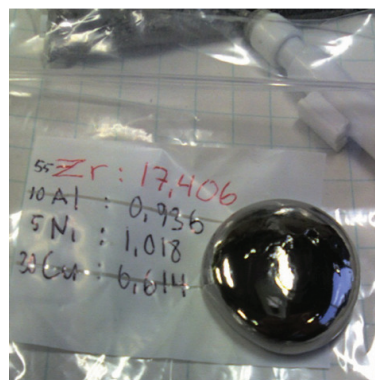


**Figure 3.10.** Melted ingot after five meltings with flipping the ingot between the meltings.



**Figure 3.11.** Induction casting furnace. The piston on top of the furnace moves the V-shaped quartz crucible from heating position inside the induction coil to direct contact with the copper mold orifice, when the large black button on the front of the machine is pressed.

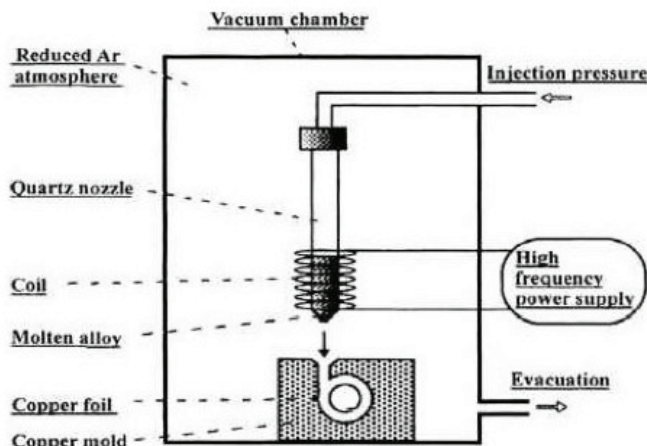


**Figure 3.12.** The principle of the used quartz crucible shape and motion from heating position to mold orifice of unrelated mold geometry [71].



**Figure 3.13.** Induction furnace cast 3 mm diameter BMG rods.



**Figure 3.14.** Cast BMG tensile test specimen in as-cast condition.

the quartz crucible can be seen in figure 3.12, as the distance of the arrow between the tip of the crucible and the orifice of the mold. After positioning the crucible and the mold, the furnace was closed and pumped to  $<1 \times 10^{-5}$  mbar vacuum.

After pumping the vacuum, in this case with oil-sealed rotary vane fore-pump (not visible) and high vacuum diffusion pump (gray cylinder above the black fan on the right of figure 3.11), the crucible was heated inside the induction coil, as shown in figure 3.12, until it was evaluated through the window, seen in figure 3.11, to be completely molten.

Optionally the melt temperature could be verified through the chamber viewing port with a spot infrared thermometer. In practice, the color of the molten metal and the knowledge of the melting point were used with well known alloys. After melting the ingot, the big black button shown on front of the furnace in figure 3.11 was pressed, which lowered the crucible from inside the induction coil to contact with the mold and immediately after reaching contact pressurized argon was used to eject the molten metal into the mold. The most often produced specimens were cylindrical rods of varying diameters, as shown in figure 3.13. As shown in figures 3.12 and 3.14, other forms can also be produced with relatively little adjustment.

The benefit of using V-tipped crucible was the good sealing it achieved with the mold orifice. The mold orifice mechanically supports the tip of a quartz crucible reducing the probability of the crucible breaking. This effectively removes the need for bottom half of the crucible shown in figure 3.4. This construction makes individual crucibles much less expensive, but requires linear piston motion to move a crucible from the induction coil to the mold orifice. This motion is not needed in the casting furnace shown in figure 3.3, because the bottom end of an hour-glass shaped quartz crucible provides sufficient distance between the induction coil and the copper mold for induction melting to operate.

### 3.3.1 High pressure die casting

The methods discussed in chapters 3.1 and 3.3 are sometimes referred to as die casting [72]. However, the pressures that can be used with fused quartz crucible are limited by the softening of the fused quartz. One common casting failure in this system is that the fused quartz crucible breaks and releases the high speed melt in a direction other than the mold. A high pressure die casting set-up usually consists of materials more able to withstand the casting pressures. Also a hydraulic plunger instead of gas pressure is used to accurately control the melt displacement speed and the force used [73, 74]. This kind of high pressure and high displacement method, schematically illustrated in figure 3.15 fills the mold fast enough to form relatively complex specimens, such as those shown in figure 3.16. Liquid Metal Company has produced the samples in figure 3.16 with a customized aluminum die casting method [27].

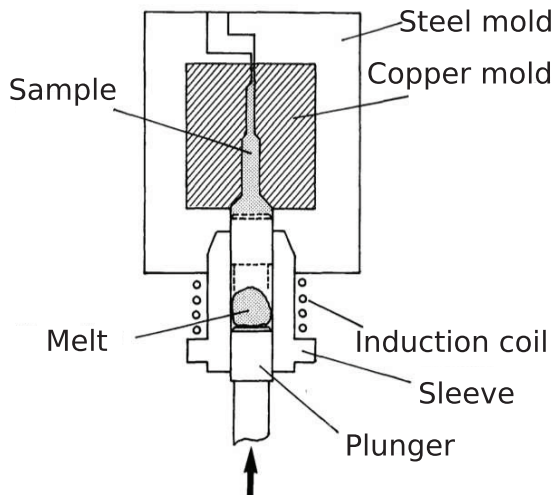


**Figure 3.15.** A schematic representation of a high pressure metallic glass die casting set-up [74].

The downside of the die casting methods discussed in chapters 3.1, 3.3 and here is the unreliable mechanical properties produced [72]. The mold is filled by atomized spray, at least initially, followed by consolidation as the pressure rises in the mold. The high flow velocities of die casting result in porosity in the produced samples, which can cause un-reliable mechanical properties as compared to suction-cast metallic glass specimens [27, 75]. Although suction casting produces better mechanical properties than die casting, tilt casting is known to produce better mechanical prop-



**Figure 3.16.** Examples of commercially die-cast metallic glass specimens [27].

erties than suction casting [42, 76, 77].

### 3.4 High-purity arc melting and tilt casting with suction

On considering the equipment discussed in chapters 3.1 and 3.3, the use of transparent fused quartz crucibles in both furnaces shown in figures 3.3 and 3.11 has the benefit that the melt is easy to observe. The downside of the quartz crucible is that it is a likely source of contamination with oxygen, which has been shown to cause brittleness in some Zr-based BMG alloys[78]. The alternative method is to use a graphite crucible (as done by the Schultz group in Dresden) with the same furnace. Graphite has not been reported to cause embrittlement in BMG alloys. This design needs an additional mirror or camera inside the chamber to observe the melt. Another issue with the BMG manufacturing systems presented in chapters 3.1 and 3.3 is the need for two vacuum chambers, one for alloying and one for casting. Both need a crucible and a method to melt and observe the alloy. In the case of the relatively inexpensive equipment presented in figures 3.1 and 3.3, this was accomplished by using the same vacuum system and induction power source for both furnaces, i.e. disassembly and assembly of the furnaces was needed in normal operation. This is detrimental to high-vacuum systems and often leads to hard to diagnose leaks in the furnace due to misalignment of seals, wear of sealing surfaces and dirt particles on seals. In the case of the expensive equipment presented in figures 3.8 and 3.11, both furnaces have their own independent vacuum and melting equipment. This is a practical but expensive solution,

and still specimens prepared by this method do not compare favorably to the best fatigue properties reported for cast BMG specimens [41, 43, 76]. The need to break the vacuum for transferring the ingot from one furnace to another contributes again to oxygen contamination.

Another very interesting solution using a single vacuum system integrates casting directly into the arc-melting copper hearth, as illustrated in figure 3.17. However, the downside of this method is that the cold-spot, where the melt touches the copper hearth is very likely to be sucked into the mold when the melt is sucked from beneath in arc-melting.

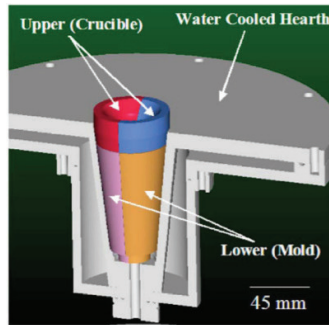


**Figure 3.17.** Drop-suction-casting furnace [79].

Ideally therefore, the casting method would avoid using the cold spot material. One example of such a system, for making golf clubs in this case, is shown in figure 3.18. Here clamp casting serves to move the melt in uniform fashion away from cold spot into the mold. However, this set-up is no longer very useful for alloying, with all the vacuum-feedthroughs that are needed to operate moveable parts inside the vacuum chamber.

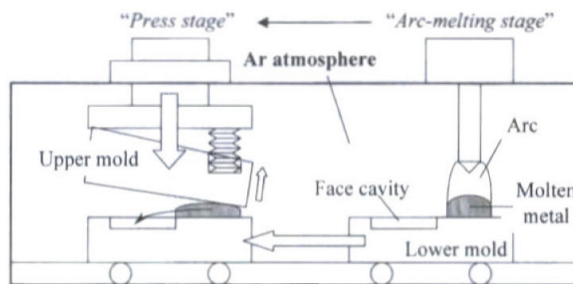


**Figure 3.18.** Clamp casting to produce golf club strike plates with attractive mechanical properties [43].

The most promising fatigue properties of BMG alloys have been reported with all-metal crucibles using tilt casting [42, 76], which makes this method particularly attractive for further study. In tilt casting, the BMG specimen is first melted, usually with arc melting, and then the

molten alloy is gently poured into the mold, as is schematically illustrated in figure 3.19. The set-up shown in figure 3.19 usually requires the use of high-torque rotary vacuum feedthroughs which severely limit the atmosphere purity achievable in the tilt casting furnace using this fixed chamber design. As is discussed in greater detail in (thesis Paper IV), these rotating high-vacuum feedthroughs usually contain a lubricated O-ring seal, which are prone to collect dirt and known to leak in use.

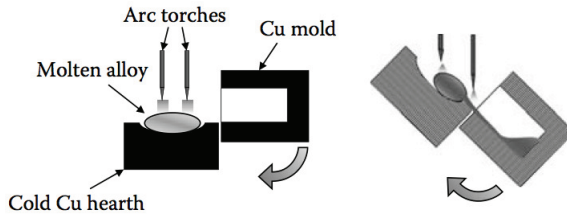


**Figure 3.19.** Tilt casting set-up with fixed chamber orientation [62]. The pre-alloyed ingot is remelted and once molten the Cu-crucible and mold are tilted together to gently pour the melt into the mold. Since the chamber stays fixed, the primary arc torch needs to be moved up before the hearth and mold are tilted. Here another arc is fixed closer to the center of rotation to heat the melt during casting.

To altogether remove the need for two systems, a higher purity one for alloying and the lower purity one for casting, a novel design was sought that would avoid the vacuum problems associated with tilt casting. By rotating the whole arc melting chamber for tilt casting —thus eliminating the need for the most troublesome feedthroughs— and generally using designs more commonly used in ultra-high vacuum systems, the vacuum leak problems associated with tilt casting were resolved without compromising the suitability of the chamber for alloying. The resulting furnace design allows arc melting and tilt casting in a single furnace. The furnace constructed according to this design is shown in figures 3.20, 3.21 and 3.22. More detail on the design methodology and the design features of the combined tilt casting and arc melting furnace that was constructed, is given in thesis Paper IV.

### 3.4.1 An example of BMG ingot melting with tilt and suction casting

A typical use of the constructed combination furnace consists of the following steps:

1. Convert the wanted alloy composition into weight percentages.
2. Cut and weigh the correct ingredient amounts.

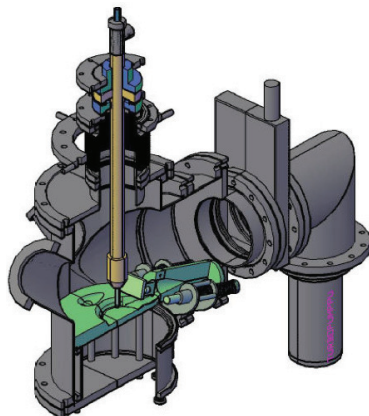


**Figure 3.20.** Cut-out view of the design of the arc melting and casting furnace (thesis Paper IV). Here the arc torch remains usable during the casting operation because it rotates with the chamber, so only one arc torch is required.

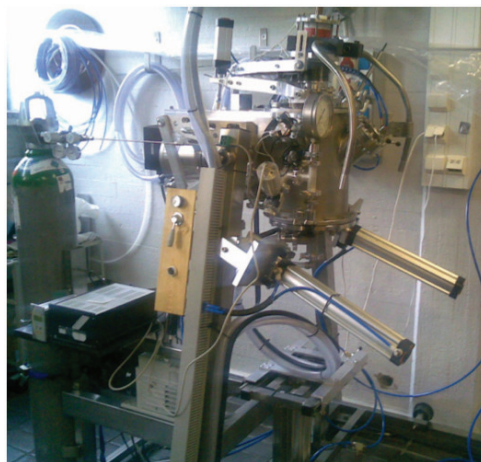


**Figure 3.21.** The combined arc melting and casting furnace, with chamber closed (thesis Paper IV).

3. Place the cut pieces on the cold copper crucible as shown in figure 3.25.
4. Close the furnace using the pneumatic lift shown in figure 3.22.
5. Start rough pumping the chamber. Turn on and start pumping through the turbo-molecular pump shown in figure 3.26, when the vacuum is better than  $5 \times 10^{-2}$  mbar.
6. Pump to a high vacuum better than  $1 \times 10^{-5}$  mbar. This usually takes less than 30 min. With a couple of hours of pumping time, a  $1 \times 10^{-6}$  mbar vacuum can be reached.



**Figure 3.22.** The combined arc melting and casting furnace, with chamber open.

7. Close the high vacuum valve, shown in closed position behind the mold in figure 3.27. This seals the chamber. Turn off the pumps. Remove electrical connections from the turbo-molecular pump to avoid possible damage from high-voltage arc-starting spark. Remove the cold-cathode high-vacuum gauge.
8. Fill the chamber with argon until desired pressure is reached. Usually this pressure is set from 0.4 bar to 0.6 bar absolute pressure (amounts are 0.6 bar and 0.4 bar under atmospheric pressure, respectively). Use only the mechanical pressure gauge shown in figure 3.21 to set this pressure.
9. Turn on the TIG power source and select 100 A starting current with high-voltage spark. Verify that cooling water is flowing both in the electrode and in the copper crucible.
10. Position the tungsten electrode tip on top of the gettering titanium as shown in figure 3.27. Adjust the tip height from the right thumb pneumatic valve shown in figure 3.32 to be as close to the titanium as possible, without touching the titanium.
11. When ready, ignite the arc plasma by pressing the right foot pedal

trigger. Make sure the plasma travels from the tip of the electrode directly to the titanium. Let the sharp end of the tungsten electrode tip heat for few seconds in the same position until the top of the tungsten electrode begins to glow red. Carefully lift the electrode to a more comfortable height, such as that shown in figure 3.28, while observing the plasma behavior and adjusting as necessary.

12. **Melt the titanium.**
13. After about one minute, move the plasma to start melting the ingredients in the main trough. Use the 100 A power to melt the pieces into a single ingot. If necessary, stop the melting and move the pieces together after they have cooled down and remelt them, always igniting the plasma on the titanium to clear the chamber of any leaked oxygen.
14. Add more power depending on the size of the melt. The molten ingot should look and move like liquid mercury as shown in figure 3.23, when properly molten. After melting the ingot for about one minute, stop the melting by lifting foot of the triggering pedal, as shown in figure 3.29.
15. Wait for the ingot to cool down. The poor wetting of the cold-copper crucible by the molten ingot and the poor thermal conduction across the ingot-crucible interface show a markedly slow cooling rate. So the ingot usually crystallizes as can be seen from the ingot surface shown in figure 3.30. Use the electrode tip and the manipulator, both shown in figure 3.30 to flip the ingot upside down as shown in figure 3.31. The ingot has no more adhesion to the crucible as the pieces it was melted from, shown in figure 3.25. This seems surprising since the melting point of copper ( $1083^{\circ}\text{C}$ ) is exceeded by approximately about  $1000^{\circ}\text{C}$ , when the zirconium is first melted.
16. Repeat steps from 10 to 15 until the ingot has been melted four to five times. The surface of the ingot should start to show uniform crystallization patterns on repetitive meltings signaling the alloy is properly mixed [80].
17. During the last melting, open the suction valve and pour the melt as shown in figure 3.24 into the mold shown in figure 3.33.



**Figure 3.23.** The arc melting of a BMG alloy ingot on top of the water-cooled copper hearth. On the right is the tip of the manipulator used to flip the ingot upside down between melting runs. The mould orifice and the melt pouring nozzle leading to it can be seen behind the arc (thesis Paper IV).



**Figure 3.24.** Tilted furnace after casting. The two large pneumatic cylinders on the right are used to tilt the chamber. The tilting is controlled from the gray pneumatic valve on the wooden panel in the middle of the picture. The furnace is mechanically reinforced with water-cut aluminium structure to survive the accelerations of the chamber tilting process. An all-metal gas line is used between the argon gas cylinder and the chamber to preserve the 99.9999 at % purity.

18. Rough pump the chamber fumes before leaking it, and open it to the position shown in figure 3.22.
19. Remove the mold from the chamber and open it as shown in figure 3.34. A typical specimen can be seen in figure 3.35. The same mold was used in figure 3.4. Tilt and suction casting help to prevent the cold shut seen in figure 3.4.



**Figure 3.25.** Measured Cu, Zr, Al and Ni on the water cooled copper crucible before closing the chamber. Titanium that is used to getter any residual oxygen is in the small trough.



**Figure 3.26.** High-vacuum pumping in progress. Turbo-molecular pump rotor is spinning behind the mold.

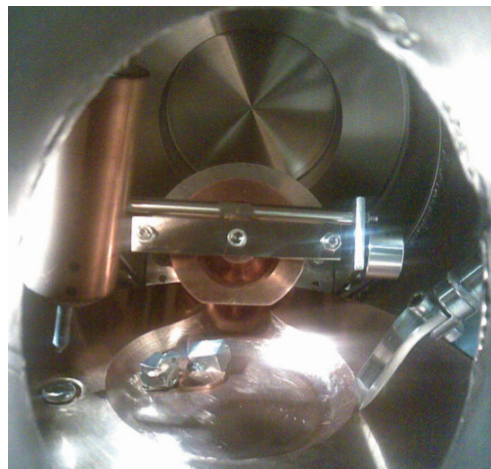


**Figure 3.27.** Preparing to ignite arc melting arc. The arc is always ignited to the titanium getter (under the electrode tip). In titanium gettering the highly reactive titanium is melted to remove oxygen impurities from the chamber atmosphere.

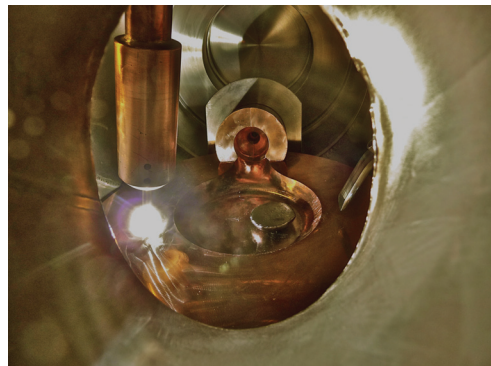


**Figure 3.28.** Titanium gettering the chamber. After about one minute of gettering, the lit arc is moved to melt the ingredients in the main trough.



**Figure 3.29.** Typical appearance of a molten BMG alloy.



**Figure 3.30.** Cooled BMG alloy ingot before flipping.



**Figure 3.31.** Flipped BMG ingot. The ingot was flipped without breaking the vacuum by moving it with the electrode to the right side of the trough, where it could be easily flipped with the manipulator tip.

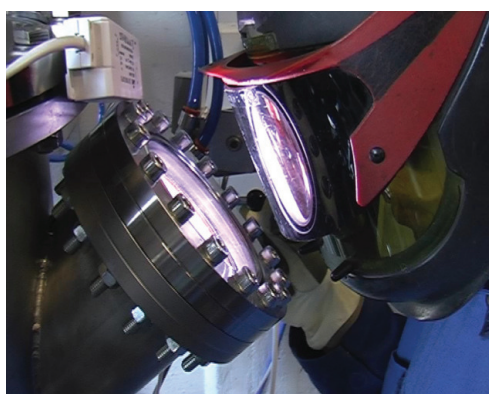


**Figure 3.32.** Arc melting in practice. The pneumatic valve in the middle of the picture is used to adjust the height of the electrode inside the chamber.



**Figure 3.33.** Inside view of the furnace after tilt casting. On the water-cooled copper crucible, titanium is in the small trough on the left and BMG alloy was poured into the mold.



**Figure 3.34.** Typical mold filling with tilt and suction casting. This is the same mold shown in figure 3.4, now with better filling probably mostly due to the use of suction in the casting. This specimen also has some cast-in copper wires for an experiment that will be covered in chapter 4.



**Figure 3.35.** Tilt and suction cast specimen. Slow pouring left a large 'skull' on the cold copper crucible.

### 3.4.2 Tilt casting more complex annular shapes

While die casting is known for its ability to produce complex specimens, although with the issue of unreliable mechanical properties, it is interesting to investigate the feasibility of casting more complex shapes with the constructed tilt casting furnace with suction casting, especially since these methods should be able to produce higher mechanical quality specimens. The chosen study case is the casting of annular or tubular specimens, in molds requiring a core.

Such shapes are also relevant for potential practical applications such as annular gaskets, active solder materials [81], jewelry, enclosures for electronic components, and as a preform for blow molding [50]. Metallic glass tubes can be used to construct precise Coriolis mass flowmeters [82]. The alternative metallic glass ring or tube manufacturing methods are discussed in (thesis Paper II).

Here we studied the possibility of casting bulk metallic glass tube into a core mold, schematically illustrated in figure 3.36 in one process. With a custom-built furnace, we start from raw materials and break the vacuum only once the tube has been cast. With the same arc melting electrode used in both alloy production and in casting, we aim to keep the ingot size under 100 g and waste as little as possible of the melt charge on runners by using tilt-casting to avoid the need for vertical runners.

Although the mold was filled nicely, as shown in figure 3.37, and a glassy  $Zr_{55}Cu_{30}Al_{10}Ni_5$  (in at.%) ring with outer diameter of 25 mm and 1.8 mm thickness, shown in figure 3.38, was produced, the amount of work to find the optimized casting parameters required was surprisingly large.

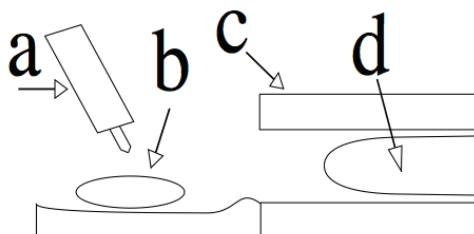


**Figure 3.36.** An illustration of the used casting set-up with (a) arc melting electrode, (b) molten alloy, (c) mold and (d) core. In casting the set-up is tilted clockwise to pour the melt into the mold (thesis Paper II).

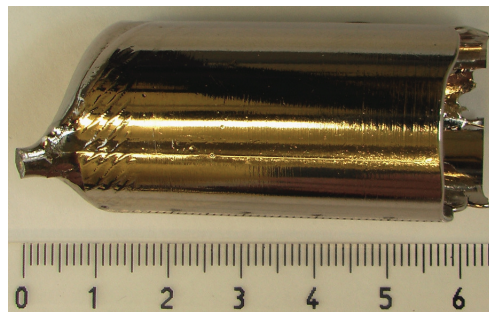


**Figure 3.37.** A fully filled casting (thesis Paper II).

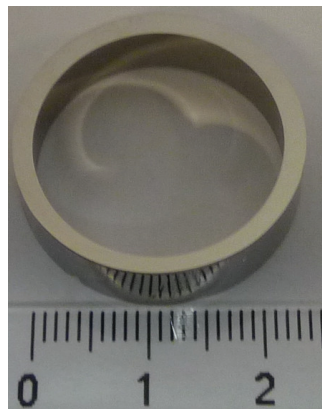


**Figure 3.38.** A glassy ring cut in cross-section from tilt cast tube (thesis Paper II).

### 3.4.3 Tilt casting with cap casting

One way to improve the tilt-casting process mold filling is to use a separate plunger to push the melt, as is illustrated in figure 3.39, into contact with the mold. Besides helping to fill the mold, this method improves the thermal contact between the cooling melt and the mold enabling greater glass forming ability. Also the plunger removes excess heat from the top of the melt [42, 76–78, 83]. An optional cap casting feature is currently under construction to the constructed furnace.

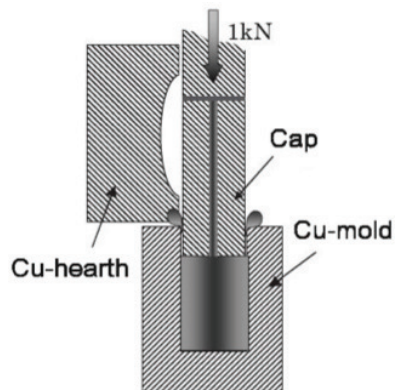


**Figure 3.39.** Yokoyama design for the cap casting technique [83].

## 4. Production facilities for thermoplastic forming of bulk amorphous metal

Thermoplastic forming of metallic glass is seen as a promising method for producing shapes that are difficult or impossible to cast. By decoupling the casting process from the final shaping, the cast specimen can be relatively simple to produce compared to the final shape. In practice, the preform material is alloyed and cast normally into a metallic glass by metal mold casting, as is schematically illustrated by the blue arrow first cooling segment in figure 4.1. This first manufacturing step is very similar to the ordinary metal mold casting represented by the grey arrow in figure 4.1. In thermoplastic forming, the cast sample is reheated between  $T_G$  and  $T_X$  temperatures, where a larger forming time than in direct casting, is available before crystallization, as is schematically illustrated by the reheating part of the blue arrow in figure 4.1.

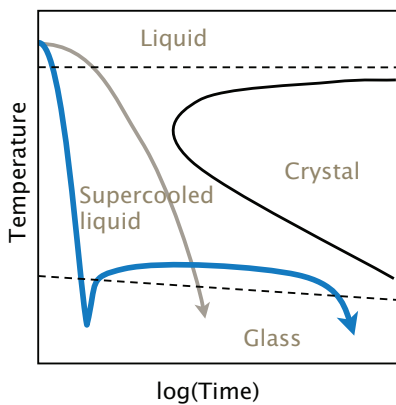


**Figure 4.1.** The principal idea of thermoplastic forming.

#### 4.1 Effect of friction between metallic glass and mold in thermoplastic forming of metallic glass

Thermoplastic forming processes that have been successfully carried out with bulk metallic glasses include imprinting [51, 84–86], extrusion [27], injection molding [72], friction welding [87], manipulation with forceps [85] and blow molding [50]. Depending on the used experimental set-up, the thermoplastic forming is done either in constrained or un-constrained flow. In fully constrained flow, the friction of the alloy surface against the mold wall requires shearing inside the alloy for continued deformation. In fully un-constrained flow there is no shearing caused by friction limiting the achievable deformations. The larger deformations available in unconstrained flow are represented in figure 4.2 by thermoplastic flattening diameters of cylindrical specimens [88].

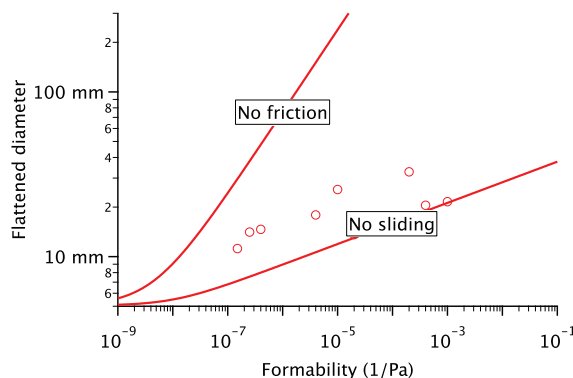


**Figure 4.2.** The significance of constrained or un-constrained flow in the flattening of a cylindrical sample in compression test [88].

The amount of thermoplastic deformation that can be achieved in constant heating of metallic glass before crystallization can be characterized by the figure of merit

$$F = \frac{1}{3} \frac{\partial T}{\partial t} \int_{T_G}^{T_X} \frac{1}{\eta(T)} dT, \quad (4.1)$$

where  $\eta$  is viscosity,  $T_G$  and  $T_X$  are glass transformation temperature and crystallization temperature, respectively [89]. The blow-molded nominal composition  $Zr_{44}Ti_{11}Cu_{10}Ni_{10}Be_{25}$  metallic glass bottle (from a cast metallic glass parison) in figure 4.4 and the blow molded hologram in figure 4.5 are examples of thermoplastic forming with very little hindrance from friction between metallic glass and mold. As a result of no metal-

mold friction, much larger aspect ratios can be manufactured with blow-molding type thermoplastic forming, as is shown in figure 4.3, where the diameters of figure 4.2 are represented as achievable aspect ratios. The thermoplastically compression molded corrugated plate (from a flat plate preform) in figure 4.6 is an example of thermoplastic molding, where friction between metallic glass and mold hinders the achievable deformations.

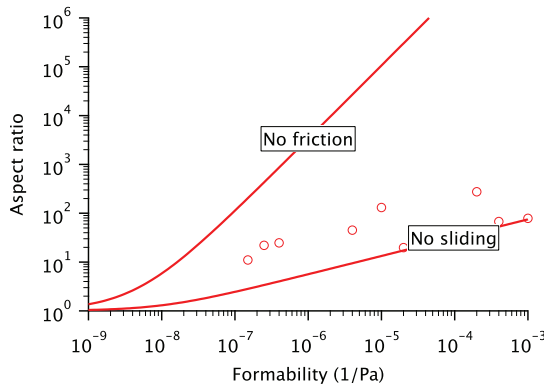


**Figure 4.3.** The significance of constrained or un-constrained flow in the flattening of a cylindrical sample in compression test with the effect to achievable aspect ratios [88].



**Figure 4.4.** A blow molded nominal composition  $Zr_{44}Ti_{11}Cu_{10}Ni_{10}Be_{25}$  metallic glass bottle [27].

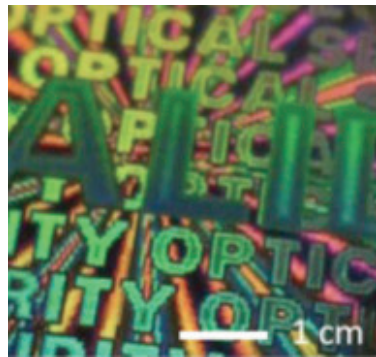


**Figure 4.5.** A blow molding replicated hologram [27].



**Figure 4.6.** A thermoplastically compression molded nominal composition  $Zr_{44}Ti_{11}Cu_{10}Ni_{10}Be_{25}$  metallic glass plate [27].

## 4.2 Effect of reheating rate on thermoplastic forming of metallic glass

Usually in the reheating process, the sample is heated to a temperature much lower than melting temperature to avoid crystallization, however in some cases, with very high heating rate temperatures above melting temperature have also been achieved [90]. The difference between casting and thermoplastic forming is sometimes blurred, as some recent capacitive discharge thermoplastic forming processes actually can heat the glassy preform above their melting point [90]. The usual case, especially with slower heating rate is to keep the temperature between the  $T_G$  and  $T_X$  temperatures [27].

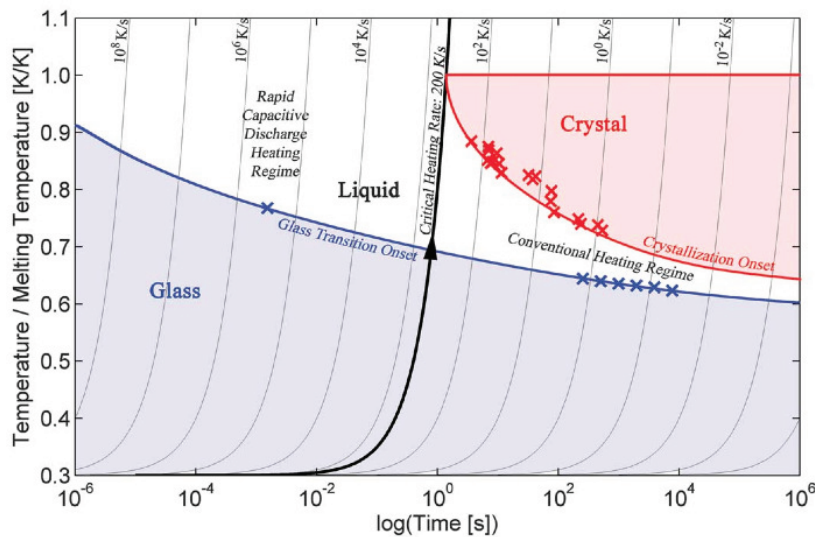


**Figure 4.7.** Glass-transition onset temperature and crystallization onset temperature versus time for metallic glass Vitleroy 1 at varying heating rates. The critical heating rate to completely bypass crystallization on heating from the glass through the liquid is about  $200 \text{ K s}^{-1}$ . Conventional heating rates on the order of  $1 \text{ K s}^{-1}$  provide access to the undercooled liquid over a relatively narrow temperature range, above which crystallization becomes kinetically favorable. Capacitive discharge heating rates on the order of  $1 \times 10^6 \text{ K s}^{-1}$  make the undercooled liquid accessible at any temperature above the glass transition, through the melting point and beyond, where the liquid enters the equilibrium state [90].

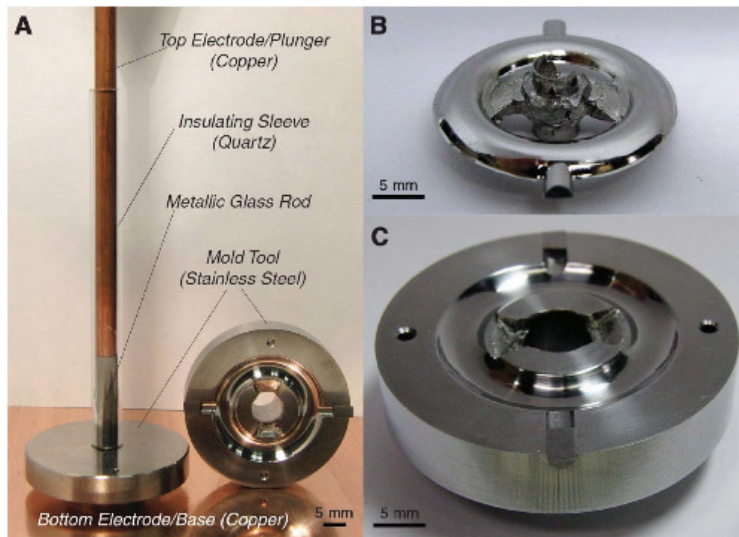


**Figure 4.8.** A set-up for demonstrating the use of capacitive discharge heating for injection molding of a metallic glass component. Also, 'as-molded'  $\text{Pd}_{43}\text{Cu}_{27}\text{Ni}_{10}\text{P}_{20}$  toroidal metallic glass part formed at processing temperature of  $\sim 720\text{ K}$  using a plunger pressure of  $\sim 20\text{ MPa}$  is shown [90].

### 4.3 An example of thermoplastic flow facility construction and its use for tensile viscous flow forming

Blow molding of cast metallic glass parisons is an interesting method, because unlike most forming methods, it does not consist of using high pressure to force supercooled liquid through narrow mold orifices, but instead deforms the preform mostly by tensile forces induced by pressure differences [27, 50]. The tensile forces can also be induced directly by heating a metallic glass specimen under tension above its glass forming temperature. To further test this method, a tensile viscous flow forming rig, shown in figure 4.9 was designed and built (thesis Papers III and V). The constructed forming apparatus shown in figure 4.9 consists of fused quartz tube, which is sealed from above, and open from lower end. On the upper end, there is a connection for helium gas, which is used both to increase the convective cooling rate and to protect the deforming specimen from excess oxidation. The fused quartz tube and ends are held in place by a support mechanism, which allows the induction coil to move up and down during the process.



**Figure 4.9.** The constructed wire drawing apparatus (thesis Paper V).

The thermoplastic forming of metallic glass wire is seen interesting because it potentially allows high flexibility in the produced wire diameters just by changing the process parameters even during the test. The controlled mid-process wire diameter change could be useful in novel suspension design. A variable diameter in a spring would result in a nonlinear

spring, where stiffness increases as the deflection increases. Also the low intrinsic loss and high elastic deformation properties of metallic glass can have applications where wire form is useful, such as for acoustic applications (thesis Paper III).

With the constructed tensile viscous forming facility, the cast preform is thermoplastically formed into a wire without the need for high-vacuum chamber or high-end process control in an essentially self-stabilizing method. The finite element calculations are used to evaluate optimal specimen geometries and the functioning of the used induction coils. The reported melt quenching metallic glass wire production methods use a rapidly spinning thin disk, the edge of which is brought into contact with the molten glass-forming alloy during the wire extraction part of this melt extraction method [91, 92]. Alternatively, the melt is poured onto a spinning disk with suitably sized groove for thicker wire formation [93]. The use of thermoplastic forming for metallic glass wire production is reported relatively seldom [94], (thesis Paper III). The unconstrained flow of material on the surface of the precursor material during thermoplastic forming enables much larger tensile deformations than are possible in a confined flow situation such as casting into a long and narrow mold [89], (thesis Paper III). The simplest geometry to produce by this method is custom diameter profile amorphous wire, which also may have practical applications in acoustics (thesis Paper III) or as non-linear springs (thesis Paper V).

#### **4.3.1 Finite element modeling of induction heating**

Finite element modelling was used to evaluate the focusing of the induction heating on the specimen. A finite element model used in (thesis Paper III) was further developed to evaluate the various schemes to focus the induction heating away from the sample suspension wires. A failure to focus the induction heating away from the sample grips was found to result in highly elliptical cross-section wires. To overcome this problem without the use of bucking coil, the slots shown at the ends of figure 4.10a specimen were machined. This is a working solution, although with the downside of requiring much work in sample preparation. As shown in figure 4.10a, the slots successfully focus the electromagnetic power loss density i.e. heating in the middle of the specimen. To avoid the need of machining the slots at each end of the sample, a combination of using a bucking coil and

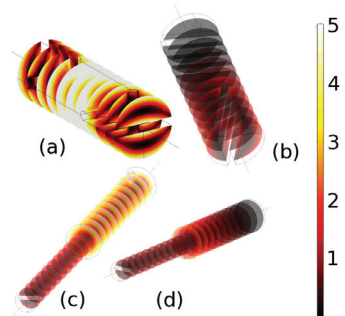


**Figure 4.10.** Tested wire drawing preform specimen geometries, (a) 7 mm cylindrical sample heated in normal induction coil. Sample has holes for attaching it to the wire drawing rig. Sample also has slits cut to the ends to reduce the heating of the sample ends. (b) Sample from a. heated with a bucking coil. The top of the sample is heated much less due to the bucking coil. (c) Specimen with diameters 5 mm and 3 mm heated in normal induction coil. The heating of the sample at the thicker upper part is focused too much near the gripping holes. However, the lower gripping holes do not suffer from overheating due to the smaller diameter. (d) Sample from c. is heated with bucking coil. Here the bucking coil reduces the heating at the thicker upper part and the smaller diameter reduces the heating at the lower thinner part. Both sample grips are protected from overheating (thesis Paper V).

a smaller diameter lower part sample was planned. The electromagnetic power loss of this 40 mm long 5 mm to 3 mm diameter sample is shown in figure 4.10c without the use of bucking coil and in figure 4.10d with the use of bucking coil. It is seen that the upper sample gripping hole region in the figure 4.10c preform heats up too much. However, this problem is successfully avoided in the identical geometry preform shown in figure 4.10d with the use of a custom-built bucking coil. To take into account the different diameters, i.e. smaller diameter section needs less heating to start to flow, the electromagnetic power loss was integrated along the length of the specimen and divided by the cross-section. The results of the calculations are shown in figure 4.11, where the reduction of heating caused by the use of the bucking coil is clearly seen as a downward slope of the bucking coil curve.

The success with the bucking coil led to the question, if the need of machining the sample could be removed altogether, thus significantly simplifying the process of producing wire with thermoplastic deformation. By carefully positioning wires in both top and lower parts of the mold before casting, a ready to use wire drawing specimen, shown in figure 4.9 was successfully cast and successfully used to draw wire. The effect of the force used to draw the wire was qualitatively analyzed by continuing to draw the wire by hand after the 0.2 kg weight had descended its full free

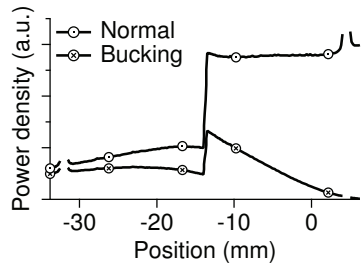


**Figure 4.11.** A comparison of calculated power loss densities per sample length with and without the use of bucking coil. The use of bucking coil successfully prevents the sample from heating near the top of the sample (thesis Paper V).

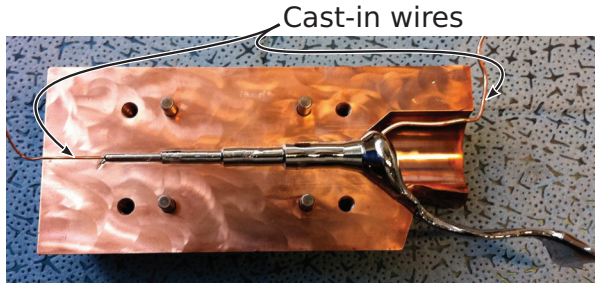


**Figure 4.12.** A sample with cast-in wires.

fall distance of 0.5 m. The produced wire thickness was found to be very sensitive to the amount of force used, which could enable the tailoring of wire thickness profile by changing the force and rate of the drawing during the process. These tailored thickness profile wires could be used as non-linear springs, benefiting from the excellent spring properties of bulk metallic glasses [95].

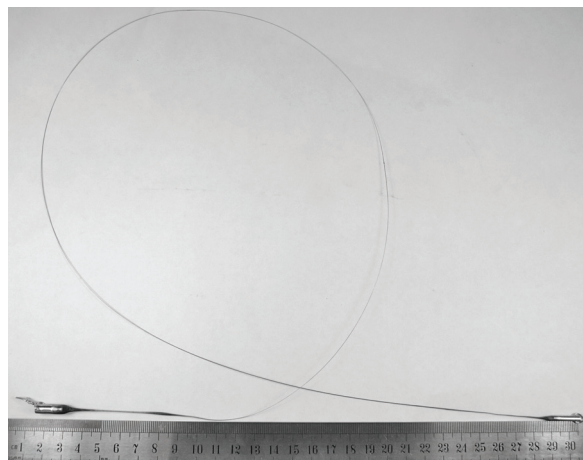


**Figure 4.13.** An example of produced glassy wire (thesis Paper V).



## **5. Production facilities for bulk amorphous coating with physical vapor deposition**

As discussed in chapter 1.2.3, one of the great advantages of BMG alloys is their potential in miniaturization. The lack of grain boundaries in amorphous metals removes this natural limit encountered, when miniaturizing with polycrystalline metals. The high thermal stability of the amorphous structure in BMG alloys further enhances their potential in miniaturization by providing the possibility for superplastic forming. As discussed in chapters 1.2.4 and 1.2.3, the small plastic zone size in BMG alloys often leads to problems in the form of too high strain localization. Making specimens of sufficiently small size avoids this problem without the need to modify the BMG alloy for increased ductility [14]. An interesting way to achieve this is to use the BMG alloy as a coating. As discussed in chapters 1.2.2 and 1.2.3, basic physical vapor deposition methods, such as magnetron sputtering can be used both to produce fatigue strength enhancing coatings and to produce MEMS / NEMS parts. In addition, magnetron sputtering is an environmentally friendly dry process, with existing mass production applications.

### **5.1 Magnetron sputtering target manufacturing**

In magnetron sputtering, the most practical way to deposit a fixed composition multi-component alloy is to manufacture a target of the same composition. As shown in chapter 3, melting reactive alloys with high-purity requirements can be done either with induction or arc melting on a water-cooled copper crucible. Due to the relatively large size requirement of 72.2 mm diameter with thickness of 3 mm to 10 mm, arc melting was selected. The BMG alloy ingot shown in figure 5.1 was produced with normal arc melting, as discussed in chapter 3.4.1. The main difference

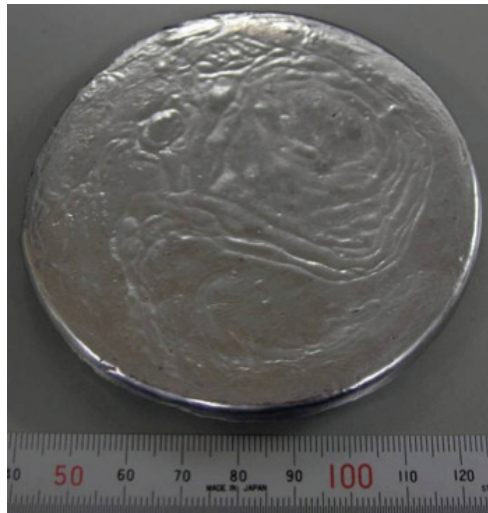


**Figure 5.1.** Arc-melted nominal composition Zr<sub>55</sub>Cu<sub>30</sub>Al<sub>10</sub>Ni<sub>5</sub> BMG alloy ingot.

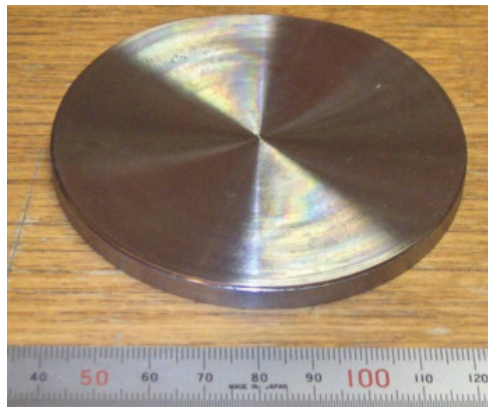


**Figure 5.2.** Arc-melted BMG ingot after machining with a lathe. The 72.3 mm (3") diameter disk is ready for use as a magnetron sputtering target.

to chapter 3.4.1 is that the ingot was left to cool on the water-cooled cold copper crucible. Since it is not necessary to produce amorphous target disks for amorphous magnetron sputtering coatings, the slow cooling rate and crystallization of the target disk were not a problem. After melting, the ingot was machined with a lathe to the correct dimensions for the magnetron sputtering target holder assembly. The finished target disk is shown in figure 5.2.

## 5.2 Bulk amorphous metal coating of polymers with magnetron sputtering

As discussed in chapter 1.2.4, the wider industrial use of BMG alloys suffers from the costly high-purity requirements of the materials and the manufacturing processes. It is therefore interesting to study the possibility of minimizing the amount of high-strength BMG and the possibility to use the known processability of polymers to produce hybrid material parts with a high contact strength surface and a high specific strength interior. Also in display manufacture, replacing the glass as the transparent electronics substrate with flexible polymers can enable new durable flexible displays. The applicability of BMG alloys for this substrate of polymers is of interest because of its attractive MEMS / NEMS properties discussed in chapter 1.2.3. To evaluate the feasibility of these BMG polymer composites it is necessary to determine if it is possible to create sufficient adhesion between the two and what the properties of the deposited BMG alloy are. Vacuum can perform transport medium function analogous to that of a solution in electrolytic metallization, as shown in figure 5.3. Generally physical power is provided to target material (coating material) to vaporize it so it can travel to the substrate material (material that is coated). To work the chamber needs to be vacuum-purified meaning that it is pumped to high enough vacuum before letting the necessary plasma gases in. This leaking is done in a controlled fashion measuring the amounts of gasses leaked into the chamber, while at the same time pumping the chamber. [96, 97]

The methods used to vaporize target material can be divided to thermal and nonthermal methods [96]. Thermal methods include heating deposited material by various means to cause evaporation. Nonthermal methods include sputtering where ejection of deposited material is induced by bombardment of ions. The ions are excited with alternating current and focused on the target material by magnetic fields as shown in figure 5.4b [96, 97]. It can be thought, that the hit target material is very briefly and locally heated for a short time to a high temperature causing it to evaporate into the chamber, where it will be colliding with the plasma gases while travelling towards the substrate, where it will travel and do most of its possible diffusion and chemical reactions on the surface. If the substrate surface is rough, then the now adsorbed atom (adatom) can travel deeper into the substrate face before nucleating or joining previous

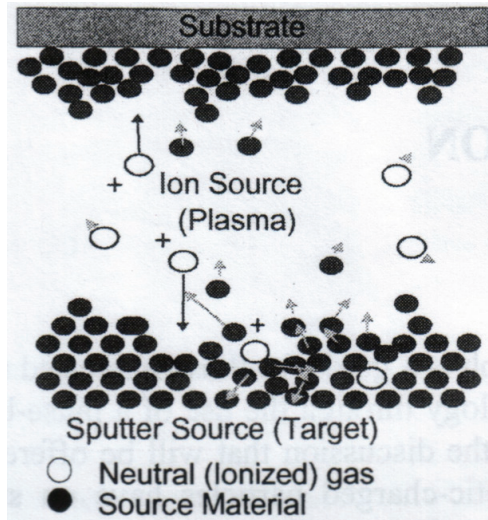


**Figure 5.3.** The principle of material transfer from the target to the substrate in magnetron sputtering [98].

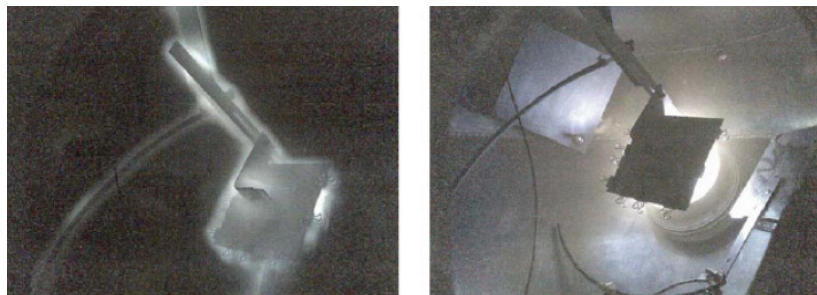


**Figure 5.4.** a) Plasma-activation plasma treatment corona around plastic substrate holder. b) Magnetron sputtering for the metallization of polymer substrates [99].

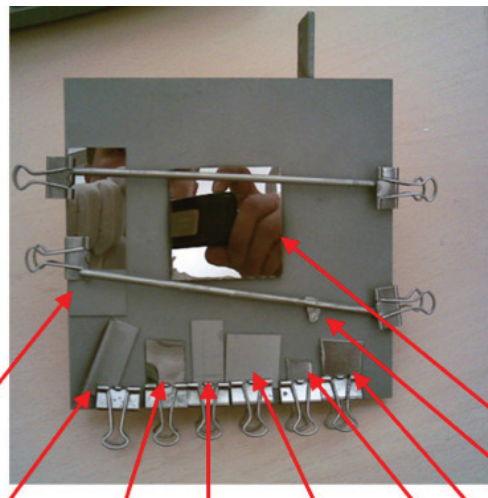


**Figure 5.5.** BMG alloy coated substrates in the used industrial purity substrate holder.

nuclei. In this way the surface roughness of the substrate can increase coating adhesion by inducing mechanical locking between the coating and the substrate [96–98].

The diffusion of metal into polymer substrate depends on the chemical reactivity of the metal with the polymer. If the metal is reactive like Cr or Ti, it will travel a very short distance before immobilizing due to chemical reaction. If the metal is noble and not considered reactive then the distance traveled depends on the deposition rate. At any practical deposition rate a metal film will form on the polymer surface and because these metals are chemically attracted to each other they will not diffuse to the polymer. Only if the deposition rate is so small that the metal film does not have time to form do the metal atoms diffuse deeper into the polymer. Even then these supposedly non-reactive metals significantly reduce local chain movement by temporary metal-atom-induced cross-linking and so stiffen the polymer also making it an effective diffusion barrier for further diffusion [100, 101]. In general, it can be said that metal deposited on polymer surface stays very near to the surface. Without chemical reaction between the polymer side groups or mechanical adhesion from the surface roughness the adhesion will be due to Van der Waals forces. Methods like the plasma treatment in figure 5.4a to increase the diffusion depth at the substrate surface will significantly increase the mechanical adhesion and also affect favorably the mechanical properties of the composite because there will be a less abrupt change in the material properties. Less



**Figure 5.6.** The UHV magnetron sputtering furnace used. The aluminum foil wrapping is for UHV baking the chamber, which is necessary after disassembly to achieve UHV conditions.

abrupt change from metal to polymer will reduce the stress concentration at the interface which will have beneficial effect on adhesion under stress [100, 101]. Usually physical vapor deposited metal on plastic substrates possesses relatively high adhesion. Often adhesion is increased with a surface roughening plasma treatment, like the one shown in figure 5.4a. Irrespective of the precise deposition method used for metallization there are some very powerful adhesion improvement methods that can be used to improve adhesion between metallization and plastic [96, 97, 102–107].

Magnetron sputtering under reduced Ar pressure, discussed in chapter 5, was used to deposit the target alloy onto various substrates without excessive heating. The base pressure of the industrial purity deposition chamber shown in figure 5.4 was  $1 \times 10^{-5}$  mbar. A typical industrial purity coating can be seen in figure 5.5. These tests are compared to the results from a high-purity deposition chamber, shown in figures 5.6, 5.7, and 5.8, with a base pressure less than  $1 \times 10^{-7}$  mbar. A typical high-purity coating can be seen in figure 5.9. The details of this equipment are listed in ref. [22]. Polycarbonate (PC), polymethyl methacrylate (PMMA), polyamide 12 (PA12), polyarylamide (PAA+50GF), polyphenylene sulfide

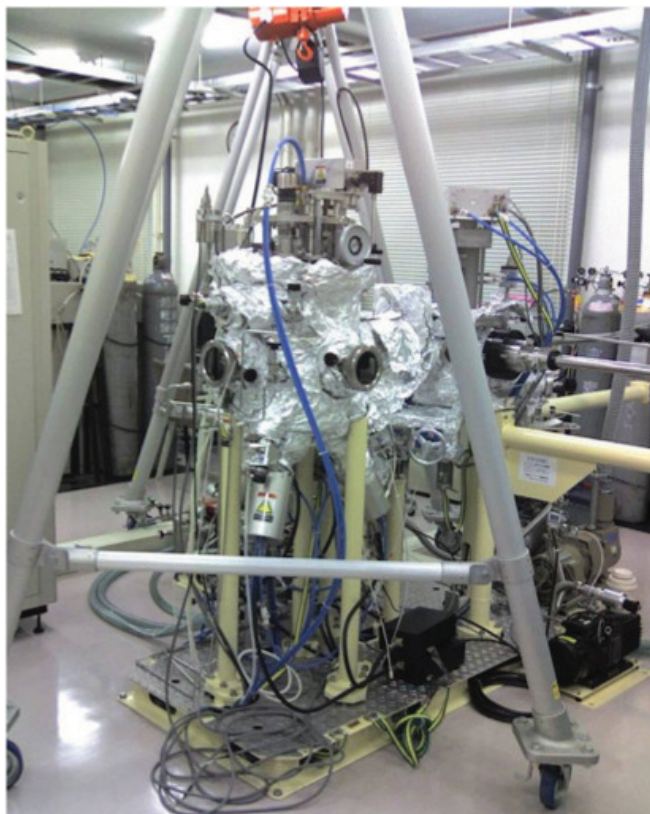


**Figure 5.7.** The UHV magnetron sputtering furnace used. The long horizontal rod on the right of the picture is used to transport the substrates from the load lock to the processing chamber.



**Figure 5.8.** Magnetron sputtering deposition of BMG alloy on a polymer substrate.

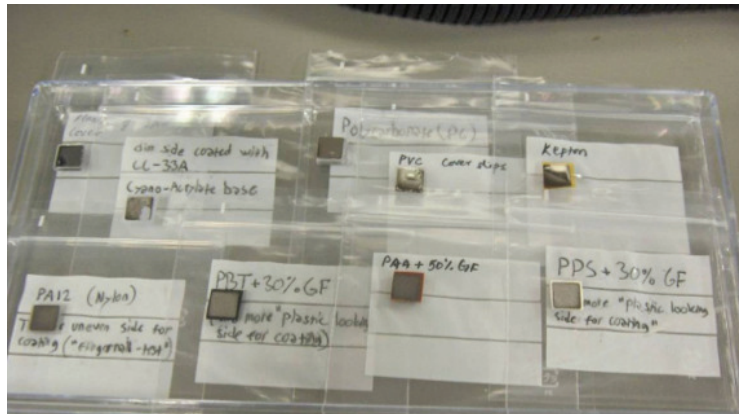


**Figure 5.9.** BMG alloy coated substrates after UHV magnetron sputtering coating.



**Figure 5.10.** Zr-based BMG alloy deposited on a polymer substrate.

(PPS+30GF), polybutylene terephthalate (PBT+30GF) were used as substrates. The numbers in the three last codes refer to the content of glass fibre filler (GF) in weight %. Thin films of about 400 nm were deposited on each polymer substrate.

### 5.2.1 Methods to improve the metal-polymer adhesion

Due to the very high difference in hardness and Young's modulus between polymers and BMG alloys, the interface of the materials may experience large shearing forces unless appropriate measures are taken. These forces together with thermal and mechanical stresses may lead to poor adhesion. As shown in figure 5.11, there are basically three methods that are used, when good mechanical strength is desired at the polymer-metal interface [98]. Surface preparation of a polymer surface before metal deposition can be divided to [96]:

- External cleaning which takes place outside the deposition system in a controlled environment.
  - May include 'gross cleaning' which removes portion of the substrate

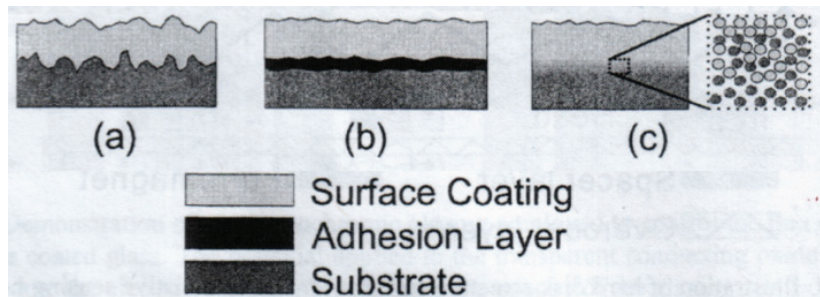


**Figure 5.11.** Methods used to improve adhesion between a substrate and a coating. a) Increased surface area by rough interface. b) Addition of an adhesion layer. c) Interphase region with atomic mixing of the two materials [98].

material.

- May include 'specific cleaning' which removes specific contaminants such as hydrocarbons and salts.
- In-situ cleaning takes place inside the deposition system.
  - For example, hydrocarbon pollution may be removed from some inert enough surfaces with oxygen or tetrafluoromethane ( $\text{CF}_4$ ) plasma [106].

Surface treatments of the polymer substrate can be used to [96, 97, 103]:

- Roughen or smoothen the surface for better mechanical adhesion and wetting. For example, the plasma treatment shown in figure 5.4a.
- Activating the surface by breaking bonds to create chemically reactive side groups for chemical adhesion [103].

The diffusion depth of a metal can be increased with electrodes in suitable potentials which together form an ion gun towards the substrate surface. The ions will hit some of the coating atoms and like billiard balls accelerate them to penetrate deeper into the substrate creating an interphase region between the coating and the substrate as shown in figure 5.12. To some extent ion bombardment will act to remove any poorly adhered deposited material before it is coated over [102]. The ions hitting the growth front have been shown to influence the very initial stages of film growth, including nucleation rates, nucleation densities, and adatom

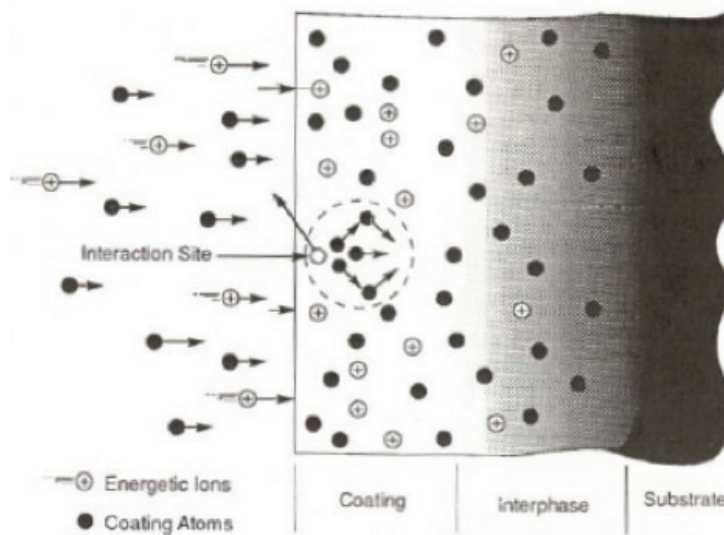


**Figure 5.12.** Physically forced diffusion in ion-beam assisted deposition [102].

(an atom adsorbed on a surface so that it will migrate over the surface) mobilities. These interactions can influence the interface between the substrate and the growing film as well as the final microstructure of the deposited film. In this way ion bombardment (or substrate biasing) significantly increases the parameters to tailor the deposition process for good adhesion basically without any imposed restrictions [98, 104]. Ion-beam assisted deposition can be made to join almost any two materials by just adjusting the bombardment parameters such as using heavier ions at greater velocities when more power is needed. The limit is set by what the substrate material can handle or can be pre-treated or modified to handle [104]. For the specific case of BMG polymer interfaces, the substrate surface roughening by plasma treatment, as shown in figure 5.4a, can produce mechanical locking which provides adhesion. However, the best method to provide high quality interfaces for mechanically demanding applications uses physical force, as shown in figure 5.12, to overcome the lack of diffusion from deposited metal into the polymer substrate. The created interphase region has the added benefit that it reduces any stresses acting on the substrate coating interface.

## 6. Discussion

Metallic glasses are metals that have been solidified by cooling from the molten state to below the glass transition temperature, without crystallizing. They have the amorphous structure of the metallic liquid, but they are not able, in a finite amount of time, to flow into the shape of the container they are in; they are solids. Despite the conceptual simplicity of the amorphous structure —its defining characteristic is that there is no structure above the scale of the fluctuations in a dense random packing of atoms— fundamental questions remain about the nature of the glassy state and the glass transition. Nobel laureate P.W. Anderson has called this the most important open question in solid state physics [108].

Bulk metallic glasses are also technologically relevant. Ordinary metals need to be cooled at extremely high cooling rates,  $>1 \times 10^6 \text{ K s}^{-1}$ , to avoid crystallization and form a glass. This is possible with rapid quenching equipment for thin foils and ribbons, thin wires and small droplets, but not for bulk material. In the 1980's, however, it was realized that there are alloy compositions where crystallization can be avoided already at moderate cooling rates, which can be achieved by fairly conventional metal casting processes for bulk samples. There is still a maximum section thickness that can be cooled quickly enough to avoid crystallization, but this thickness is  $>1 \text{ mm}$  for a critical cooling rate around  $1 \times 10^3 \text{ K s}^{-1}$ , ranging to 100 mm and  $0.1 \text{ K s}^{-1}$  for the very best bulk metallic glasses discovered to date.

Different methods may be used to produce amorphous metals, each with its own advantages and disadvantages, whose relative importance depends on the alloy composition and the intended purpose. Strictly speaking, an amorphous solid is called a glass only if it was formed when a liquid state underwent a glass transition. Thus, metallic glasses are formed by melting the constituents to obtain a molten alloy with the desired com-

position, and then quenching the molten alloy below its glass transition temperature. Often, pre-alloying to obtain the desired composition, and casting to obtain the desired shape while quenching to the glassy state, are entirely separate processes, carried out in different apparatuses.

The methods most frequently used to study bulk amorphous alloys were covered shortly to provide a useful primer for reading the measurement methods used in the publications, that this thesis consists of. The combination of XRD and DSC is probably the most common study performed in metallic glass manufacturing. The compression tests usually aim to study shear banding and the malleability of the studied BMG alloy. The most useful property of instrumented indentation is the measurement of indentation modulus and hardness from a small specimen. Indentation mapping was found to provide useful function in evaluating larger metallic glass specimens for microstructural variations (thesis Paper II).

The manufacturing of bulk metallic glasses is a very specific process, one that usually fails miserably if tried on commonly found metal industry laboratory equipment and process purities. To successfully study the manufacturing of bulk metallic glasses one must study the design and test the different manufacturing methods empirically. All bulk metallic glass manufacture begins with alloying the correct composition; two methods, i.e. induction melting and arc melting were tested. In the case of amorphous coatings, it is possible to co-deposit from multiple target materials and alloy in-situ in the deposition phase, but only single target deposition systems were used in this thesis.

In the scheme of manufacturing, the casting has two conflicting goals that it must succeed. The casting method must solidify the BMG-alloy into right shape and simultaneously cool it fast enough to avoid crystallization, i.e. the faster the cooling rate required the less time there is to fill the mold. If filling the mold is emphasized too much, crystallization occurs and ruins the desired microstructure and possibly also the surface of the cast specimen. If fast cooling is emphasized too much a freeze-frame of the metal about to fill the mold is captured in a glassy specimen of wrong—and probably useless—shape. The different casting methods also significantly influence the mechanical properties of the solidified glassy alloy. The die casting methods, which excel in filling even complex molds compromise on mechanical properties by producing a lot of microscopic flaws and inclusions into the cast material. Suction casting and tilt casting produce better mechanical properties but are also more difficult to

use in the production of complex shapes. Ideally bulk metallic glass caster wants the formability of die casting with the mechanical properties of tilt casting.

Thermoplastic formability of bulk metallic glasses has larger formability than die casting, and the preforms can be manufactured with high quality sample producing methods such as suction and tilt casting. Thermoplastic forming does not replace casting, because it still needs a glassy (or deposited amorphous in the case of physical vapor deposition) preform. The quality and shape of the glassy preform significantly influence the quality of the thermoplastically shaped sample. The most important benefit of thermoplastic forming of metallic glasses, is that there is significantly bigger processing window than there is in casting, while still avoiding crystallization. Also the process purity requirements are not as strict, i.e. the processing can be done without vacuum chambers even in air atmosphere. To fully utilize the benefits of thermoplastic forming methods for large aspect ratio specimen production, it is necessary to minimize or eliminate the mold–supercooled-liquid interface friction caused shearing in the supercooled liquid. These shear minimizing methods include blow-molding and tensile viscous forming. Currently a significant part of the processing window is wasted by inefficient contact heating of the metallic glass preform, the use of induction heating and capacitive discharge heating can be used to improve the achieved results.

Physical vapor deposition does not directly produce metallic glass, as the metallic material is not molten during the process, instead individual atoms are mobile (and energized) during their travel from their target origin to the substrate final destinations. However, if the PVD is carried out in a pure enough environment, the resulting amorphous coating can be reheated for thermoplastic patterning or shaping, and if it is subsequently cooled fast enough, a literally glassy coating results. PVD provides extremely versatile amorphous metal shaping possibilities, mostly limited by the shaping of the substrate, but most importantly, it is possible to coat sensitive materials, which can not withstand the casting temperatures of the BMG. These materials include microchip silicon wafers and various polymers. When PVD methods are used, whether to improve metal part fatigue and corrosion resistance, or coat heat sensitive materials, the composite part quality requires good adhesion between the coating and substrates. This adhesion and the steepness of mechanical property change needs to be controlled to produce the best quality products. The downside

of PVD is that it is relatively slow for anything except thin coatings, and the quality of these coatings is sensitive to all impurities they encounter while in atomized state. Ultra-high-vacuum chambers need to be used for nominal composition  $Zr_{55}Cu_{30}Al_{10}Ni_5$  coatings, which are subsequently used for thermoplastic processes.

## 7. Conclusions

A novel combined tilt-casting arc-melting furnace was designed and constructed for the preparation of high-quality bulk metallic glass specimens. Using this apparatus, the complete process from pre-alloying to final casting can be carried out in one sequence, without need to vent and re-establish the inert atmosphere. Specimens of  $Zr_{55}Cu_{30}Al_{10}Ni_5$  cast into cylinders up to 10 mm diameter using this apparatus were confirmed to be glassy and to exhibit fracture behavior similar to the highest-quality specimens of this alloy studied elsewhere. Also, a glassy  $Zr_{55}Cu_{30}Al_{10}Ni_5$  (in at.%) ring with outer diameter of 25 mm and 1.8 mm thickness was produced, using the constructed arc-melting tilt-casting furnace. Both tilt and suction casting were used to ensure mold filling. Tilt casting was found to fill one side of the tube mold first, with the rest of the tube circumference filled subsequently by suction casting.

Two methods were tried for tensile viscous flow forming of copper mold cast  $Zr_{55}Cu_{30}Al_{10}Ni_5$  preforms with induction heating, and both methods worked. The glassy microstructure of the drawn wire was verified with X-ray diffraction (XRD) and differential scanning calorimetry (DSC) measurements. The mechanical properties of the produced wires were tested with instrumented indentation to be very similar to those measured from a glassy cast specimen cross-section of the same composition  $Zr_{55}Cu_{30}Al_{10}Ni_5$  (in at.%). Finite element simulation was used to evaluate the performance of the induction heating and specimen geometries. In the first method (symmetric set-up) the focusing of the induction heating was achieved by machining the preform specimen so that the inductive currents heated the middle of the specimen. In the second method (asymmetric set-up) the focusing of the induction heating was accomplished by using preforms with smaller diameter at the lower end, in a bucking coil which minimizes heating in the upper end of the preform. The preforms

used for the asymmetric set-up are simpler to produce than those required for the symmetric set-up. Furthermore, the asymmetric set-up offers the possibility to continue the wire forming process indefinitely in a steady state, as long as the preform does not crystallize and the preform does not run out. Unlike other glassy wire production methods, this method allows some real-time control over the produced wire diameter, which could be very useful for the production of glassy non-linear springs. The presented asymmetric test set-up may also have some potential as a method to characterize thermoplastic forming behavior of different metallic glasses, if more instrumentation is added to monitor the temperature profiles and a more comprehensive numerical model is constructed to relate the resulting thickness profile to the material parameters.

BMG alloy Zr<sub>55</sub>Cu<sub>30</sub>Al<sub>10</sub>Ni<sub>5</sub> (in at.%) was successfully deposited on various engineering polymer substrates by magnetron sputtering as thin homogeneous layers of about 400 nm. The deposited alloys were shown to have amorphous structure and elemental composition close to the target alloy. According to the crosscut tape tests good adhesion was achieved between the studied BMG alloy and all other polymer substrates with the exception of polycarbonate. The mechanical properties of coating and cast BMG appear similar when tested with the same method. These results with the novel BMG-polymer hybrid structures look promising and may open new opportunities for BMG alloy applications.

The research hypothesis of this thesis was that there remain significant opportunities for improvement of processing facilities used in bulk metallic glass research. Further it was thought that studying and developing such facilities contributes both to practical applications of these materials and to advances in basic science of liquid and amorphous states of matter. Based on the obtained results, it is safe to say that the development of practical applications has been advanced, by proposing and verifying several innovations that reduce the cost of manufacture of bulk metallic glasses while increasing the quality of the produced specimens. With the development of the combined arc melting and tilt casting furnace, the increase in quality dominates, although the ability to produce samples with a single apparatus also lowers the initial cost to start producing high-quality bulk metallic glass specimens in limited quantities. The custom-designed and -built tensile forming facility lowers cost by drastically simplifying and streamlining the preform preparation process. Furthermore, it provides new manufacturing possibilities, e.g., to make controlled vari-

able diameter wires for non-linear spring applications. Advances in the basic science of metallic glasses are expected on two fronts. Firstly, more widespread availability of the highest quality bulk metallic glass specimens will contribute indirectly to the research on these specimens. Secondly, the asymmetric viscous forming set-up has potential as a method to characterize and study thermoplastic forming behavior of different metallic glasses. Therefore, the goals of the research have been achieved.



# Bibliography

- [1] E. Soinila, T. Pihlajamäki, S. Bossuyt, H. Hänninen, Tilt casting arc melter, Finnish patent application. No. FI-20115527, Status: Examination, 2010.
- [2] M. Miller, P. K. Liaw, Bulk metallic glasses, Springer, USA, first edition, 2008.
- [3] R. Cotterill, The material world, Cambridge University Press, Cambridge CB2 8RU, UK, second edition, 2008.
- [4] A. Inoue, B. L. Shen, A. Takeuchi, Materials Transactions 47 (2006) 1275–1285.
- [5] W. H. Wang, C. Dong, C. H. Shek, Materials Science and Engineering Review 44 (2004) 45–89.
- [6] C. A. Schuh, T. C. Hufnagel, U. Ramamurty, Acta Materialia 55 (2007) 4067–4109.
- [7] M. Rageghi, Fundamentals of solid state engineering, Kluwer Academic Publishers, USA, first edition, 2002.
- [8] A. Inoue, A. Takeuchi, Acta Materialia 59 (2011) 2243–2267.
- [9] K. Takenaka, T. Wada, N. Nishiyama, H. Kimura, A. Inoue, Materials Transactions 46 (2005) 1720–1724.
- [10] M. F. Ashby, A. L. Greer, Scripta Materialia 54 (2006) 321–326.
- [11] F. Spaepen, Acta Metallurgica 25 (1977) 407–415.
- [12] C. A. Schuh, A. C. Lund, T. G. Nieh, Acta Materialia 52 (2004) 5879–5891.
- [13] R. Maas, D. Klaumünzer, J. F. Löffler, Acta Materialia 59 (2011) 3205–3213.
- [14] R. D. Conner, W. L. Johnson, N. E. Paton, W. D. Nix, Journal of Applied Physics 94 (2003) 904–911.
- [15] B. Lemley, Discover 25 (2004) 45–51.
- [16] M. F. Ashby, Materials selection in mechanical design, Butterworth-Heinemann, England, 2 edition, 1999.

- [17] A. Inoue, Introduction, <<http://www.inoue.imr.tohoku.ac.jp/en/intro.html>>, 2007. Laboratory of non-equilibrium materials, Tohoku University.
- [18] A. L. Greer, K. L. Rutherford, I. Hutchings, International Materials Reviews 47 (2002) 87–112.
- [19] Y. Yokoyama, S. Fukumoto, Y. Oka, M. Yatsuzuka, H. Tsubakino, A. Inoue, Materials Transactions 47 (2006) 1999–2005.
- [20] F. X. Liu, C. L. Chiang, J. P. Chu, Y. F. Gao, P. K. Liaw, Materials Research Society Symposium Proceedings 903 (2006).
- [21] C. L. Chiang, F. X. Liu, P. K. Liaw, R. A. Buchanan, Applied Physics Letters 88 (2006) 1–3.
- [22] P. Sharma, N. Kaushik, H. Kimura, Y. Saotome, A. Inoue, Nanotechnology 18 (2007) 1–6.
- [23] C. T. Pan, T. T. Wu, M. F. Chen, Y. C. Chang, C. J. Lee, J. C. Huang, Sensors and Actuators 141 (2008) 422–431.
- [24] T. Miyashita, Japanese Journal of Applied Physics 46 (2007) 5391–5396.
- [25] A. Inoue, T. Zhang, Materials Transactions 37 (1996) 185–187.
- [26] S. Hata, Y. Liu, T. Kato, A. Shimokohbe, 10th International Conference on Precision Engineering (ICPE) (2001).
- [27] J. Schroers, Advanced Materials 22 (2010) 1566–1597.
- [28] M. D. Demetriou, M. Launey, G. Garrett, J. P. Schramm, D. Hofman, W. L. Johnson, W. R. Ritchie, Nature Materials 10 (2011) 123–128.
- [29] J. Schroers, W. L. Johnson, Physical Review Letters 93 (2004) 255506.
- [30] K. F. Yao, F. Ruan, Y. Q. Yang, N. Chen, Applied Physics Letters 88 (2006) 122106.
- [31] Y. Yokoyama, K. Fujita, A. R. Yavari, A. Inoue, Philosophical Magazine Letters 89 (2009) 322–334.
- [32] Y. Yokoyama, H. Tokunaga, A. R. Yavari, M. Yamada, T. Yamasaki, K. Fujita, A. Inoue, Intermetallics 19 (2011) 1683–1687.
- [33] G. Kumar, T. Ohkubo, K. Hono, Scripta Materialia 57 (2007) 173–176.
- [34] J. J. Lewandowski, M. Shazly, A. Nouri, Scripta Materialia 54 (2006) 337–341.
- [35] C. C. Hays, C. P. Kim, W. L. Johnson, Materials Science and Engineering 304–306 (2001) 650–655.
- [36] D. Hofman, J. Suh, A. Wiest, M. Lind, M. D. Demetriou, W. L. Johnson, Proceedings of the National Academy of Sciences 105 (2008) 20136–20140.
- [37] S. Pauly, S. Gorantia, G. Wang, U. Kühn, J. Eckert, Nature Materials 9 (2010) 473.
- [38] E. S. Park, D. H. Kim, T. Ohkubo, K. Hono, Journal of Non-crystalline Solids 351 (2005) 1232–1238.

- [39] A. L. Greer, *Materials Today* 12 (2009) 14–22.
- [40] J. Schroers, C. Veazey, W. L. Johnson, *Applied Physics Letters* 82 (2003) 370–372.
- [41] I. Seki, D. V. Louzguine-Luzgin, A. Inoue, *Materials Transactions* 48 (2007) 821–825.
- [42] Y. Yokoyama, P. K. Liaw, M. Nishijima, K. Hiraga, R. A. Buchanan, A. Inoue, *Materials Transactions* 47 (2006) 1286–1293.
- [43] H. Kakiuchi, A. Inoue, M. Onuki, Y. Takano, T. Yamaguchi, *Materials Transactions* 42 (2001) 678–681.
- [44] W. H. Kui, A. L. Greer, D. Turnbull, *Applied Physics Letters* 45 (1984) 616–617.
- [45] A. Inoue, N. Nishiyama, *MRS Bulletin* 32 (2007) 651–658.
- [46] G. Xie, W. Zhang, D. V. Louzguine-Luzgin, H. Kimura, A. Inoue, *Scripta Materialia* 55 (2006) 687–690.
- [47] C. Y. Luo, Y. H. Zhao, X. K. Xi, G. Wang, D. Q. Zhao, M. X. Pan, W. H. Wang, S. Z. Kou, *Journal of Non-crystalline Solids* 352 (2006) 185–188.
- [48] J. H. Kim, J. S. Park, H. T. Jeong, W. T. Kim, D. H. Kim, *Materials Science and Engineering* 386 (2004) 186–193.
- [49] J. Schroers, *JOM* 57 (2005) 35–39.
- [50] J. Schroers, Q. Pham, A. Peker, N. E. Paton, R. V. Curtis, *Scripta Materialia* 57 (2007) 341–344.
- [51] B. Zhang, D. Q. Zhao, M. X. Pan, W. H. Wang, A. L. Greer, *Physical Review Letters* 94 (2005) 205502.
- [52] Y. Liu, S. Hata, K. Wada, A. Shimokohbe, *Japanese Journal of Applied Physics* 40 (2001) 5382–5388.
- [53] Y. Zeng, N. Nishiyama, T. Wada, D. Louzguine-Luzkin, A. Inoue, *Materials Transactions* 47 (2006) 175–178.
- [54] A. Castellero, S. Bossuyt, M. Stoica, J. Deledda, G. Eckert, G. Z. Chen, D. J. Fray, A. L. Greer, *Scripta Materialia* 55 (2006) 87–90.
- [55] B. D. Cullity, S. R. Stock, *Elements of X-ray diffraction*, Prentice-Hall, USA, 3 edition, 2001.
- [56] R. Busch, E. Bakke, W. L. Johnson, *Acta Materialia* 46 (1998) 4725–4732.
- [57] E. Watson, Differential microcalorimeter, U.S. Patent No. 3,263,484, 1966.
- [58] D. Klaumünzer, R. Maas, F. H. Dalla Torre, J. F. Löfller, *Applied Physics Letters* 96 (2010) 061901.
- [59] F. H. Dalla Torre, D. Klaumünzer, R. Maas, J. F. Löfller, *Acta Materialia* 58 (2010) 3742–3750.
- [60] W. Oliver, G. Pharr, *Journal of Materials Research* 7 (1992) 1564–1583.

- [61] J. Eckert, A. Kübler, L. Schultz, *Journal of Applied Physics* 85 (1999) 904–911.
- [62] C. Suryanarayana, A. Inoue, *Bulk metallic glasses*, CRC Press, USA, first edition, 2011.
- [63] E. Soinila, High strength amorphous copper alloys, M.S. thesis, Helsinki University of Technology, Laboratory of Engineering Materials, 2005.
- [64] I. Heating, Induction skull melting offers Ti investment casting benefits, 2001. Retrieved 4.2.2005.
- [65] A. Sneyd, H. K. Moffatt, *Journal of Fluid Mechanics* 117 (1982) 45–70.
- [66] E. Okress, D. Wroughton, G. Comenetz, P. Brace, J. C. K. Kelly, *Journal of Applied Physics* 23 (1982) 545–552.
- [67] D. Herlach, R. Cochrane, I. Egry, H. J. Fecht, A. L. Greer, *International Materials Reviews* 38 (1993) 273–347.
- [68] E. Fromm, H. John, *British Journal of Applied Physics* 16 (1965) 653–663.
- [69] S. Arajs, G. P. Wray, *Journal of Scientific Instruments (Journal of Physics e)* 2 (1969) 518–520.
- [70] G. J. Bowden, R. Day, *Journal of Scientific Instruments (Journal of Physics e)* 4 (1971) 922–923.
- [71] S. Wu, B. L. Shen, A. Inoue, *Intermetallics* 1-4 (2004) 1261–1264.
- [72] A. Wiest, J. S. Harmon, M. D. Demetriou, R. D. Conner, W. L. Johnson, *Scripta Materialia* 60 (2009) 160–163.
- [73] A. Inoue, T. Nakamura, N. Nishiyama, T. Matsumoto, *Materials Transactions* 33 (1992) 937–945.
- [74] A. Inoue, T. Nakamura, T. Sugita, T. Zhang, T. Masumoto, *Materials Transactions* 34 (1993) 351–358.
- [75] A. Inoue, T. Zhang, *Materials Transactions* 36 (1995) 1184–1187.
- [76] Y. Yokoyama, K. Fukaura, A. Inoue, *Intermetallics* 10 (2002) 1113–1124.
- [77] Y. Yokoyama, E. Soinila, personal communication, 2007.
- [78] V. Keryvin, C. Bernard, J. C. Sangleboeuf, Y. Yokoyama, T. Rouxel, *Journal of Non-crystalline Solids* 352 (2006) 2863–2868.
- [79] J. Wall, C. Fan, P. K. Liaw, C. Liu, T. Choo, *Review of Scientific Instruments* 77 (2006) 2863–2868.
- [80] S. Bossuyt, Microstructure and crystallization behavior in bulk glass forming alloys, PhD dissertation, CalTech, 2001.  
< <http://etd.caltech.edu/etd/available/etd-07022001-164944/unrestricted/Bossuyt.pdf> >.
- [81] X. C. Zhang, Y. Zhang, X. Chen, G. Chen, *International Journal of Minerals, Metallurgy and Materials* 16 (2009) 108–111.

- [82] C. Ma, N. Nishiyama, A. Inoue, Materials Science and Engineering A 407 (2005) 201–206.
- [83] Y. Yokoyama, E. Mund, A. Inoue, L. Schultz, Materials Transactions 48 (2007) 3190–3192.
- [84] Y. Saotome, K. Itoh, T. Zhang, A. Inoue, Scripta Materialia 44 (2001) 1541–1545.
- [85] A. Kundig, A. Dommann, W. L. Johnson, P. Uggowitzer, Materials Science and Engineering A 375 (2004) 327–331.
- [86] G. Kumar, H. X. Tang, J. Schroers, Nature 457 (2009) 868–872.
- [87] Y. Kawamura, Y. Ohno, Scripta Materialia 45 (2001) 279–285.
- [88] S. Bossuyt, J. Schroers, The role of friction in measurements of the formability of bulk metallic glasses, 2009. TMS Annual meeting.
- [89] J. Schroers, Acta Materialia 56 (2008) 471–478.
- [90] W. L. Johnson, G. Kaltenboeck, M. D. Demetriou, J. P. Schramm, X. Liu, K. Samwer, P. Kim, D. C. Hofmann, Science 332 (2011) 828–833.
- [91] T. Nagase, K. Kinoshita, Y. Umakoshi, Materials Transactions 49 (2008) 1385–1394.
- [92] T. Masumoto, A. Ohnaka, A. Inoue, M. Hagiwara, Scr. Metall. 15 (1981) 293–296.
- [93] K. Son, H. Soejima, N. Nishiyama, X. M. Wang, A. Inoue, Materials Science and Engineering A 449 (2007) 248–252.
- [94] A. Inoue, Proc. Japan Acad. 73 (1997) 19–24.
- [95] A. I. Salimon, M. F. Ashby, Y. Brechet, A. L. Greer, Materials Science and Engineering A 375 (2004) 385–388.
- [96] D. M. Mattox, Growth and growth-related properties of films formed by physical vapor deposition, volume 5 of *ASM Handbook Surface Engineering*, ASM, Metals Park, Ohio, 10 edition, pp. 538–555.
- [97] D. Rohde, Sputter deposition, volume 5 of *ASM Handbook Surface Engineering*, ASM, Metals Park, Ohio, 10 edition, pp. 573–581.
- [98] E. V. Barnat, T. Lu, Pulsed and pulsed bias sputtering principles and applications, Kluwer Academic Publishers, USA, first edition, 2003. A full BOOK entry.
- [99] E. Soinila, P. Sharma, M. Heino, K. Pischedow, A. Inoue, H. Hänninen, New amorphous alloys in metal layers, 2008. Presentation at MIICS 2008.
- [100] F. Faupel, R. Willecke, A. Thran, Materials Science and Engineering Review 22 (1998) 1–55.
- [101] W. J. Tian, H. Y. Zhang, J. C. Shen, Surface Review and Letters 4 (1997) 703–708.

- [102] R. Moody, T. G. Tetreault, J. Hirvonen, Enhanced metal/polymer adhesion by ion assisted deposition, *Metallized plastics 2 fundamental and applied aspects*, Plenum Press, Canada, first edition, 1991.
- [103] C. S. Rastomjee, M. Keil, H. Sotobayashi, A. M. Bradshaw, C. L. A. Lamont, D. Gador, E. Umbach, *Applied Surface Science* 136 (1998) 280–297.
- [104] G. K. Hubler, J. Hirvonen, Ion-beam assisted deposition, volume 5 of *ASM Handbook Surface Engineering*, ASM, Metals Park, Ohio, 10 edition, pp. 593–601.
- [105] E. David, A. Lazar, A. Armeanu, *Materials Processing Technology* (2004) 284–289.
- [106] W. Li, R. Charters, B. Luther-Davies, L. Mar, *Applied Surface Science* 233 (2004) 227–233.
- [107] J. Cognard, C. R. Chimie (2004) 13–24.
- [108] P. W. Andersen, *Science* 267 (1995) 1616.

# Publication I

Erno Soinila, Parmanand Sharma, Markku Heino, Kaj Pischedow, Akihisa Inoue, Hannu Hänninen. Bulk metallic glass coating of polymer substrates. *Journal of Physics: Conference Series*, 144, 012051, 1–4, doi:10.1088/1742-6596/144/1/012051, 2009.

© 2009 IOP Publishing.  
Reprinted with permission.



## Bulk metallic glass coating of polymer substrates

**Erno Soinila<sup>1</sup>, Parmanand Sharma<sup>2</sup>, Markku Heino<sup>3</sup>, Kaj Pischedow<sup>4</sup>, Akihisa Inoue<sup>2</sup> and Hannu Hänninen<sup>1</sup>**

<sup>1</sup> Laboratory of Engineering Materials, Helsinki University of Technology, Espoo, Finland.

<sup>2</sup> Institute for Materials Research, Tohoku University, Sendai, 980-8577, Japan.

<sup>3</sup> Nokia Research Center, NanoSciences, Itämerentie 11-13, 00180 Helsinki, Finland.

<sup>4</sup> Savcor Coatings, Insinöörikatu 7, 50100 Mikkeli, Finland.

E-mail: erno.soinila@hut.fi

**Abstract.** Bulk Metallic Glass (BMG) alloy with the composition of Zr<sub>55</sub>Cu<sub>30</sub>Al<sub>10</sub>Ni<sub>5</sub> was deposited by sputtering as thin films on several different engineering polymers and polymer composites. Polycarbonate, polymethyl methacrylate, polyamide 12, polyarylamide (50GF=50 % glass fibers), polyphenylene sulfide (30GF) and polybutylene terephthalate (30GF) were used as substrates. The microstructure of the deposited BMG coatings was studied by X-ray diffraction (XRD) and scanning electron microscopy (SEM). The results of XRD and SEM studies were consistent with amorphous microstructure. Elemental compositions of the coatings were verified by energy dispersive spectroscopy (EDS). Mechanical properties of the coatings were compared to copper mould cast BMG using nano-indentation tests with similar results. According to the cross-cut tape tests good adhesion was achieved between the studied BMG alloy and all other polymer substrates except polycarbonate. Nano-indentation results showed similar mechanical properties for coating and cast BMG. The results of this study look promising as they open new opportunities for BMG-polymer composite applications.

### 1. Introduction

Bulk metallic glasses (BMG) are amorphous metals that can be cast into a copper mould with a diameter larger than 1 mm before detectable crystallization appears [1]. In heating these alloys often have a glass transition temperature ( $T_g$ ), followed by a super-cooled liquid region (SLR) before crystallizing. Enhanced stability against crystallization is usually achieved by alloying multiple elements with significant size difference in atomic radius above 12 % and negative heats of mixing among the constituent elements. Typically the obtainable critical casting diameters of known BMG alloys range from 1 to ~100 mm depending on the alloy composition and process conditions. BMG alloys have been found in many different alloy groups and new alloys have been discovered and reported with a variety of different properties. The known alloy groups include Mg-, La-, Zr-, Ti-, Fe-, Co-, Pd-Cu-, Ni- and Cu-based systems. Because of the large number of possible alloy compositions and the atomic level structures, adjusting mechanical properties, electrical resistance, corrosion resistance and magnetic properties can be done in large degree with relatively minor alloying changes.

With BMG alloys it is possible to achieve different combinations of strength, stiffness and ductility. Properties reported in the literature include very high strength in the as-cast state, typically ranging from 1500 to more than 5500 MPa, and Young's modulus ranging from 70 to 275 GPa with unusually large elastic strain of almost 2 % compared to crystalline alloys [2]. The lack of grain boundaries produces very accurate surface finishes and enhances corrosion resistance.

The methods to produce BMG alloys are combinations of high-vacuum melting of the elements for alloying and various ways to solidify the end-product in the desired shape. The most used methods to produce relatively large components are copper mould casting, quench casting and sintering from atomized powder [7, 8]. The most studied methods to produce coatings include high velocity oxygen fuel (HVOF) and physical vapour deposition such as magnetron sputtering [5, 6]. BMG alloys can be very accurately deformed in the SLR region without causing crystallization, either during cooling from the molten state or with a separate reheating from the quenched state.

The wider industrial use of BMG alloys suffers from the costly high purity requirements of the materials and the manufacturing processes. Here we study the possibility of minimizing the amount of high strength BMG and the possibility to use the known processability of polymers to produce hybrid material parts with high contact strength surface and high specific strength interior. To evaluate the feasibility of these BMG-polymer composites it is necessary to determine if it is possible to create sufficient adhesion between the two and what the properties of the deposited BMG alloy are.

Although many results of BMG coating of various substrates have been published and made, so far we have not found any published studies of BMG coating of polymer substrates. We have studied here the possibility to deposit one BMG alloy on selected engineering polymer substrates using magnetron sputtering. The coating micro-structure, composition, hardness, Young's modulus and adhesion to the substrate were evaluated.

## 2. Experimental

Target alloy of composition Zr<sub>55</sub>Cu<sub>30</sub>Al<sub>10</sub>Ni<sub>5</sub> (at-%) was weighed from the elements of Zr (+Hf) 99.99 mass-%, Cu 99.999 mass-%, Ni 99.99 mass-% and Al 99.99 mass-% purity. The cut and weighed pieces were melted in a titanium gettered laboratory arc-melter under reduced pressure in argon atmosphere. The vacuum-chamber was evacuated to a vacuum of higher than 1E-3 Pa before filling the chamber with argon. The ingot was melted and flipped over five times to ensure even distribution of alloying elements.

The target was machined with a lathe from the ingot to the final dimensions for use in the magnetron sputtering. The cast bulk specimens were manufactured in a casting furnace where they were remelted with induction heater inside a quartz crucible and cast with Ar pressure into a copper mould under vacuum atmosphere better than 1E-3 Pa. The glassy nature of the copper mould cast BMG was verified with X-ray diffraction (XRD) and differential scanning calorimetry (DSC). The compression tests were performed with strain rates  $5 \times 10^{-6}$ ,  $1 \times 10^{-5}$ ,  $5 \times 10^{-5}$  and  $1 \times 10^{-4} \text{ s}^{-1}$  with an Instron-type machine. The Young's moduli were obtained from recorded strain-gage data. Magnetron sputtering under reduced Ar pressure was used to deposit the target alloy to various substrates without heating them too much. The base pressure of the industrial purity deposition chamber was 1E-3 Pa. These tests are compared to the results from a high purity deposition chamber with base pressure <1E-5 Pa. The details of this equipment are listed in ref. [5].

Polycarbonate (PC), polymethyl methacrylate (PMMA), polyamide 12 (PA12), polyarylamide (PAA+50GF), polyphenylene sulfide (PPS+30GF), polybutylene terephthalate (PBT+30GF) were

used as substrates. The numbers in the last three codes refer to the content of glass fibre filler (GF) in weight %. Thin films of about 400 nm were deposited on each polymer substrate.

The microstructures of the deposited alloys were studied with Zeiss Ultra 55 field emission gun scanning electron microscope (FEG-SEM) and the elemental composition was analyzed with Bruker AXS energy dispersive spectrum (EDS) analyzer connected to the SEM. The X-ray diffraction (XRD) patterns of the samples were analyzed with Siemens Kristalloflex 710H X-ray generator and Inel CPS 120 position sensitive detector. Transmission electron microscopy (TEM) samples were prepared with Leica UC6 ultramicrotome using a diamond knife and studied with FEI 120 kV LaB6 electron gun and Gatan UltraScan CCD 2048\*2048 pix detector for pictures and CCD 1392\*1040 pix for transmission electron microscopy selected area electron diffraction (TEM-SAED) pattern. Adhesion of the BMG coating to the polymer substrates was studied with tape tests and cross-cut tape tests. The nano-indentation results were measured with a CSM Ultra Nanoindentation Tester.

### 3. Results and Discussion

Elemental compositions of the coatings were characterized by FEG-SEM and EDS and they were compared to the target composition. Coatings made by both industrial purity process ( $Zr_{54.7}Cu_{32.0}Al_{6.8}Ni_{6.6}$ ) as well as the high purity process ( $Zr_{49.2}Cu_{27.4}Al_{14.9}Ni_{8.5}$ ) were rather close to the intended composition  $Zr_{55}Cu_{30}Al_{10}Ni_5$  (at%). Composition of deposit varied slightly with different sputtering parameters. Ni and Cu contents were measured to be slightly higher than the composition of the target alloy. The exceptionally large 30 mm critical casting diameter of the target alloy ensures that the deposited alloy is in the high glass forming region.

X-ray diffraction patterns shown in figure 1 were obtained to determine the structure of the deposited coating. The selected area diffraction pattern in figure 2 does not show any indication of crystallization, but does show the diffuse ring characteristic of an amorphous structure. According to Chen and Spaepen, amorphous structure can be difficult to distinguish from ultra-fine-grained polycrystals without DSC-measurements [3]. The cross-section in figure 2 shows a section of characteristic smooth BMG coating on the polyamide substrate. The TEM sample was prepared by cutting the hard BMG coating on top of a very soft polyamide substrate with an ultramicrotome having Ø1 nm diamond edge. Based on the XRD, TEM and TEM-SAED results, it can be stated that the studied coating material is amorphous. This is in good accordance with the DSC studies of the same alloy reported in literature in sputtered[5] and cast[4] form.

The adhesion test results indicate that the studied BMG alloy can be coated on various polymer substrates by magnetron sputtering. The coating was successfully attached to all studied polymers except polycarbonate. The mechanical test results in table 1 and the similarity of the load-displacement patterns of figures 3 and 4 show that the mechanical properties of the coatings are similar to copper mould cast BMG when tested with the same method.

**Table 1.** Mechanical property test results.

	Coating	Cast BMG	Coating (literature) [5]
Hardness (nano-indentation) <sup>1</sup>	$9.1 \pm 0.2$ GPa	$8.0 \pm 0.1$ GPa	10.3 GPa
Young's modulus (nano-indentation)	$130 \pm 5.6$ GPa	$118 \pm 2.3$ GPa	128 GPa
Hardness HV <sub>1</sub>	-	$489 \pm 16$ HV <sub>1</sub> ( $3.45 \times 0.489 = 1.7$ GPa)	-
Young's modulus <sup>2</sup> (compression test)	-	$93 \pm 2.3$ GPa	-

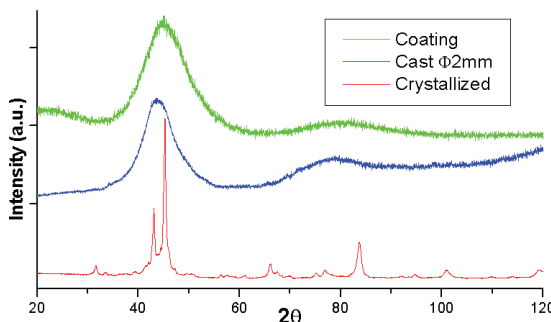


**Figure 1.** X-ray diffraction (Co K<sub>α</sub>) patterns of deposited coating (top), cast bulk sample (middle) and arc-melted ingot (bottom)

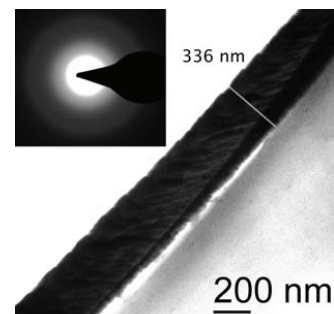


**Figure 2.** Selected Area Electron Diffraction and ultramicrotomy of the cross-section of the coating.

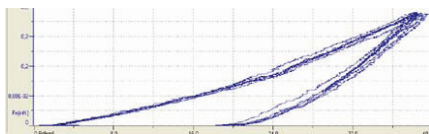


**Figure 3.** Nano-indentation load-displacement of the industrial purity coating.

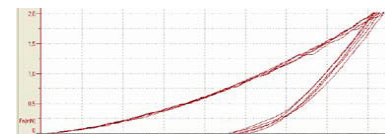


**Figure 4.** Nano-indentation load-displacement of the cast BMG.

#### 4. Conclusions

BMG alloy Zr<sub>55</sub>Cu<sub>30</sub>Al<sub>10</sub>Ni<sub>5</sub> (at-%) was successfully deposited on various engineering polymer substrates by magnetron sputtering as thin homogeneous layers of about 400 nm. The deposited alloys were shown to have amorphous structure and elemental composition close to the target alloy. According to the cross-cut tape tests good adhesion was achieved between the studied BMG alloy and all other polymer substrates with the exception of polycarbonate. The mechanical properties of coating and cast BMG appear similar when tested with the same method. These results with the novel BMG-polymer hybrid structures look promising and may open new opportunities for BMG alloy applications.

#### 5. Acknowledgements

Funding by TEKES is greatly appreciated for making this work possible. This work was done in part while visiting IMR, Institute for Materials Research, Tohoku University, Sendai, Japan. The contribution of various persons at IMR, especially that of Assistant Professor Yoshiko Yokoyama, are appreciated. The efforts of Prof. Janne Ruokolainen with TEM-studies and Savcor R&D team in sputtering experiments are gratefully acknowledged.

#### 6. References

- [1] Schuh C A, Hufnagel T C and Ramamurty U 2007, *Acta Mater.* **55**, 4067-109
- [2] Inoue A, Shen B L and Takeuchi A 2006, *Mater. Trans. JIM* **47**, 1275-85
- [3] Chen L C and Spaepen F 1988, *Nature* **336**, 366-368
- [4] Inoue A 2000, *Acta Mater.* **48**, 279-306
- [5] Sharma P, Kaushik N, Kimura H, Saotome Y and Inoue A 2007, *Nanotechnology* **18**, 035302
- [6] Chiang C, Chu J, Liu F, Liaw P, Buchanan A 2006, *Appl. Phys. Lett.* **88** (13), 131902
- [7] Inoue A and Takeuchi A 2004, *Mat. Sci. and Eng. A* **375-377**, 16-30
- [8] Wang W, Dong C, Shek C 2004, *Mat. Sci. and Eng. R* **44**, 45-89

## Publication II

E. Soinila, K. Antin, S. Bossuyt, H. Hänninen. Bulk metallic glass tube casting. *Journal of Alloys and Compounds*, 509S, 210–213, doi:10.1016/j.jallcom.2010.12.145, 2010.

© 2010 Elsevier.  
Reprinted with permission.





## Bulk metallic glass tube casting

E. Soinila\*, K. Antin, S. Bossuyt, H. Hänninen

Department of Engineering Design and Production, Aalto University, School of Science and Technology, Espoo, Finland

### ARTICLE INFO

#### Article history:

Received 31 July 2010

Received in revised form

17 December 2010

Accepted 17 December 2010

Available online 28 December 2010

#### Keywords:

Bulk metallic glasses

Tubular shape

Atomic force microscopy

Calorimetry

X-ray diffraction

### ABSTRACT

Tubular bulk metallic glass specimens were produced, using a custom-built combined arc-melting tilt-casting furnace. Zr<sub>55</sub>Cu<sub>30</sub>Al<sub>10</sub>Ni<sub>5</sub> tubes with outer diameter of 25 mm and 0.8–3 mm wall thicknesses were cast, with both tilt and suction casting to ensure mold filling. Tilt casting was found to fill one side of the tube mold first with the rest of the tube circumference filled subsequently by suction casting. Optimized casting parameters were required to fully fill the mold and ensure glass formation. Too small melt mass and too low arc power filled the mold only partially. However, too large melt mass and higher arc power which lead to the best mold filling also lead to partial crystallization. Variations in processing parameters were explored, until a glassy ring with 1.8 mm thickness was produced. Different sections of the as-cast ring were investigated by X-ray diffraction (XRD), differential scanning calorimetry (DSC), and instrumented indentation to ensure amorphous microstructure. Atomic force microscopy (AFM) was used to compare the surface qualities of the first- and last-filled sections. These measurements confirmed the glassy structure of the cast ring, and that, the tilt cast tube section consistently showed better surface quality than the suction cast section. Optimized casting parameters are required to fully realize the potential of directly manufacturing complex shapes out of high-purity bulk metallic glasses by tilt casting.

© 2010 Elsevier B.V. All rights reserved.

### 1. Introduction

Metallic glasses are amorphous metals that solidified without detectable crystallization. Upon heating from the solid state these alloys exhibit a glass transition, after which they remain metastable for a finite length of time in the super-cooled liquid region, before crystallizing. For some alloys, rapid quenching is not necessary to avoid crystallization. If the diameter of the glass is larger than 1 mm, it can be called a bulk glass. Enhanced stability against crystallization is usually achieved by alloying multiple elements with significant difference, greater than 12%, in atomic radius and negative heats of mixing among constituent elements. The critical casting diameters of known BMG alloys typically range from 1 mm to 100 mm. BMG alloys have been found in many different alloy groups (Pd-, Mg-, Ln-, Zr-, Ti-, Fe-, Co-, Ni- and Cu-based systems) and new alloys have been discovered and reported with a variety of different properties. By casting BMG alloys, without cold working or heat treatment, complex shapes can be produced with excellent mechanical properties: purely elastic deformation up to a yield strain of typically 2%, resulting in tensile or compressive strength of 1500–5500 MPa, with Young's modulus of 70–275 MPa [1]. The lack of grain boundaries in the BMG materials also results in very

accurate surface finish and enhances corrosion resistance. Several recent reviews testify to the widespread interest in these materials both from a fundamental science perspective and for practical applications [2–4].

For practical applications, the ease of forming complex shapes out of metallic glass is particularly important, but most reports in the academic literature focus on simple shapes achievable with simple molds. Recently a lot of attention has been focused on the use of thermoplastic forming processes or "visco-forming" for manufacturing metallic glass products from cast preforms [5]. Thermoplastic forming allows to form complex shapes that would be practically impossible to produce directly by casting, but does not obviate the need for casting complex shapes. Rather, they are complementary processes, wherein the preform produced by casting provides the right amount of material in the right starting position for the thermoplastic forming step. For example, blow-molding a bottle starts with a parison in the shape of a tube closed at one end [6]. The casting of annular or tubular specimens, in molds requiring a core, allows to investigate some of the issues arising when bulk metallic glasses are cast in complex molds. Such shapes are also relevant for potential practical applications such as annular gaskets, active solder materials [7], jewelry, and enclosures for electronic components. Metallic glass tubes can be used to construct precise Coriolis mass flowmeters [8]. Bulk metallic glass rings or tubes have previously been manufactured by centrifugal casting [9], machining [10], modified water quenching [7], copper mold

\* Corresponding author. Tel.: +358 050 5376172; fax: +358 09 470 23537.  
E-mail address: [Erno.Soinila@hut.fi](mailto:Erno.Soinila@hut.fi) (E. Soinila).

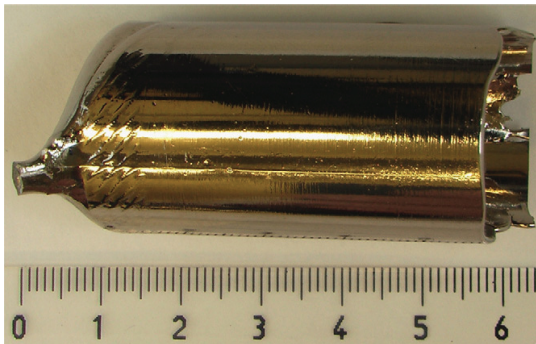


**Fig. 1.** A fully filled casting.

casting [11–13] and coreless mold suction casting [8,14]. Centrifugal casting [9] and suction casting [8,14] were done without a core. Modified water quenching [7] used a fused silica core. The copper mold casting [12,13] used vertical argon pressure ejection of induction-heated melt from a quartz crucible into the ring mold with minimal vertical runner length. MingZhen et al. [11] used a more traditional lip pour ladle with both vertical and horizontal runners before the mold with a copper core.

The published methods for bulk metallic glass tube and ring casting use two furnaces: one for alloy production and another for casting. Often the melt is cooled only from one side, possibly limiting the achievable tube wall thickness. When a core is used, the melt size has been very large, e.g., 780 g in [11], or the length of the ring was the smallest dimension [12,13]. When temporary molds are used [7], the molten alloy comes in contact with fused silica, which may cause embrittlement [15].

Here we study the possibility of casting bulk metallic glass tube into a core mold in one process. With a custom-built furnace, we start from raw materials and break the vacuum only once the tube has been cast. With the same arc melting electrode used in both alloy production and casting, we aim to keep the ingot size under 100 g and waste as little as possible of the melt charge on runners using tilt-casting to avoid the need for vertical runners (Figs. 1 and 2).

## 2. Experimental procedures

Alloy constituents for the target composition of  $Zr_{55}Cu_{30}Al_{10}Ni_5$  (in at.%) were weighed from the elements with purity (in mass%) of 99.99% for Zr(+Hf), 99.99% for Cu, 99.99% for Ni, and 99.99% for Al. The cut and weighed pieces were melted in a custom built combined arc melting and tilt casting furnace under reduced pressure titanium gettered argon atmosphere. The vacuum-chamber was evacuated to a vacuum of better than  $5 \times 10^4$  Pa before filling the chamber with 99.9999% purity argon. Any remaining oxygen in the chamber was reduced by titanium gettering. To ensure an even distribution of the alloying elements, the ingot was melted, observed while it was allowed to crystallize, flipped over and remelted repeatedly, until the crystallization process appeared to follow a uniform and repeatable pattern over several remelting cycles. Once the ingot was deemed mixed, it was melted again for casting. The suction casting line valve was opened and the furnace tilted to tilt cast the melt into a cylindrical mold located at the edge of the copper hearth. The furnace is designed so that these steps can be carried out without opening the chamber to air between the first melting and the final casting, maintaining the high-purity atmosphere throughout the entire process.

In our casting set-up, schematically shown in Fig. 3, filling of the mold begins as the chamber is tilted, when the melt flows over the hump separating the hearth and the mold orifice. The melting arc is still powered during the tilting, keeping the rest of the melt molten as it flows over the hump. However, until the chamber has finished tilting, the melt pours into one side of the mold first. The chamber tilting rate depends on the constriction caused by a pneumatic valve feeding the two pneumatic actuators that tilt the chamber. For best results, the valve is fully opened and tilting takes less than 2.5 s. A small longitudinal draft is used in the core; the diameter of the core increases towards the bottom of the mold to facilitate withdrawing the core from the cast tube.

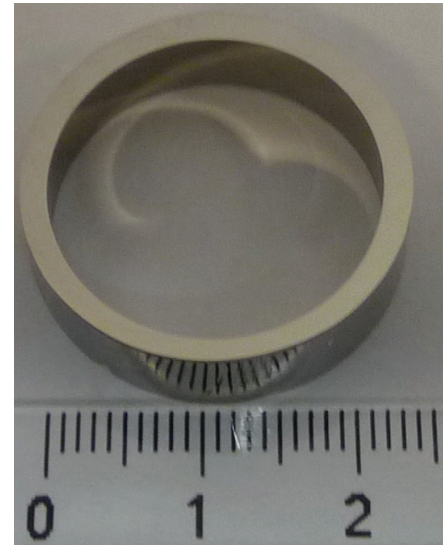


**Fig. 2.** A glassy ring cut in cross-section from the optimized parameter casting.

The X-ray diffraction (XRD) patterns of the cast specimens were measured with a Siemens Kristalloflex 710H X-ray generator and Inel CPS-120 position sensitive detector. Instrumented indentation tests were conducted with a Berkovitch diamond indenter on a CSM Instruments nanoindenter tester. Linear loading with few seconds of holding time was used. The indentation force used was 40 mN.

Contact mode atomic force measurements were done with an AFM-S-AE-004X atomic force microscope ( $xy = 40 \mu\text{m}$ ,  $z = 4 \mu\text{m}$ ) integrated into the nanoindenter platform. A 450  $\mu\text{m}$  long silicon contact probe with  $\leq 10 \text{ nm}$  tip was used in the measurements (Fig. 4).

## 3. Experimental results and discussion

The wall thickness of 0.8–3 mm used in this study is relatively large, allowing the molten alloy to flow into the first-filled portion of the mold cavity during tilt casting, without the application of a suction pressure difference. As a result, preliminary trials using smaller melt charges only filled one side of the mold. A larger melt charge allowed the filling of the entire mold circumference, so that the rest of the mold could be filled by suction casting after the one side was filled by tilt casting. However, there was a longitudinal cold shut running on both sides of the tube. This casting defect, which impacts the mechanical integrity, varied in severity along the length of the tube. Thus, there were very large differences in thermal history between different sections of the casting, with variations both longitudinally along the tube and circumferentially. In essence, one side of the casting was filled quickly, fed from a high-

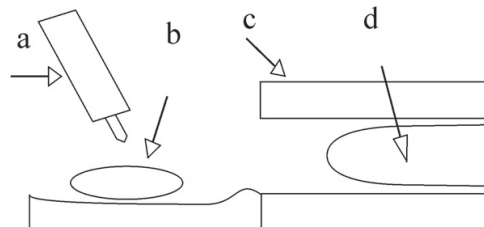


**Fig. 3.** An illustration of the used casting setup with (a) arc melting electrode, (b) molten alloy, (c) mold and (d) core. In casting the setup is tilted clockwise to pour the melt into the mold.

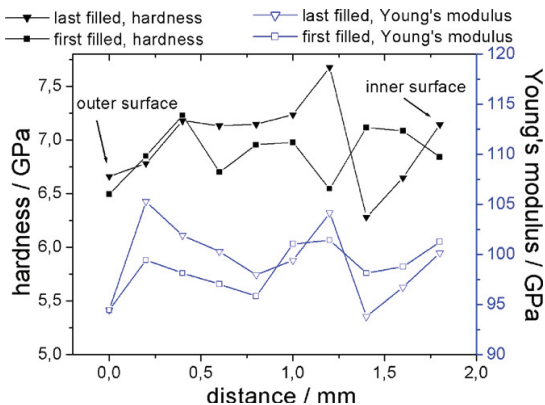


**Fig. 4.** Young's modulus and hardness profiles as a function of the distance from the outer surface to the inner surface for the as-cast ring. Results for both the first-filled and the last-filled sections are shown.

temperature running melt, and near the bottom already solidified, before the other side was filled more slowly, fed from a lower-temperature standing melt, in a mold already preheated by the material on the first-filled side. Nevertheless, both tube halves were found to be fully amorphous when tested by X-ray diffraction and differential scanning calorimetry to be amorphous.

MingZhen et al. [11] discuss the effects of latent heat release from the melt and heat transfer to the mold upon freezing of the melt as the mold is filled. The heat transfer from the melt to the mold is much affected by any created thermal shrinkage gaps between the mold and the specimen surface, and the atmosphere in these gaps [16]. The latent heat is affected by both the size of the melt charge and the power with which it is heated just before casting. To improve the rate at which the second side of the mold is filled during suction casting, in an effort to eliminate the cold shuts, their conclusions indicate a melt charge with more latent heat to begin with should be used. More latent heat would thus need to be removed from the melt before it solidified, simultaneously increasing the time available to fill the mold, and lowering the melt viscosity so that the mold cavity would fill more quickly. In addition, the suction line of the casting setup was modified, increasing its diameter and improving its vacuum sealing. These modifications also reduced the mass of the mold. With improved suction, higher melt mass and higher arc power just before casting, the tube shown in Fig. 1 was produced. The mold was completely filled and the cross-section showed no cold shut formation. Unfor-

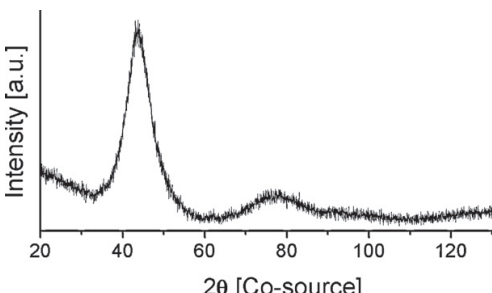


**Fig. 5.** X-ray diffraction ( $\text{Co K}_\alpha$ ) pattern of cast tube segment, showing amorphous structure. Samples were prepared with a water-cooled aluminium oxide impregnated cut-off wheel. Cut-off wheel residue was removed with  $1 \mu\text{m}$  diamond paste polishing.

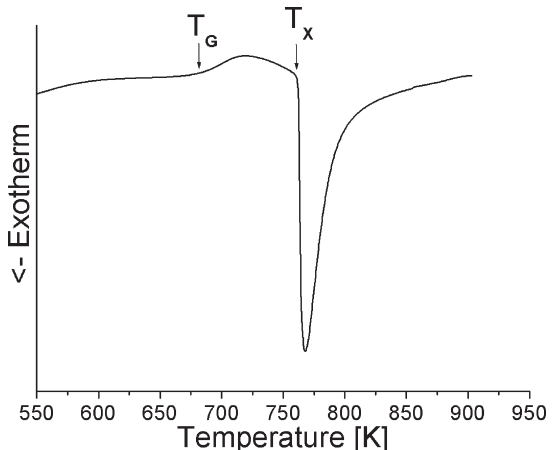


**Fig. 6.** Differential scanning calorimetry measurement from a cast tube segment showing distinctive glassy region between  $T_g$  and  $T_x$ .

tunately, despite the high gloss surface quality, the cross-section instrumented indentation results pointed to a partially crystallized microstructure, as shown in Fig. 7. The instrumented indentation measurement provides a convenient method of evaluating variations in process parameters: fluctuations in the measured hardness, over a cross section of the specimen, indicate partial crystallization.

Clearly, the modifications had the intended effect, so much so that the melt was cooled too slowly to form fully glassy (or amorphous) structure. Optimal process parameters were clearly located between these two values. Hence, with lower arc power and melt mass, the glassy ring cross-section shown in Fig. 2 was produced. Both tube halves were found to be fully amorphous when tested with X-ray diffraction and differential scanning calorimetry. Typical results of these measurements are shown in Figs. 5 and 6. Unlike in the tube shown in Fig. 1, the indentations taken from the ring cross-section shown in Fig. 2 show almost no difference between the first-filled and last-filled portions and thus indicate no signs of partial crystallization, as shown in Figs. 4 and 7 and in Table 1.

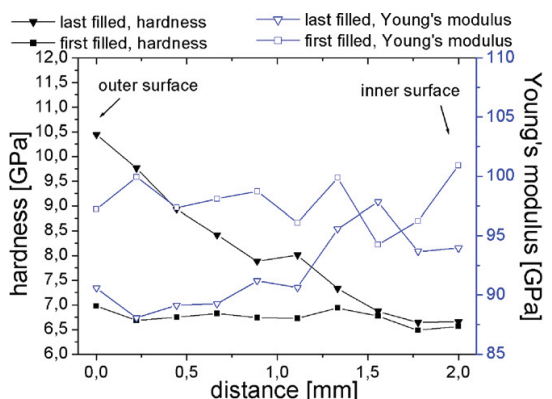


**Fig. 7.** Young's modulus and hardness profiles as a function of the distance from the outer surface to the inner surface for the as-cast partially crystallized ring. Results for both the first-filled and the last-filled sections are shown. The large hardness on the cross-section near the outer surface of the last-filled section indicates composite structure.

**Table 1**

Hardness and Young modulus at initial unloading, with their standard deviations, as measured by instrumented indentation.

	Hardness (GPa)	Modulus (GPa)
Tilt-cast side	6.88 (0.24)	98.6 (2.4)
Suction-cast side	6.99 (0.4)	99.4 (3.8)

#### 4. Conclusions

A glassy Zr<sub>55</sub>Cu<sub>30</sub>Al<sub>10</sub>Ni<sub>5</sub> (in at.%) ring with outer diameter of 25 mm and 1.8 mm thickness was produced, using a custom-built combined arc-melting tilt-casting furnace. Both tilt and suction casting were used to ensure mold filling. Tilt casting was found to fill one side of the tube mold first, with the rest of the tube circumference filled subsequently by suction casting. Different sections of the as-cast ring were investigated by X-ray diffraction (XRD), differential scanning calorimetry (DSC), and instrumented indentation to ensure glassy microstructure.

Optimized casting parameters are required to fully realize the potential of directly manufacturing complex shapes out of high-purity bulk metallic glasses by tilt casting.

#### Acknowledgements

Funding by TEKES and the Academy of Finland are greatly appreciated for making this work possible. The staff of Department of Engineering Design are acknowledged for help with the

numerous manufacturing steps. The discussions with Assistant Professor Yoshiko Yokoyama, Tuomas Pihlajamäki, Jarmo Raikisto, Markku Heino, Heikki Westman, Jari Hellgren, Laura Tiainen, Paula Kainu, Voitto Vanhatalo and Kaj Pischorow are appreciated.

#### References

- [1] A. Inoue, B. Shen, A. Takeuchi, Materials Transactions 47 (2006) 1275–1285.
- [2] A. Inoue, N. Nishiyama, MRS Bulletin 32 (2007) 651–658.
- [3] M. Chen, The Annual Review of Materials Research 38 (2008) 445–469.
- [4] C. Schuh, T. Hufnagel, U. Ramamurty, Acta Materialia 55 (2007) 4067–4109.
- [5] J. Schroers, Advanced Materials 22 (2010) 1566–1597.
- [6] J. Schroers, Q. Pham, A. Peker, N. Paton, R. Curtis, Scripta Materialia 57 (2007) 341–344.
- [7] X.C. Zhang, Y. Zhang, X. Chen, G. Chen, International Journal of Minerals, Metallurgy and Materials 16 (2009) 108–111.
- [8] C. Ma, N. Nishiyama, A. Inoue, Materials Science and Engineering A 407 (2005) 201–206.
- [9] Q. Zhang, D. Guo, A. Wang, H. Zhang, B. Ding, Z. Hu, Intermetallics 10 (2002) 1197–1201.
- [10] H. Shin, J. Park, Y. Yokoyama, 16th International Symposium on Metastable, Amorphous and Nanostructured Materials, Journal of Alloys and Compounds 504 (2010) S275–S278.
- [11] M. MingZhen, Z. HaiTao, W. HaiYan, Q. YanPeng, L. SunXing, S. Aijun, Z. WeiGuo, W. Qiang, Z. XinYu, J. Qin, L. Gong, L. RiPing, Science in China Series G: Physics, Mechanics and Astronomy 51 (2008) 438–444.
- [12] T. Mizushima, K. Ikarashi, S. Yoshida, A. Makino, A. Inoue, Materials Transactions 40 (1999) 1019–1022.
- [13] S.S. Wu, B. Shen, A. Inoue, Intermetallics 12 (2004) 1261–1264.
- [14] N. Nishiyama, K. Amiya, A. Inoue, Journal of Non-crystalline Solids 353 (2007) 3615–3621.
- [15] I. Setki, D. Louguine-Luzgin, A. Inoue, Materials Transactions 48 (2007) 821–825.
- [16] H. Setyawan, J. Kato, A. Saida, Inoue, Journal of Applied Physics (2008) 103.

## Publication III

Sven Bossuyt, Erno Soinila, Henri Penttinen, Ville Pulkki, Hannu Hänninen. Thermoplastic wire drawing from bulk metallic glass. 2010 *MRS Fall Meeting*, 1–6, MRSF10-1300-U08-04.R1, 2010.

© 2010 ScholarOne Manuscripts.  
Reprinted with permission.



## Thermoplastic Wire Drawing from Bulk Metallic Glass

Sven Bossuyt<sup>1</sup>, Erno Soinila<sup>1</sup>, Henri Penttinen<sup>2</sup>, Ville Pulkki<sup>2</sup> and Hannu Hänninen<sup>1</sup>

<sup>1</sup>Dept. Engineering Design and Production, Aalto University School of Science and Technology,  
FI-02015 Espoo, Finland.

<sup>2</sup> Dept. Signal Processing and Acoustics, Aalto University School of Science and Technology,  
FI-02015 Espoo, Finland.

### ABSTRACT

The low loss coefficient and high elastic energy storage of amorphous metals may provide novel opportunities in the design of stringed musical instruments. To produce prototypes for metallic glass music wire, bulk metallic glass pre-forms were reheated into the supercooled liquid region and stretched into wires. Investigations of these wires' geometrical, mechanical, and physical properties are reported. The process is relatively simple and could be practical for producing continuous wire. A theoretical analysis shows the importance of the interaction between heating power input, radiative and convective cooling, and area reduction in determining the wire's final properties.

### INTRODUCTION

Bulk metallic glasses are here defined as amorphous metals which exhibited a glass transition upon cooling from the molten alloy, without detectable crystallization, in a shape with minimum dimension greater than 1 mm. By Fourier's law of heat flow, the maximum cooling rate that can be achieved in a bulk object is inversely related to the square of its minimum dimension, so this definition implies that the crystallization kinetics in bulk metallic glass-forming alloys are unusually sluggish. As a result, these materials exhibit a practically useful window of time and temperature in the supercooled liquid state above the glass transition temperature, where the shape obtained when the glass was made in the first cooling is only the starting point for easy deformation processes leading to much more complicated shapes. If flow of the material is unconstrained at the surface, particularly in uniaxial tensile testing, strains much larger than unity can be achieved [1,2]. In confined flow, much larger strain rate gradients are needed for large deformations, so the achievable strain is limited by a material formability parameter that takes into account the temperature dependence of viscosity and of crystallization kinetics [3,4]. Thermoplastic forming processes [5] that have been successfully carried out with bulk metallic glasses include imprinting [6-9], extrusion [10], injection molding [11], friction welding [2], manipulation with forceps [7], and blow molding [5].

Inspired by the similarities and differences between blow molding of bulk metallic glasses and the ancient art of glass blowing with silicate glasses, the possibility of fiber drawing by thermoplastic processing of bulk metallic glass was examined. The aim of the process is to reduce the diameter and increase the length of a cylindrical section of a bulk metallic glass

casting, as a precursor to developing capabilities for more complex thermoplastic forming operations. Conventionally, the fiber drawing process would start from a high-temperature melt rather than a glass at room temperature. Thin wires, up to a few 100  $\mu\text{m}$ , can be produced directly using rapid quenching methods. Using these methods, amorphous wires can be produced from even marginally glass-forming alloys [12,13]. Bulk metallic glass coil springs, with wire of 1-2 mm diameter, have also been produced by casting into a groove on a rotating copper mould [14]. In this work. The thermoplastic wire drawing technique allows to produce intermediate diameters as well. Metallic glasses could be of interest for novel stringed musical instruments, given their unique combination of high resilience and low intrinsic loss. However, it is by enabling design changes that make full use of the thermoplastic forming process that these materials generate real enthusiasm for innovation in musical instrument design. This work therefore examines the possibility of thermoplastically forming metallic glass wires.

## EXPERIMENT

### Method

$\text{Zr}_{55}\text{Cu}_{30}\text{Al}_{10}\text{Ni}_5$  bulk metallic glass specimens were prepared by copper mold casting. A 20 mm long segment was cut from a 7 mm diameter cylindrical section, and holes were drilled at each end. With the aid of some copper wire, these holes allowed the specimen to be suspended between a rigid support and a 1 kg weight, inside a glass tube with flowing helium gas. The assembled setup is shown inside the induction heating coil in figure 1a. The specimen was heated to the supercooled liquid region, between the glass transition temperature  $T_G$  and crystallization temperature  $T_X$ , where it deformed into a 0.5 m long wire, as shown in figure 1b.



Figure 1. a) The assembled setup for wire drawing in the supercooled liquid region. b) the glassy wire produced using this setup.

## **Results**

The microstructure of the drawn wire was determined to be glassy based on the X-ray diffraction (XRD) and differential scanning calorimeter (DSC) measurements, shown in figures 2 and 3. The mechanical properties of the produced wire were measured with instrumented indentation, and compared to those of a copper mold cast 10 mm diameter bar cross-section. Very similar hardnesses were measured from both, as is shown in Table 1. A somewhat smaller indentation modulus was measured from the wire cross-section than from the cast bar cross-section.

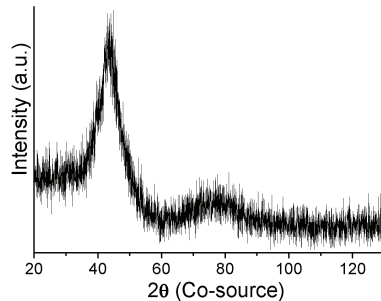


Figure 2. X ray diffraction (Co K $\alpha$ ) patterns of the supercooled liquid region stretched wire.

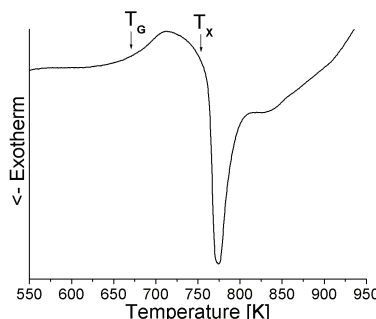


Figure 3. Differential scanning calorimeter (DSC) measurement of the supercooled liquid region stretched wire with glass transition  $T_G$  and crystallization  $T_X$  temperatures, 670.8 K and 754.3 K respectively.

	hardness [GPa]	modulus [GPa]
supercooled liquid region stretched wire, cross section	7.1 (0.14)	79.7 (1.0)
cast 10 mm rod, cross section	7.2 (0.27)	96.0 (2.7)

Table 1: Hardness and Young's modulus at initial unloading, with their standard deviations, as measured by instrumented indentation.

### **Modelling**

The wire in figure 1b had a slightly elliptical cross-section, probably resulting from the bar heating also at the very ends, thus producing a non-circular cross-section during the super-cooled liquid drawing process. To evaluate, the focusing of the induction heating, a finite element model was created to evaluate, whether the heating of the specimen ends could be reduced by cutting the ends of the bar perpendicular to the drilled holes. The cuts effectively reduce the induced surface currents at the unwanted bar ends, as is shown in figure 4. To get a quantitative estimate of the power that is induced per length of the specimen, a linear line projection plot shown in figure 5 was calculated. This plot shows that the induction heating is focused at the center of the specimen, which gives the wanted round preform cross-section for the super-cooled liquid region wire drawing. This simulated result was verified with subsequent tests. Better understanding of the test conditions from simulations allowed a drastic reduction in the number of real tests.

### **CONCLUSIONS**

Supercooled liquid region stretching with induction heating was successfully used to manufacture glassy wires from cylindrical cast glassy preforms. The microstructures of the drawn wires were verified with XRD and DSC measurements. The mechanical properties of the produced wires were tested with instrumented indentation to be very similar to those measured from a glassy cast specimen cross-section of the same composition Zr<sub>55</sub>Cu<sub>30</sub>Al<sub>10</sub>Ni<sub>5</sub>. Finite element simulation was used to better understand and optimize the process for producing circular cross-section wires. In theory, these produced wires can have novel acoustical properties, but more research is still needed to evaluate these possibilities.

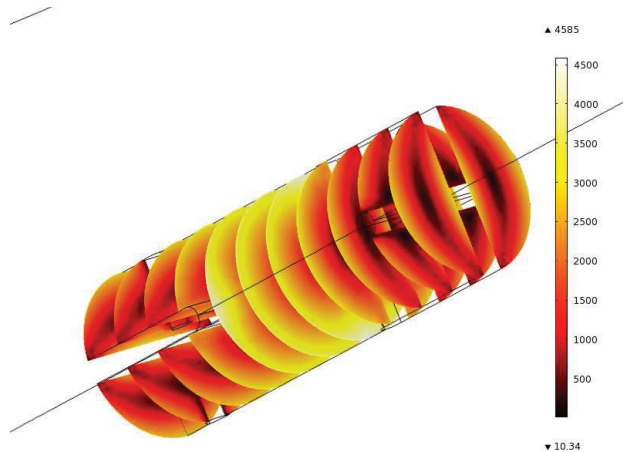


Figure 4. Finite element magnetic field simulation of induced current density in the 7 mm diameter, 20 mm long glassy wire drawing preform.

The round holes are used to attach the preform during the drawing process. The longitudinal cut in each end of the specimen, help focus the inductive heating into the middle of the specimen, which is desirable for round cross-section wire drawing.

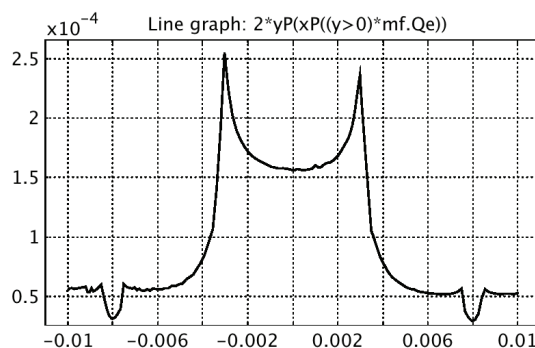


Figure 5. The calculated inductive heating power per unit length, in W/m, vs. distance, in m, along the longitudinal axis of the wire drawing preform. The dips in the curve at 2 mm from each end correspond to the holes through which the specimen is attached, and the spikes at 3 mm from the center result from concentrations in the current density at the edge of the slots cut into the sample. Approximately three times more power is delivered to the center of the specimen than to the ends, so the longitudinal slots cut into the ends seem to serve their purpose.

## ACKNOWLEDGEMENTS

The research leading to these results has received funding from TEKES, IA-Graduate School, the Academy of Finland (project no. 128689 and 130019), and the European Research Council under the European Community's Seventh Framework Programme (FP7/2007-2013) / ERC grant agreement no. [240453]. Tuomas Pihlajamäki, Miikka Aalto, Jari Hellgren, Heikki Vestman and Laura Tiainen contributed to the design and realization of the experimental setup.

## REFERENCES

- 1 A. Inoue, "Stabilization of Supercooled Liquid and Opening-up of Bulk Glassy Alloys," *Proc. Japan Acad. B* **73**, 19-24 (1997).
- 2 Y. Kawamura and Y. Ohno, "Superplastic bonding of bulk metallic glasses using friction," *Scr. Mater.* **45**(3), 279-285 (2001).
- 3 J. Schroers, "On the formability of bulk metallic glass in its supercooled liquid state," *Acta Mater.* **56**(3), 471-478 (2008).
- 4 S. Bossuyt, "The Role of Friction in Measurement of the Formability of Bulk Metallic Glasses," *TMS Ann. meeting*, (2009).
- 5 J. Schroers., Q. Pham, A. Peker, N. Paton and V. Curtis, "Blow molding of bulk metallic glass," *Scr.Mater.* **57**(4), 341-344 (2007).
- 6 Y. Saotome, K. Itoh, T. Zhang and A. Inoue, "Superplastic nanoforming of Pd-based amorphous alloy," *Scripta Mater.* **44**, 1541-1545 (2001).
- 7 A. A. Kundig, A. Dommann, W. L. Johnson and P. J. Uggowitzer, "High aspect ratio micro mechanical structures made of bulk metallic glass," *Mater. Sci. Eng. A* **375**, 327-331 (2004).
- 8 B. Zhang, D.Q. Zhao, M.X Pan, W.-H. Wang and A.L. Greer, "Amorphous metallic plastic," *Phys. Rev. Lett.* **94**(20), 205502 (2005).
- 9 G. Kumar, H.X. Tang and J. Schroers, "Nanomoulding with amorphous metals," *Nature* **457**(7231), 868-872 (2009).
- 10 Jan Schroers, "Processing of Bulk Metallic Glass," *Adv. Mater.* **22**(14), 1566-1597 (2010).
- 11 A. Wiest, "Injection molding metallic glass," *Scr. Mater.* **60** (3), 160-163 (2009).
- 12 T. Masumoto, I. Ohnaka, A. Inoue and M. Hagiwara, "Production of Pd–Cu–Si amorphous wires by melt spinning method using rotating water," *Scr. Metall.* **15**(3), 293-296 (1981).
- 13 T. Nagase, K. Kinoshita and Y. Umakoshi, "Preparation of Zr-based metallic glass wires for biomaterials by are-melting type melt-extraction method," *Mater. Trans.* **49**(6), 1385-1394 (2008).
- 14 K. Son, H. Soejima, N. Nishiyama, X.-M. Wang and A. Inoue, "Process development of metallic glass wires by a groove quenching technique for production of coil springs," *Mater. Sci. Eng. A* **449**, 248-252 (2007).

## Publication IV

E. Soinila, T. Pihlajamäki, S. Bossuyt, H. Hänninen. A combined arc-melting and tilt-casting furnace for the manufacture of high-purity bulk metallic glass materials. *Review of Scientific Instruments*, 82, 1–4, doi:10.1063/1.3606444, 2011.

© 2011 American Institute of Physics.  
Reprinted with permission.



# A combined arc-melting and tilt-casting furnace for the manufacture of high-purity bulk metallic glass materials

E. Soinila,<sup>a)</sup> T. Pihlajamäki, S. Bossuyt, and H. Hänninen

*Department of Engineering Design and Production, Aalto University School of Science and Technology, Espoo, Finland*

(Received 12 January 2011; accepted 9 June 2011; published online 8 July 2011)

An arc-melting furnace which includes a tilt-casting facility was designed and built, for the purpose of producing bulk metallic glass specimens. Tilt-casting was chosen because reportedly, in combination with high-purity processing, it produces the best fatigue endurance in Zr-based bulk metallic glasses. Incorporating the alloying and casting facilities in a single piece of equipment reduces the amount of laboratory space and capital investment needed. Eliminating the sample transfer step from the production process also saves time and reduces sample contamination. This is important because the glass forming ability in many alloy systems, such as Zr-based glass-forming alloys, deteriorates rapidly with increasing oxygen content of the specimen. The challenge was to create a versatile instrument, in which high purity conditions can be maintained throughout the process, even when melting alloys with high affinity for oxygen. Therefore, the design provides a high-vacuum chamber to be filled with a low-oxygen inert atmosphere, and takes special care to keep the system hermetically sealed throughout the process. In particular, movements of the arc-melting electrode and sample manipulator arm are accommodated by deformable metal bellows, rather than sliding O-ring seals, and the whole furnace is tilted for tilt-casting. This performance of the furnace is demonstrated by alloying and casting  $Zr_{55}Cu_{30}Al_{10}Ni_5$  directly into rods up to  $\phi 10$  mm which are verified to be amorphous by x-ray diffraction and differential scanning calorimetry, and to exhibit locally ductile fracture at liquid nitrogen temperature. © 2011 American Institute of Physics. [doi:10.1063/1.3606444]

## I. INTRODUCTION

Bulk metallic glasses (BMG) are amorphous metals, with a diameter larger than 1 mm, that solidified without detectable crystallization. Upon heating from the solid state these alloys exhibit a glass transition, after which they remain metastable for a finite length of time in the super-cooled liquid region, before crystallizing. Enhanced stability against crystallization is usually achieved by alloying multiple elements with significant difference (>12%) in atomic radius and negative heats of mixing among constituent elements. The critical casting diameters of known BMG alloys typically range from 1 mm to 100 mm. BMG alloys have been found in many different alloy groups (Pd-, Mg-, Ln-, Zr-, Ti-, Fe-, Co-, Ni-, and Cu-based systems) and new alloys have been discovered and reported with a variety of different properties. By casting BMG alloys, without cold working or heat treatment, complex shapes can be produced with excellent mechanical properties: purely elastic deformation up to a yield strain of typically 2%, resulting in tensile strength from 1500 MPa to 5500 MPa, with Young's modulus from 70 GPa to 275 GPa. The lack of grain boundaries in the BMG materials also results in very accurate surface finish and enhances corrosion resistance. Several recent reviews testify to the widespread interest in these materials both from a fundamental science perspective and for practical applications.<sup>1–3</sup>

Different methods may be used to produce amorphous metals, each with its own advantages and disadvantages, whose relative importance depends on the alloy composition

and the intended purpose. Strictly speaking, an amorphous solid is called a glass only if it was formed when a liquid state underwent a glass transition. Thus, metallic glasses are formed by melting the constituents to obtain a molten alloy with the desired composition, and then quenching the molten alloy below its glass transition temperature. Often, pre-alloying to obtain the desired composition and quenching to the glassy state are entirely separate processes, carried out in different apparatuses. Prior to the discovery of bulk glass-forming alloy compositions, the rapid quenching methods required to avoid crystallization for most metallic glass-formers meant that these materials could be produced in glassy form only as thin ribbons, foils, or wires. The significance of BMGs can be attributed in large part to the versatility of metal mold casting methods in producing different shapes, not merely larger objects, out of metallic glass. If needed, casting can be followed by additional shaping or patterning steps—Involving machining operations or superplastic forming in the viscous supercooled liquid region<sup>4</sup>—but usually the pre-alloying and casting steps are decisive for the quality of the final part.

For alloying, induction melting and arc-melting under inert atmosphere are commonly used, both with water-cooled copper crucibles. Both methods allow precise control of the melting process in laboratory scale production. Typically, the process chamber is repeatedly evacuated to a pressure around 0.1 Pa or lower and backfilled with purified argon, then purged of any remaining oxygen by titanium gettering before the constituent metals are melted for alloying. It is standard practice to flip over the pre-alloyed ingot and remelt it, several times,

<sup>a)</sup>Electronic mail: Erno.Soinila@hut.fi.

to ensure that its composition is uniform. When the process chamber must be opened to air to flip the ingot, renewing the inert atmosphere takes time, wastes argon, and risks contaminating the BMG with oxygen. Oxygen is harmful for BMG manufacture because, for some of the phases whose crystallization competes with glass formation, the crystallization kinetics are enhanced by oxygen.<sup>5</sup> As a result, BMG samples contaminated with oxygen typically are inferior to high-purity samples.<sup>6–8</sup> So not only is it quicker and more economical to perform the necessary manipulations of the ingot without repeatedly opening the process chamber; it also produces better samples.

For casting BMG, variants of metal mold casting are most commonly used. The method of quenching described in the earliest reports of bulk metallic glass formation in the Pd-Ni-P system<sup>9,10</sup>—and earlier work on marginally bulk glass forming Pd-Si based alloys<sup>11</sup>—did not involve metal mold casting. For some alloys, direct quenching of remelted pre-alloyed ingots in a fused silica container, especially in combination with fluxing, is still the preferred method for making high-quality BMG samples. However, it is difficult to produce complex shapes by this method, and the dimensional tolerances and surface quality obtained by direct quenching methods are not as good as those obtained by metal mold casting. A relatively simple version of metal mold casting consists of induction melting a pre-alloyed ingot in a fused silica crucible that has an orifice at the bottom, and then applying gas pressure to eject the molten BMG forming alloy into a mold placed beneath the crucible. High vacuum induction melting and argon pressure casting apparatus, with a linear feedthrough for moving the fused quartz crucible from the induction coil to the mold orifice, was found to be very versatile in easily producing different specimen shapes, such as rectangular and cylindrical rods,<sup>12,13</sup> wedges,<sup>14</sup> tubes,<sup>15</sup> and “dogbone” tensile specimens.<sup>16</sup> In a laboratory setting—where process conditions are often varied—it is particularly convenient to be able to view the sample through the quartz crucible during melting. However, because the same quartz crucible is a possible source of oxygen contamination,<sup>7</sup> it may sometimes be preferable to use other crucible materials, such as graphite. More sophisticated casting methods such as suction casting, tilt casting, squeeze casting, and cap casting may produce better quality specimens, e.g., because they can more consistently and more uniformly fill the mold. In particular, BMG specimens produced by the combination of tilt casting with cap casting or squeeze casting, compared to those produced by conventional tilt casting, have been reported to exhibit larger critical casting diameter<sup>17</sup> and improved ductility.<sup>18</sup>

## II. DESIGN METHODOLOGY

It is a truism of high vacuum technology that each feedthrough and each seal represents a leak. Sliding O-ring seals, where a moving surface slides against the O-ring that provides the vacuum seal, are particularly prone to leaking. Also, when a vacuum chamber has been opened to atmosphere, it takes a long time to evacuate moisture adsorbed from the air onto the inside surfaces of the vacuum chamber.<sup>19–21</sup> To provide the high-purity conditions desired

for BMG processing, the main process chamber should therefore have as few feedthroughs and as little surface area as possible. Nevertheless, the apparatus should allow the full range of motions and manipulations needed to carry out each step of the process, preferably without opening the chamber to atmosphere.

Based on previous experience<sup>22,23</sup> with both induction- and arc-melting for alloying and with various methods for casting, a choice was made to construct a multifunctional arc-melting and tilt-casting apparatus.

It is equipped with a manipulator arm so that, for pre-alloying, the sample can be flipped and remelted without opening the chamber. It also has provisions for piston suction casting and cap casting for small specimens. For a wide range of alloy compositions and sample sizes, the complete process from pre-alloying to high-quality net-shape casting can be carried out in a continuous sequence using this apparatus. Furthermore, the critical feedthroughs in this apparatus feature ultra-high vacuum construction methods, using flexible metal bellows for all moveable parts, and an all-metal gas line connects the chamber to a supply of high-purity inert gas. Thus, a high-purity atmosphere can be maintained throughout the entire processing sequence.

Tilt-casting under high purity conditions is seen as a method to reduce the incidence of casting defects, and produce samples of the highest quality.<sup>24</sup> The reasoning is that impurities in a casting process are collected on the surface of the melt, so that the cleanest alloy with the least inclusions is found in the interior of the melt. Also, material from cold spots at the bottom of the sample, where it touches the hearth during melting, may not be completely molten or sufficiently overheated. Tilt-casting is a comparatively gentle casting method, where the molten metal moves as one large drop of liquid instead of a narrow stream or atomized spray. The flow pattern is such that the melt charge is smoothly turned inside out into the mould and the material from the bottom and from the surface of the melt, if it is not part of the excess material left in the nozzle when the mould is completely filled, is mostly the last material to flow through the mould orifice. Thus, tilt-casting fills the mould primarily with the cleanest part of the melt. By contrast, when the mould is filled by squirting the melt out of a crucible through an orifice, the turbulent melt flow involves the rapid creation of new surface, which is sealed together again as the mould is filled. Even in high purity conditions, this process distributes the impurities from the melt surface to the interior of the specimen, resulting in inclusions. It may also cause significant variations in thermal history between adjoining material, affecting crystallization behavior, and residual stresses. Small amounts of inclusions and localized residual stresses may be unimportant for some measures of a specimen’s quality, but eliminating them can significantly improve properties related to fracture and fatigue.<sup>8</sup> For instance, Tilt-casting effectively minimizes both the amount of newly created melt surface and complexity of the fluid flow pattern during the casting process. As a result, compared with casting methods where the mould is filled by turbulent flow, it produces specimens with a more uniform and consistent thermal history, fewer inclusions, and essentially no porosity.

### III. DESIGN DESCRIPTION

The main chamber was constructed by modifying a standard 250 mm ISO-K T-section, oriented so that the flanges are at the top, bottom, and back of the chamber, as shown in Fig. 1. The arc-melting electrode passes through the top flange, the water-cooled hearth is raised from the bottom flange, and vacuum pumping is done through the back flange. In a similar setup to that reported by Arajs,<sup>25</sup> three additional flanges were TIG-welded to the chamber, providing feedthroughs for lighting, ingot manipulation, and viewing. Connections for suction casting and cap casting, and extra room for the moulds, are provided in an extension to the back flange. The water-cooled copper hearth inside the chamber features a single large melting trough with a pouring nozzle leading to the mould orifice, and a smaller trough for titanium gettering. The hearth is attached from below, to avoid any “internal leaks” from gas pockets that might otherwise be trapped between the hearth and the chamber. A standard ISO-K 200 O-ring seal with centering ring separates the vacuum from the cooling water circulating underneath the copper hearth. Belleville spring washers ensure that differential thermal expansion when the furnace is operated does not cause excessive decreases or increases in the clamp force maintained on the O-ring seal. Heli-Coil<sup>TM</sup> inserts help prevent damage to the threaded bolt holes in the copper hearth, considering that these must support bolt tension up to 1 kN with thermal cycling. To load a new charge into the furnace, the assembly of the bottom flange with the copper hearth is released from the rest of the chamber and lowered on a pneumatic lift provided for that purpose.

An arc-melter necessarily includes a feedthrough for the arc-melting electrode: a water-cooled conductor that can carry an electrical current up to 500 A and can handle the 30 kV high-voltage arc-ignition spark. This current needs to be electrically isolated from the chamber potential at operating pressures and atmospheres to avoid damage to the chamber. Furthermore, the electrode should be moveable; with a freely moveable electrode tip, the operator can deliver the energy of the plasma arc precisely where it is needed to melt the sample. The feedthrough should allow a range of motions covering every possible position of the sample in the melting trough as well as the titanium getter. This freedom of movement is realized with a flexible edge-welded metal bellows, between the top flange of the chamber and the electrical feedthrough for the electrode. The electrical feedthrough is constructed of two fluoropolymer insulators clamped onto either side of a copper flange which is brazed onto the electrode rod. Standard ISO-K 100 O-ring seals and centering rings seal the vacuum side. The tungsten electrode tip is secured with two screws to the brazed electrode tip assembly (visible at the top of Fig. 2) which seals the end of the water-cooled electrode rod.<sup>25</sup>

To assist the operator with delicate movements of the electrode tip and to prevent movements that would damage the hearth or the bellows, a mechanism for supporting the electrode is also necessary. The weight of the electrode rod and the atmospheric pressure when the chamber is evacuated amount to a force in excess of 800 N drawing the electrode towards the copper hearth. A mechanism with pneumatically actuated servo control in the vertical direction carries this

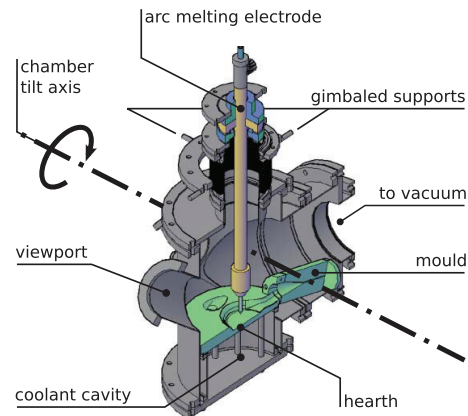


FIG. 1. (Color online) Cutout view showing the design of the vacuum chamber.

load. At the touch of a valve on the electrode handlebar, near the right-hand thumb of the operator, precise adjustments can be made to the elevation of the electrode tip above the hearth. The attachment of the electrode rod to this mechanism by a pair of concentric gimbals lets the operator tilt the electrode rod to move the electrode tip forwards, backwards or sideways. Similarly, a clamp, connected by a ball joint to another pneumatically actuated servo mechanism, supports the sample manipulator arm.

Tilt-casting requires a mechanism for pouring the melt from the crucible into the mold. Often this is done with a sliding O-ring seal, in which a rigid connector carrying cooling water for the metal crucible also allows to tilt the crucible towards the mold. In this apparatus, the whole chamber is tilted. This eliminates a potentially troublesome sliding O-ring seal, but requires a more elaborate structure to support the chamber.



FIG. 2. (Color online) The arc-melting of a BMG alloy ingot on top of the water-cooled copper hearth. On the right is the tip of the manipulator used to flip the ingot upside-down between melting runs. The mould orifice and the melt pouring nozzle leading to it can be seen behind the electrode tip assembly.

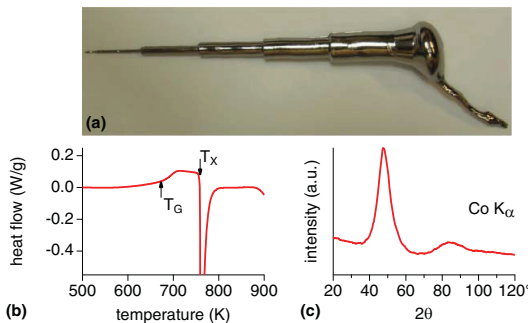


FIG. 3. (Color online) (a) Tilt- and suction-cast specimen with 1, 3, 5, 7, and 10 mm diameters. (b) Typical glassy DSC measurement from the tilt- and suction-cast BMG-rod showing distinctive glassy region between  $T_G$  and  $T_X$ . (c) X-ray diffraction ( $\text{Co } K\alpha$ ) pattern of a tilt- and suction-cast specimen shows amorphous structure for  $\phi$  10 mm. Samples were prepared with a water-cooled aluminium oxide impregnated cutoff wheel. Cutoff wheel residuum was removed by polishing with 1  $\mu\text{m}$  diamond paste when necessary.

#### IV. RESULTS AND DISCUSSION

The results obtained with the constructed furnace are more focused on evaluating the functionalities of the furnace than the properties of the particular cast specimens. Several samples of Inoue alloy  $\text{Zr}_{55}\text{Cu}_{30}\text{Al}_{10}\text{Ni}_5$  (At. %) was tilt- and suction-cast into a mold with 10, 7, 5, 3, and 1 mm diameters, as shown in Fig. 3(a). The x-ray diffraction spectrum from the largest cast diameter is shown in Fig. 3(c). In each case, a broad diffuse peak typical of the amorphous alloy was seen, confirming that the as-cast samples did indeed vitrify during the casting process. A differential scanning calorimetry (DSC) study shown in Fig. 3(b) was performed to verify the glassy nature of the cast alloy. The measured glass transition onset and crystallization onset temperatures were  $T_G = 673.1$  K and  $T_X = 758.9$  K, respectively, with a 40.8 J/g heat release in the primary crystallization peak.

Complete characterization of the purity of the argon gas under actual process conditions and the purity of the resulting specimen would be interesting, but would require much additional time and specialized instrumentation. However, the work of Keryvin *et al.*<sup>8</sup> allows to use low-temperature toughness as a proxy for sample purity. Studying the effect of sample purity on fracture behavior for the same  $\text{Zr}_{55}\text{Cu}_{30}\text{Al}_{10}\text{Ni}_5$  alloy, they observed that at liquid nitrogen temperature, only the highest-purity samples still exhibited fracture surfaces with the vein-like features typical of locally ductile failure in metallic glasses. Therefore, beams of approximately 1 mm  $\times$  1 mm  $\times$  10 mm were cut from the  $\phi$  10 mm and  $\phi$  7 mm parts of a specimen, cooled in liquid nitrogen, placed over a gap in a bench vise and broken using a hammer and chisel. Figure 4 shows a fracture surface typical of these experiments with specimens produced in the constructed furnace, indicating that these specimens are similar to the highest-purity specimens of this alloy.

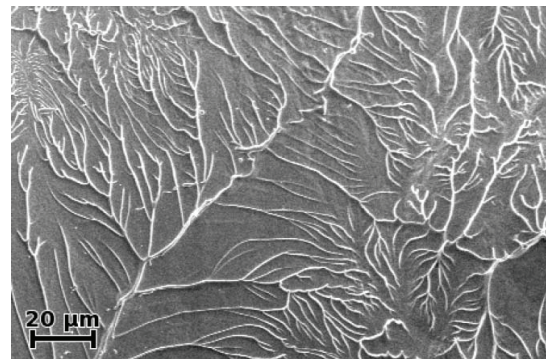


FIG. 4. Fracture surface of a small beam cut from the specimen shown in Fig. 3(a), broken at liquid nitrogen temperature in a 3-point bending geometry.

#### V. CONCLUSIONS

A combined tilt-casting arc-melting furnace was designed and constructed for the preparation of high-quality bulk metallic glass specimens. Using this apparatus, the complete process from pre-alloying to final casting can be carried out in one sequence, without need to vent and re-establish the inert atmosphere. Specimens of  $\text{Zr}_{55}\text{Cu}_{30}\text{Al}_{10}\text{Ni}_5$  cast into cylinders up to 10 mm diameter using this apparatus were confirmed to be glassy and to exhibit fracture behavior similar to the highest-purity specimens of this alloy studied elsewhere.

#### ACKNOWLEDGMENTS

Funding by TEKES and the Academy of Finland are greatly appreciated for making this work possible. The staff of Department of Engineering Design and Production and Lydwin Rös from Trinos Vacuum are acknowledged for help with the numerous manufacturing steps. The discussions with Assistant Professor Yoshiko Yokoyama, Jarmo Raikko, Markku Heino, Heikki Vestman, Jari Hellgren, Laura Tainanen, Samuli Laine, Paula Kainu, Voitto Vanhatalo, Kaj Pischedow, and the Savcor Research and Development team are appreciated.

- <sup>1</sup>A. Inoue and N. Nishiyama, *MRS Bull.* **32**, 651 (2007).
- <sup>2</sup>M. Chen, *Annu. Rev. Mater. Sci.* **38**, 445 (2008).
- <sup>3</sup>C. Schuh, T. Hufnagel, and U. Ramamurthy, *Acta Mater.* **55**, 4067 (2007).
- <sup>4</sup>J. Schroers, *Adv. Mater.* **22**, 1566 (2010).
- <sup>5</sup>X.-H. Lin, W. L. Johnson, and W.-K. Rhim, *Mater. Trans., JIM* **38**, 473 (1997).
- <sup>6</sup>R. D. Conner, R. E. Maire, and W. L. Johnson, *Mater. Sci. Eng., A* **419**, 148 (2006).
- <sup>7</sup>I. Seki, D. Louzguine-Luzgin, and A. Inoue, *Mater. Trans.* **48**, 821 (2007).
- <sup>8</sup>V. Keryvin, C. Bernard, J. Sangleboeuf, Y. Yokoyama, and T. Rouxel, *J. Non-Cryst. Solids* **352**, 2863 (2006).
- <sup>9</sup>A. Drehman, A. L. Greer, and D. Turnbull, *Appl. Phys. Lett.* **41**, 716 (1982).
- <sup>10</sup>H. Kui, A. L. Greer, and D. Turnbull, *Appl. Phys. Lett.* **45**, 616 (1984).
- <sup>11</sup>H. Chen and D. Turnbull, *Acta Metall.* **17**, 1021 (1969).
- <sup>12</sup>A. Inoue, T. Zhang, and T. Masumoto, *Mater. Trans., JIM* **31**, 425 (1990).
- <sup>13</sup>A. Peker and W. L. Johnson, *Appl. Phys. Lett.* **63**, 2342 (1993).
- <sup>14</sup>A. Inoue, Y. Shinohara, Y. Yokoyama, and T. Masumoto, *Mater. Trans., JIM* **36**, 1276 (1995).
- <sup>15</sup>A. Inoue, T. Saito, H. Yamamoto, and T. Masumoto, *J. Mater. Sci. Lett.* **12**, 946 (1993).

- <sup>16</sup>R. D. Conner, H. Choi-Yim, and W. L. Johnson, *J. Mater. Res.* **14**, 3292 (1999).
- <sup>17</sup>Y. Yokoyama, E. Mund, A. Inoue, and L. Schultz, *Mater. Trans.* **48**, 3190 (2007).
- <sup>18</sup>Y. Yokoyama, K. Fukaura, and A. Inoue, *Intermetallics* **10**, 1113 (2002).
- <sup>19</sup>J. Hanlon, *A User's Guide to Vacuum Technology*, 1st ed. (Wiley, New York, 1988).
- <sup>20</sup>H. Hablanian, *High Vacuum Technology, A Practical Guide*, 1st ed. (Marcel Dekker, New York, 1990).
- <sup>21</sup>N. C. Harris, *Modern Vacuum Practice*, 1st ed. (McGraw-Hill, London, 1989).
- <sup>22</sup>E. Soinila, M.S. thesis, Helsinki University of Technology, 2005.
- <sup>23</sup>E. Soinila, Lic.S. thesis, Helsinki University of Technology, 2009.
- <sup>24</sup>Y. Yokoyama, private communication (2008)
- <sup>25</sup>S. Arajs and G. Wray, *J. Phys. E: Sci. Instrum.* **2**, 518 (1969).



## Publication V

E. Soinila, S. Bossuyt, H. Hänninen. Steady-state tensile viscous flow forming of bulk metallic glass. *Journal of Alloys and Compounds*, Available online (doi:10.1016/j.jallcom.2012.01.153) from 7th of February 2012.

© 2012 Elsevier.  
Reprinted with permission.





Contents lists available at SciVerse ScienceDirect

## Journal of Alloys and Compounds

journal homepage: [www.elsevier.com/locate/jallcom](http://www.elsevier.com/locate/jallcom)



# Steady-state tensile viscous flow forming of bulk metallic glass

E. Soinila\*, S. Bossuyt, H. Hänninen

Department of Engineering Design and Production, Aalto University, School of Engineering, Espoo, Finland

## ARTICLE INFO

### Article history:

Received 24 June 2011

Received in revised form 25 January 2012

Accepted 30 January 2012

Available online xxx

### Keywords:

Bulk metallic glass

Amorphous

Fiber

Metal

## ABSTRACT

Tensile viscous flow is explored as a forming method for metallic glasses in their supercooled liquid temperature region. Bulk amorphous preforms with nominal alloy composition Zr<sub>55</sub>Cu<sub>30</sub>Al<sub>10</sub>Ni<sub>5</sub> were produced by arc melting and tilt- and suction casting into a copper mould. A simple loading rig, in which the preform is suspended from a wire, combined with selective heating of the section to be deformed, avoids the need for complicated loading grips. Different strategies are evaluated to attach the sample to the rig and to selectively heat the central part of the specimen.

Finite element models were compared with experiments to verify the design of the induction heating coil and optimize process parameters. Differential scanning calorimetry and X-ray diffraction measurements show that the material is glassy before and after deformation. The rapid decrease of flow stress with increasing temperature means that the process can be controlled thermally at constant load instead of mechanically at constant temperature. An asymmetric configuration, where the selective heating zone is moved relative to the specimen during the deformation, allows to form rods into wire by a steady-state process. The effect of deformation on induction heating under constant tension was found to be inherently self-stabilizing, reducing the need for precise process control.

© 2012 Elsevier B.V. All rights reserved.

## 1. Introduction

Bulk metallic glasses are amorphous metals, with a diameter larger than 1 mm, that have solidified without detectable crystallization. Upon heating from the solid state these alloys exhibit a glass transition, after which they remain metastable for a finite length of time in the super-cooled liquid region, before crystallizing. Increased stability against crystallization is usually achieved by alloying multiple elements with significant difference, greater than 12%, in atomic radius and negative heats of mixing among constituent elements [1].

The critical casting diameters of known BMG alloys typically range from 1 mm to several centimeters. BMG alloys have been found in many different alloy groups (Pd-, Mg-, Ln-, Zr-, Ti-, Fe-, Co-, Ni- and Cu-based systems) and new alloys have been discovered and reported with a variety of different properties. Complex shapes can be produced, with excellent mechanical properties in the as-cast stage: purely elastic deformation up to a yield strain of typically 2%, resulting in reported tensile or compressive strengths of 1500–5500 MPa, with Young's modulus of 70–275 GPa [1]. Accurate dimensions and surface finish can be achieved with BMG materials, due to the uniform shrinkage during solidification and the lack of grain boundaries. Several recent reviews testify to the

widespread interest in these materials both from a fundamental science perspective and for practical applications [1–3].

For practical applications, it is often necessary to form application specific shapes, such as wires. In general, the final shape in metallic glasses is obtained either during solidification from a molten state directly, or by reheating a glassy preform to allow thermoplastic forming [4]. Thermoplastic forming processes that have been successfully carried out with bulk metallic glasses include imprinting [5–8], extrusion [4], injection molding [9], friction welding [10], manipulation with forceps [6] and blow molding [11]. Usually the reheating process is limited to a temperature much lower than melting temperature to avoid crystallization. However, in some cases, with very high heating speeds, temperatures above melting temperature have also been achieved [12].

Previously reported metallic glass wire forming methods, operating directly from melt, use a rapidly spinning disk that comes into contact with arc-melted glass forming alloy melt [13,14]. Alternatively, the melt is poured onto a spinning disk with suitably sized groove for thicker wire formation [15]. The use of thermoplastic forming for metallic glass wire production is reported relatively seldom [16,17].

Thermoplastic forming of metallic glass is seen as a promising method for producing shapes that are difficult or impossible to cast. By decoupling the casting process from the final shaping, the cast specimen can be relatively simple to produce compared to the final shape. In practice, the preform material is alloyed and cast normally into a metallic glass by metal mold casting. Then, in the

\* Corresponding author. Tel.: +358 50 5376172.

E-mail addresses: Erno.Soinila@aalto.fi, Erno.Soinila@gmail.com (E. Soinila).

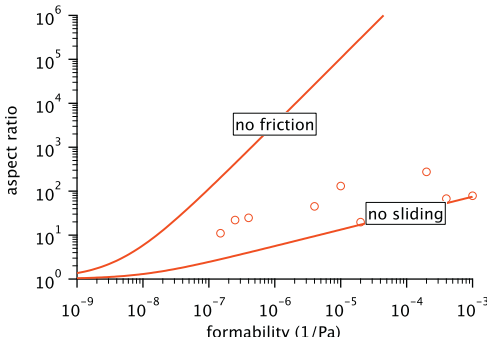


**Fig. 1.** Theoretical limits [19] to thermoplastic forming (solid lines) for flattening of cylindrical specimens with a force of 4450 N under constant heating at 20 K min<sup>-1</sup>, and corresponding experimental data [18] for different alloys with different figures of merit for formability (open circles).

thermoplastic forming step, the cast sample is reheated between  $T_g$  and  $T_x$  temperatures, where a larger forming time is available before crystallization than in direct casting. The amount of thermoplastic deformation that can be achieved in constant heating of metallic glass, before crystallization puts an end to further deformation, depends on the alloy. It can be characterized by the figure of merit [18]

$$F = \frac{1}{3(\partial T/\partial t)} \int_{T_g}^{T_x} \frac{1}{\eta(T)} dT \quad (1)$$

where  $\eta$ ,  $T_g$  and  $T_x$  are viscosity, glass transformation temperature and onset temperature of crystallization, respectively. However, as shown in Fig. 1, even for alloys with good formability the amount of deformation that can be achieved in constrained flow is limited. In fully constrained flow, such as injection molding into a long and narrow mold, the friction of the alloy surface against the mold wall requires shearing inside the alloy for continued deformation. In unconstrained flow, such as blow molding [11], the absence of metal-mold friction allows the material to deform by nearly uniform extensional flow, and much larger aspect ratios can be manufactured.

Here the idea of a simple setup for unconstrained thermoplastic forming of bulk metallic glass in uniaxial tension [17] is developed further. Through selective heating of that part of the material that is to be deformed, the temperature dependence of the viscosity of glass-forming alloys can be exploited to allow high mechanical stress in parts of the material that should not deform. In particular, this allows drastically simplified construction of the end grips for a tensile specimen. Furthermore, induction heating and convective cooling conspire to automatically switch from net heating to net cooling as a result of tensile deformation.

Ideally there is a balance between:

- The amount of heat that is extracted via convective cooling: the thinner the material at a given cross-section the more rapidly it cools (Newton's law of cooling).
- The amount of heat that is brought into a cross-section: the thinner the cross-section, the less it heats up from inductive currents. Excess heating must be avoided, as it leads to crystallization of the feedstock, which rapidly stops the wire pulling process.
- The amount of heat that is extracted along with the material making up the wire as it is pulled out of the deformation zone.

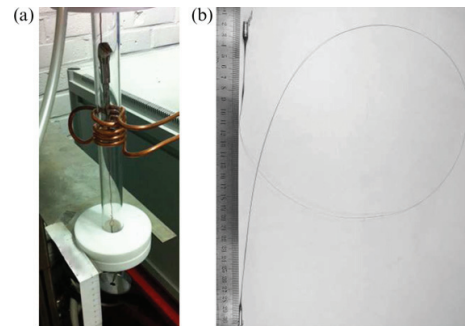


**Fig. 2.** (a) The constructed wire pulling apparatus. The preform specimen in the fused quartz chamber contains 20 mm long segments of 10, 7, 5, 3 and 1 mm diameters, and can be made without machining steps. Here this specimen type can only be used because the bucking coil prevents the top of the specimen from heating too much before the wire production begins from the smaller diameter portion. The wire production begins from the 5 to 3 mm diameter step similarly as if a specimen shown in Fig. 4b was used. (b) An example of produced glassy wire.

It is expected that when a balance between these factors is achieved, the process is essentially self-stabilizing. This allows a thermoplastic forming process for producing metallic glass wire without the need for high-vacuum chamber or high-end instrumentation. In addition, the induction heating and the preform geometry can be designed to minimize the number of process steps required. Preliminary experiments can be complemented by finite element calculations to evaluate suitable specimen geometries for different induction coils.

## 2. Experimental procedures

The Zr<sub>55</sub>Cu<sub>30</sub>Al<sub>10</sub>Ni<sub>5</sub> (in at.%) bulk metallic glass specimens were prepared by copper mold casting. Alloy constituents for the target composition of Zr<sub>55</sub>Cu<sub>30</sub>Al<sub>10</sub>Ni<sub>5</sub> (in at.%) were weighed from the elements with purity (in mass%) of 99.99% for Cu, and 99.99% for Zr(+Hf), Ni and Al. The cut and weighed pieces were melted and cast in a custom built combined arc melting and tilt casting furnace, under reduced pressure titanium gettered argon atmosphere, with the same process parameters as reported in more detail elsewhere [20].

The X-ray diffraction (XRD) patterns were measured with a Siemens Kristalloflex 710H X-ray generator and Inel CPS-120 position sensitive detector. A Netzsch STA 449F1 was used for the DSC measurements with 20 K min<sup>-1</sup> heating rate. The finite element modeling calculations were done with COMSOL Multiphysics 4.1.

The constructed forming apparatus, shown in Fig. 2a, consists of a fused quartz tube and two end pieces. At the upper end piece there is a connection for helium gas, which is used both to increase the convective cooling rate and to protect the deforming specimen from excess oxidation. The upper end piece includes a hook from which the specimen is suspended by a copper wire, and the lower end piece has an opening for a second copper wire which is used to pull the metallic glass specimen, until the formed metallic glass wire is pulled through the opening and the metallic glass wire can be pulled directly. A nominally constant force is applied by suspending a mass of 0.2 kg from the second wire. It should be noted that the ends of the specimen where the copper wires are attached must remain colder than the part of the specimen to be deformed, otherwise the copper wire is pulled out of the specimen instead of deforming the specimen. This is achieved by locally heating the part of the specimen to be deformed, using induction heating with an appropriate combination of specimen geometry and induction coil geometry. The apparatus is held in place by a support mechanism, which allows the induction coil to move up and down during the process, in effect gradually feeding the specimen into the induction coil.

Two induction coils were tested. One is regular solenoidal coil, with all loops conducting current in the same direction. The other coil, shown in Fig. 2a, is a bucking coil where the highest loop conducts current in the opposite direction of the lower loops. Depending on the induction coil used, different specimen geometries were required to successfully focus the induction heating. In the symmetric set-up with the regular solenoidal coil, the specimens are straight cylinders with slots machined into the ends and holes drilled to attach the wires. Starting from an as-cast cylinder, producing a specimen in this geometry, which is shown in Fig. 4a, required up to six machining steps. In contrast, specimens for the asymmetric set-up with the bucking coil are cylinders with a step change in diameter but no slots. This geometry, the relevant part of which is shown in Fig. 4b, was produced directly by copper mold casting. As can be seen in Fig. 2a, the actual

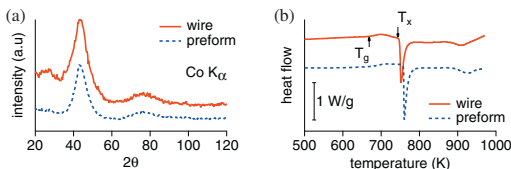


**Fig. 3.** (a) X-ray diffraction ( $\text{Co K}_\alpha$ ) patterns of drawn wire and preform, showing amorphous structure. (b) Differential scanning calorimeter (DSC) measurements of drawn wire, with its glass transition and crystallization temperatures  $T_g = 668.6\text{ K}$  and  $T_x = 748.6\text{ K}$  marked by arrows, and of a preform.

mold has several step changes in diameter. The need for drilling the gripping holes in the asymmetric set-up was avoided by placing the copper attachment wires into the mold prior to casting, and casting the metallic glass around them.

### 3. Experimental results and discussion

The amorphous structure of glassy as-cast preforms can be demonstrated [21] by combination of X-ray diffraction and differential scanning calorimeter (DSC) measurements. Fig. 3 shows a comparison of such measurements between a sample of one of the produced wires and a glassy preform, indicating that the thermal stability of the thermoplastically formed wire is reduced from the as-cast specimen— $T_x$  is 10 K lower—whereas the diffraction patterns and the heats of crystallization do not differ significantly.

Two methods were tried for tensile viscous flow forming of copper mold cast  $\text{Zr}_{55}\text{Cu}_{30}\text{Al}_{10}\text{Ni}_5$  preforms with induction heating, and both methods worked in practice. In the first method (symmetric set-up) the focusing of the induction heating was achieved by machining the preform specimen so that the inductive currents heated the middle of the specimen preferentially, as shown in Fig. 4a. In the second method (asymmetric set-up) the focusing

of the induction heating was accomplished with the use of smaller diameter at the lower end and by the use of a bucking coil in the upper end of the preform. This asymmetric set-up leads to a steady state, where high temperatures and thermoplastic flow remain essentially limited to the deformation zone, which is slowly moved up along the feedstock while newly formed wire is extracted from below. Examples of the successful asymmetric set-up are shown in Fig. 4b and in Fig. 2a. Notably in Fig. 2a the as-cast specimen was used as preform, without further machining steps.

Finite element modeling was used to evaluate the focusing of the induction heating using both approaches. A finite element model used in [17] was further developed to evaluate the various schemes to focus the induction heating away from the sample suspension wires. Experimentally, failure to focus the induction heating away from the sample grips was found to result in metallic glass wires of limited length and non-uniform, highly elliptical cross-section, where the attachment wires are pulled out of the specimen. Machining slots at both ends of the specimen—as shown in Fig. 4a—reduces the coupling of the ends of the specimen to the magnetic field of the induction coil, thereby focusing the electromagnetic power loss density, i.e., the induction heating effect, in the central part of the specimen. This is a workable solution, although it involves rather extensive sample preparation. The second approach, using a combination of using a bucking coil and a smaller diameter lower part sample, avoids the need to machine the slots at the ends of the sample. Fig. 4 shows the effect of using the bucking coil on the electromagnetic power loss density, and the effect of changing to a 40 mm long, 5–3 mm diameter sample. As shown in Fig. 4b, the combination of the bucking coil and the asymmetric sample focuses the induction heating effect near the step change in diameter, on the larger-diameter side, as desired. This observation is quantified in a plot along the length of the specimen, of the electromagnetic power loss integrated over the cross section and divided by the area of the cross-section. Thus, both approaches are effective in focusing the induction heating effect in the central part of the specimen, but the asymmetrical set-up allows much simpler sample preparation.

Another difference between the two approaches, is the possibility in the asymmetric set-up to continue the process by feeding more of the specimen into the induction coil. Because a steady state can be achieved, where a larger-diameter rod is continuously fed into the process zone and a smaller-diameter wire is continuously pulled out, producing wires of essentially unlimited length may be possible via this method; as long as the preform does not run out and does not crystallize, the process can continue indefinitely. As a result of the effect of wire diameter on the balance between inductive heating and convective cooling, and the effect of temperature on viscosity, the process is self-stabilizing both for mechanical and thermal perturbations. Issues of process control to control the diameter and thermal history of the thermoplastically formed wire, as well as the stability of dynamic perturbations are topics for further research. The effect of the force used to draw the wire was qualitatively analyzed by continuing to pull the wire by hand after the 0.2 kg weight had dropped the available 0.5 m height. The produced wire thickness was found to be very sensitive to the amount of force used, which could enable the tailoring of wire thickness profiles by changing the force and speed of the pulling during the process. Wires with such tailored thickness profile could be useful as non-linear springs, benefiting from the excellent spring properties of bulk metallic glasses [22].

### 4. Conclusions

Two methods were tried for tensile viscous flow forming of copper mold cast  $\text{Zr}_{55}\text{Cu}_{30}\text{Al}_{10}\text{Ni}_5$  preforms with induction heating,

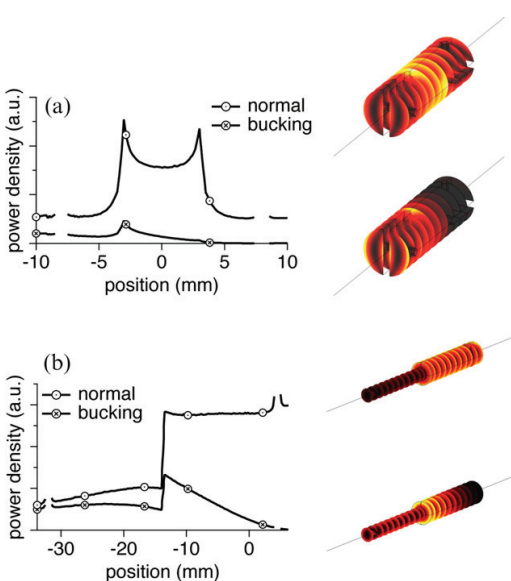


**Fig. 4.** A comparison of calculated power loss densities per sample length, with and without using a bucking coil, for both of the tested wire drawing preform geometries: (a) 7 mm cylinder with holes for attaching it to the wire drawing rig and slots cut into the ends to reduce the heating of the sample ends, where the bucking coil is not needed; and (b) specimen with step change in diameter from 5 to 3 mm, where the lower portion heats less because its diameter is smaller, and use of a bucking coil reduces heating of the upper end.

4  
and both methods worked. The glassy microstructure of the drawn wire was verified with XRD and DSC measurements. Finite element simulation was used to evaluate the performance of the induction heating and specimen geometries.

In the first method (symmetric set-up) the focusing of the induction heating was achieved by machining the preform specimen so that the inductive currents heated the middle of the specimen. In the second method (asymmetric set-up) the focusing of the induction heating was accomplished by using preforms with smaller diameter at the lower end, in a bucking coil which minimizes heating in the upper end of the preform. The preforms used for the asymmetric setup are simpler to produce than those required for the symmetric set-up. Furthermore, the asymmetric set-up offers the possibility to continue the wire forming process indefinitely in a steady state, as long as the preform does not crystallize and the preform does not run out.

Unlike other glassy wire production methods, this method allows some real time control over the produced wire diameter, which can be very useful for the production of non-linear glassy springs. The presented asymmetric test set-up may also have some potential as a method to characterize thermoplastic forming behavior of different metallic glasses, if more instrumentation is added to monitor the temperature profiles and a more comprehensive numerical model is constructed to relate the resulting thickness profile to the material parameters.

## Acknowledgments

Funding by TEKES and the Academy of Finland are greatly appreciated for making this work possible. Discussions with Tuomas

Pihlajamäki and Heikki Westman, and help with the numerous manufacturing steps from the staff of Department of Engineering Design are also acknowledged.

## References

- [1] A. Inoue, A. Takeuchi, *Acta Mater.* 59 (2011) 2243–2267.
- [2] M. Chen, *Annu. Rev. Mater. Res.* 38 (2008) 445–469.
- [3] C. Schuh, T. Hufnagel, U. Ramamurti, *Acta Mater.* 55 (2007) 4067–4109.
- [4] J. Schroers, *Adv. Mater.* 22 (2010) 1566–1597.
- [5] Y. Saotome, K. Itoh, T. Zhang, A. Inoue, *Scripta Mater.* 44 (2001) 1541–1545.
- [6] A. Kundig, A. Dommann, W. Johnson, P. Uggowitzer, *Mater. Sci. Eng. A* 375 (2004) 327–331.
- [7] B. Zhang, D. Zhao, M. Pan, W. Wang, A. Greer, *Phys. Rev. Lett.* 94 (2005) 205502.
- [8] G. Kumar, T. Hong, J. Schroers, *Nature* 457 (2009) 868–872.
- [9] A. Wiest, J. Harmon, M. Demetriou, D. Conner, W. Johnson, *Scripta Mater.* 60 (2009) 160–163.
- [10] Y. Kawamura, Y. Ohno, *Scripta Mater.* 45 (2001) 279–285.
- [11] J. Schroers, Q. Pham, N. Paton, *Scripta Mater.* 57 (2007) 341–344.
- [12] W. Johnson, G. Kaltenboeck, M. Demetriou, J. Schramm, X. Liu, K. Samwer, P. Kim, D. Hofmann, *Science* 332 (2011) 828–833.
- [13] T. Nagase, K. Kinoshita, Y. Umakoshi, *Mater. Trans. JIM* 49 (2008) 1385–1394.
- [14] I. Masumoto, A. Ohnaka, A. Inoue, M. Hagiwara, *Scr. Metall.* 15 (1981) 293–296.
- [15] K. Son, H. Soejima, N. Nishiyama, X. Wang, A. Inoue, *Mater. Sci. Eng. A* 449 (2007) 248–252.
- [16] A. Inoue, *Proc. Japan Acad.* 73 (1997) 19–24.
- [17] S. Bossuyt, E. Soinila, H. Penttilä, V. Pulkki, H. Hanninen, *Mater. Res. Soc. Symp. Proc.* 1300 (2011) 1–6.
- [18] J. Schroers, *Acta Mater.* 56 (2008) 471–478.
- [19] S. Bossuyt, J. Schroers, The role of friction in measurements of the formability of bulk metallic glasses, TMS Annual meeting, 2009.
- [20] E. Soinila, T. Pihlajamäki, S. Bossuyt, H. Hänninen, *Rev. Sci. Instrum.* 82 (2011) 0739901.
- [21] L. Chen, F. Spaepen, *Nature* 336 (1988) 366–368.
- [22] A. Salimon, M. Ashby, Y. Brechet, A. Greer, *Mater. Sci. Eng. A* 375 (2004) 385–388.



Bulk metallic glasses (BMG) are alloys that can be solidified into a diameter larger than 1 mm without detectable crystallization. The resulting amorphous solid state satisfies the thermodynamic definition of a glass: upon heating above a glass transition temperature, they reach a metastable super-cooled liquid region before crystallizing. There are many known methods for producing amorphous metals. The material properties and the ease of manufacturing amorphous metal specimens depend on the manufacturing methods and facilities used. Studying and developing such facilities contributes both to practical applications of these materials and to advances in basic science of liquid and amorphous states of matter. In this thesis, the merits of different facilities for producing bulk metallic glass are evaluated anecdotally using literature and interviews, and then in practice by designing, building and finally using different facilities to make various metallic glass specimens with composition Zr55Cu30Al10Ni5 (at.%).

ISBN 978-952-60-4691-4 (pdf)  
ISSN-L 1799-4934  
ISSN 1799-4934  
ISSN 1799-4942 (pdf)

Aalto University  
School of Engineering  
Department of Engineering Design and Production  
[www.aalto.fi](http://www.aalto.fi)

BUSINESS +  
ECONOMY

ART +  
DESIGN +  
ARCHITECTURE

SCIENCE +  
TECHNOLOGY

CROSSOVER

DOCTORAL  
DISSERTATIONS